Application of Artificial Intelligence Techniques in the Prediction of Industrial Outfall Discharges

Aakanksha Jain

A thesis submitted in partial fulfilment of the requirements for the degree of

Master of Applied Science in Environmental Engineering

Ottawa-Carleton Institute for Environmental Engineering

Department of Civil Engineering

University of Ottawa

Ottawa, Canada

Abstract

Artificial intelligence techniques have been widely used for prediction in various areas of sciences and engineering. In the thesis, applications of AI techniques are studied to predict the dilution of industrial outfall discharges. The discharge of industrial effluents from the outfall systems is broadly divided into two categories on the basis of density. The effluent with density higher than the water receiving will sink and called as negatively buoyant jet. The effluent with density lower than the receiving water will rise and called as positively buoyant jet. The effluent discharge in the water body creates major environmental threats. In this work, negatively buoyant jet is considered. For the study, ANFIS model is taken into consideration and incorporated with algorithms such as GA, PSO and FFA to determine the suitable model for the discharge prediction. The training and test dataset for the ANFIS-type models are obtained by simulating the jet using the realizable k-ε turbulence model over a wide range of Froude numbers i.e. from 5 to 60 and discharge angles from 20 to 72.5 degrees employing OpenFOAM platform. Froude number and angles are taken as input parameters for the ANFIS-type models. The output parameters were peak salinity (S_m), return salinity (S_r), return point in x direction (x_r) and peak salinity coordinates in x and y directions (x_m and y_m). Multivariate regression analysis has also been done to verify the linearity of the data using the same input and output parameters. To evaluate the performance of ANFIS, ANFIS-GA, ANFIS-PSO, ANFIS-FFA and multivariate regression model, some statistical parameters such as coefficient of determination (R^2), root mean squared error (RMSE), mean absolute error (MAE) and average absolute deviation in percentage are determined. It has been observed that ANFIS-PSO is better in predicting the discharge characteristics.

Acknowledgements

I would sincerely like to express my gratitude to my supervisors Dr. Majid Mohammadian and Dr. Majid Sartaj, for their continuous guidance, endless support, patience and help in accomplishment of this thesis work.

I would also like to acknowledge and thank Dr. Hossein Bonakdari for the collaboration and providing valuable advices and suggestions.

Furthermore, I want to thank my parents and my grandmother for their blessings and my sister for her encouragement at every stage of my life.

Table of Contents

List of Figures

List of Tables

List of Symbols

C	Concentration on the numerical mesh;
c_1 *and* c_2	learning coefficients
D	Diameter of nozzle [m], and diffusion coefficient [m^2/s];
$D_{rededined}$	Redefined Willmott's Index
E_{LM}	Legates and McCabes Index
E_{NS}	Nash-Sutcliffe coefficient
Fr_d	Densimetric Froude number;
g	Gravity acceleration [m/s^2];
g'_o	Reduced gravity acceleration [m/s^2];
I	light intensity
k	Turbulent kinetic energy;
O_i	Observed value
P_i	Predicted value
r_1 *and* r_2	random coefficients
S_m	Salinity of the jet centerline peak;
S_r	Salinity of the return point;
T	Temperature of the numerical mesh [°C];
t	Time [s];
T_0	Temperature of source [°C];
u, v, w	Velocity in the x, y, z direction, respectively [m/s];
U_0	Velocity at source [m/s];
U_0	Velocity at source [m/s];
v^i	velocity vector for particle i
w	inertia weight (Equation 4.19)
$w(r)$	attractiveness at distance r from the firefly
x, y, z	Coordinates;
x^{Gbest}	best position achieved in the group

x^i	Position vector for particle i
x_m	Location of the jet centerline peak in x-direction [m];
x^{Pbest}	Best individual position in the group
x_r	Return point [m];
y_m	Location of the jet centerline peak in y-direction [m];
y_t	Maximum terminal rise height [m];
α	Randomization coefficient
γ	Coefficient of light absorption
ε	Dissipation rate for turbulence kinetic energy in k-ε;
ε_i	Random number vector
Θ	Initial jet angle [°];
Θ_B	Offshore slope angle
μ	Dynamic viscosity [N.s/m^2];
ρ	Density on the computational mesh [kg/m^3];
ρ_0	Discharge density [kg/m^3];
ρ_a	Ambient water density [kg/m^3];
ρ_t	Density of water as a function of temperature [kg/m^3];
υ	Kinematic viscosity [m^2/s];
υ_{eff}	Effective kinematic viscosity [m^2/s];
υ_t	Turbulent kinematic viscosity [m^2/s];

List of Acronyms

AI	Artificial Intelligence
ANFIS	Adaptive Neuro Fuzzy Inference System
ANN	Artificial Neural Network
CFD	Computational Fluid Dynamics
DE	Differential Evolution
FES	Finite Element Simulation
FFA	Firefly Algorithm
GA	Genetic Algorithm
GCV	Gross Calorific Value
ICA	Imperialist Competitive Algorithm
LA	Light Attenuation
LES	Large Eddy Simulation
MAE	Mean Absolute Error
MAPE	Mean Absolute Percentage Error
MLR	Multivariate Linear Regression
MRE	Mean Relative Error
MSF	Multistage Flash
OpenFOAM	Open-source Field Operation and Manipulation
PIV	Particle Image Velocimetry
PLIF	Planar Laser Induced Fluorescence
PSO	Particle Swarm Optimization
RMSE	Root Mean Squared Error
SGS	Sub-grid Scale
SI	Scatter Index

Chapter 1: Introduction

1.1 Industrial Effluents and their Environmental Impacts

According to US EPA, any waste water which is treated or untreated, that flows out of a treatment plant or industrial outfall is termed as effluent. The effluents are generally discharged into the water bodies and cause major environmental impacts as they impact the water quality and affect the marine life (Kanu et al., 2011).

With increasing water demand all around the world, desalination plants are rapidly growing especially in semi-arid and arid regions as the best alternative to fulfil the demand for fresh and drinkable water (Purnama and Shao, 2015). However, desalination plants cause some potential effects on environment which not only include the entrainment of the marine organisms but also impacting the air quality due to emission of the pollutants while maintaining the energy demand (Lattemann and Hopner, 2008). Along with this, desalination plants discharge a type of effluent called 'brine' in the receiving water whose salt concentration is significantly higher than receiving sea water and might have elevated temperature if the desalination process occurred in Multi-stage flash (MSF) plant (Alameddine and El-Fadel, 2007; Roberts et al., 2010). The impact of brine on receiving marine environment is severe as it affects the water quality and causes sediment pollution with accompanying harmful effects on marine life (especially in the near-field region) along with damaging the functioning of the coastal eco-system (Lattemann and Hopner,2008; Gildeh et al., 2015).

Impacts caused by brine on environment depend on various factors which include the strength of brine (mass and concentrations of contaminants) released, its dilution rate, and properties of receiving water along with the geometry and hydraulic characteristics of the discharge outfall system, which play a key role on dispersion and dilution of effluent in water bodies (Alameddine and El-Fadel, 2007). Hence, outfall systems need to be properly designed and installed in order to mitigate harmful effects, which are generally observed in the range of 300m from the point of discharge (Kheirkhah Gildeh, 2013; Alameddine and El-Fadel, 2007). It has been reported that the outfall systems are often not properly designed due to improper guidelines for the effluent

discharges (Jirka,2004). To reduce the impacts, methods such as discharging the brine with the cooling water coming out from the power plant have been implemented by many plants, but most of the plants discharge the brine through long outfall pipe which creates a highly concentrated saline plume in the receiving water body (Purnama and Shao, 2015). Some other alternatives for brine disposal are: implementing long pipes with diffusers at offshore, surface disposal of the brine, diluting the brine, and treating the brine to extract salt (Einav et al., 2003; Malcangio and Petrillo, 2010).

Malcangio et al. (2010) suggested that dilution occurs into two stages:

- When the jet is discharged from the outfall system, dilution occurs in the near-field region and depends on the density gradient, flow rate and speed, momentum flux and geometrical characteristics of the outfall system.
- Further, the natural dilution takes place in far-field region which depends on the diffusion and mixing provided by the ocean currents. In this thesis, near-field region is considered. The mixing fields for negatively buoyant jet can be seen in Figure 1.1

Bleninger et al. (2010) mentioned about discharge characteristics in which the discharge site and effluent are prevalent. The discharge characteristics consist of: 1) the type of the discharge structure, which could be open channel, submerged, etc.; 2) dimensions of the structure. which could be its pipe diameter, cross-section of the channel, etc.; 3) the site for the discharge which could either be the receiving water body or the channel, etc; and 4) the orientation of the discharge structure which comprises of discharge angles, other geographical features etc. The effluent comprises of type of effluent, its physical, chemical, biological properties and fluxes such volume, momentum, etc. Also, Bleninger et al. (2010) pointed out some significant characteristics of receiving water which includes, its local conditions (type of water body, topographic conditions, physical, chemical and biological properties) and its regional conditions (proximity to other discharges, proximity to aquatic ecosystem etc.)

Effluents are discharged into the water body (Lattemann and Hopner, 2008) generally as a submerged jet as this is more effective than the surface jets. The density difference between the receiving water and effluent make the plume to rise or fall. If the density of brine is higher than the ambient water, this will cause the plume to fall. This is called

a negatively buoyant jet. If the density of effluent is lower than the receiving water, it makes the plume to rise, which is called positively buoyant jet. Hence, it is very prominent to design the outfall system properly in order to mitigate the potential environment issues (Shao and Law, 2010). An effective way to tackle the problem could be to increase the effluent dispersion in the receiving zone and installation of multiport diffusor in order to improve the efficiency of mixing (Bleninger et al., 2010). Also, if the concentration is predicted before discharging the effluent in the receiving water body, it would be helpful to implement the solutions. The salinity of the effluent discharged can be measured by experimental or numerical studies but to avoid the computational time and cost of the experimental equipment, another solution could be applying artificial intelligence (AI) techniques to predict the salinity as by implementing different algorithms it would be a faster way to predict the results.

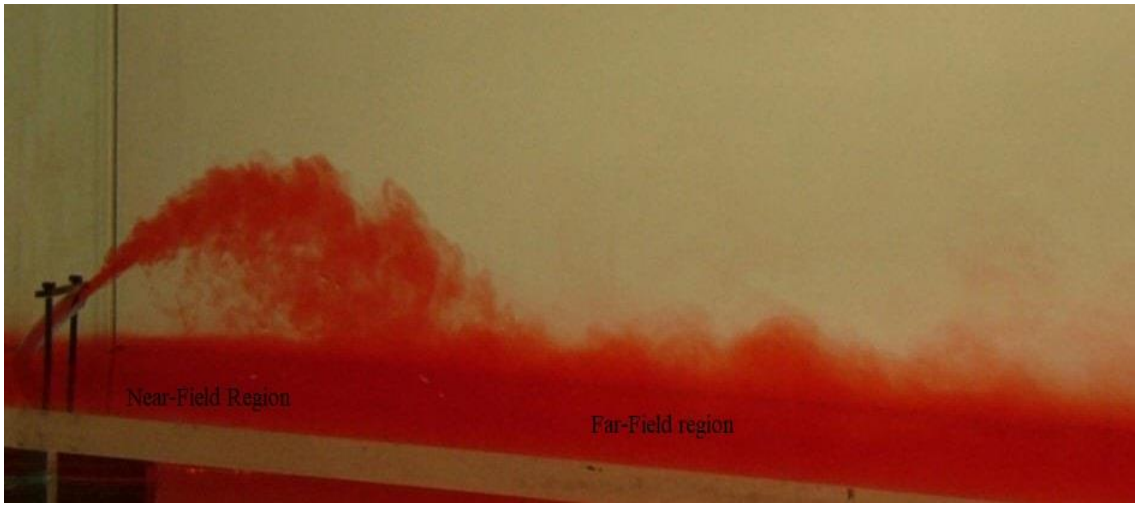

Figure 1.1: Mixing fields of negatively buoyant jet. (Source:http://www.ifh.uni-karlsruhe.de/science/envflu/Research/brinedis/results.htm)

1.2 Objectives of the study

In this study, negatively buoyant submerged jets are considered. The main objectives of this study are:

- To simulate the numerical model for negatively buoyant jets to obtain a wide range of datasets.
- To develop suitable ANFIS-type models.

- To evaluate the performance of various ANFIS-type models.
- To compare the ANFIS-type models' predictions with the numerical model.
- To compare the ANFIS-type models' performance with regression models.

In order to achieve the objectives of the study, a numerical model from the study by Gildeh et al. (2015) was considered which was carried on OpenFOAM platform. All the ANFIS-type models were run on MATLAB which is explained in Chapter 4.

1.3 Novelty of the Study

Various experimental studies have been conducted on negatively and positively buoyant jets, though numerical studies on negatively buoyant jets are less compared to experimental studies.

In the present study, negatively buoyant jets are considered. This is the first time (to the best knowledge of author) that artificial intelligence techniques are applied for prediction of industrial outfall discharges.

Moreover, ANFIS-type models incorporated with different algorithms have been examined in order to determine the suitable model for the study. In which various output parameters are investigated.

Also, the models are compared with the regression analysis as well in order to determine if there is any closeness with the linearity.

1.4 Scope of the Study

In this study, negatively buoyant jets are considered and simulations are performed based on realizable k-ε turbulence model which were ran on OpenFOAM platform. Also, ANFIS-type models incorporated with three different algorithms are investigated along with the multivariate regression model. Though, for an independent study, positively buoyant jets or other numerical models can be examined or other algorithms for soft computing can also be investigated which is beyond the scope of the current thesis.

1.5 Thesis Outline

The thesis is organized in five chapters. The first chapter i.e. Chapter 1 is the Introduction. Chapter 2 is the Literature Review in which numerical studies on

negatively buoyant jets are discussed in one section and in another section, various studies conducted on different areas using different Artificial Intelligence models and algorithms are reviewed. Also, in this section comparative studies between numerical or experimental models with AI models are shown and some of the studies are compared with regression models as well.

Chapter 3 presents a description on the numerical model which is used in the study. Chapter 4 consists of a Technical paper. In this paper, negatively buoyant jet from the study of Gildeh et al. (2015) is considered. The turbulence model used for this study is realizable k-ε turbulence model and simulated over a range of Froude number and discharge angles to predict the discharge parameters. Also, the datasets collected from numerical model are used to train and test four models: (i) Adaptive Neuro-Fuzzy Inference System (ANFIS); (ii) ANFIS-Genetic Algorithm (ANFIS-GA); (iii) ANFIS-Particle Swarm Optimization (ANFIS-PSO); and (iv) ANFIS-Firefly Algorithm (ANFIS-FFA). The numerical model is compared with Multivariate Regression model as well.

Chapter 5 consists of conclusions and suggestions for the future work. It should be mentioned that main results of the thesis are presented in Chapter 4 which is the technical paper, hence the author tried to avoid repetition as much as possible.

Chapter 2: Literature Review

2.1 Introduction

The effluent discharge from the plants into the water body occurs in one of the two ways, either as a surface discharge (Figure 2.1) or submerged discharge (Figure 2.2). Submerged discharges are widely used by the plants due to their high mixing efficiency in the water body which leads to higher dilution rate as the water entrainment in this type of discharges occurs from all the directions whereas in surface discharges the mixing efficiency is low. Submerged discharges could occur either in the form of negatively buoyant jet (Figure 2.2-b) or positively buoyant jet (Figure 2.2-c). If the density of effluent is higher than the receiving water, then it would be considered as negatively buoyant jet and if the density of effluent is lower than the receiving water then the jet plume will rise.

(a)

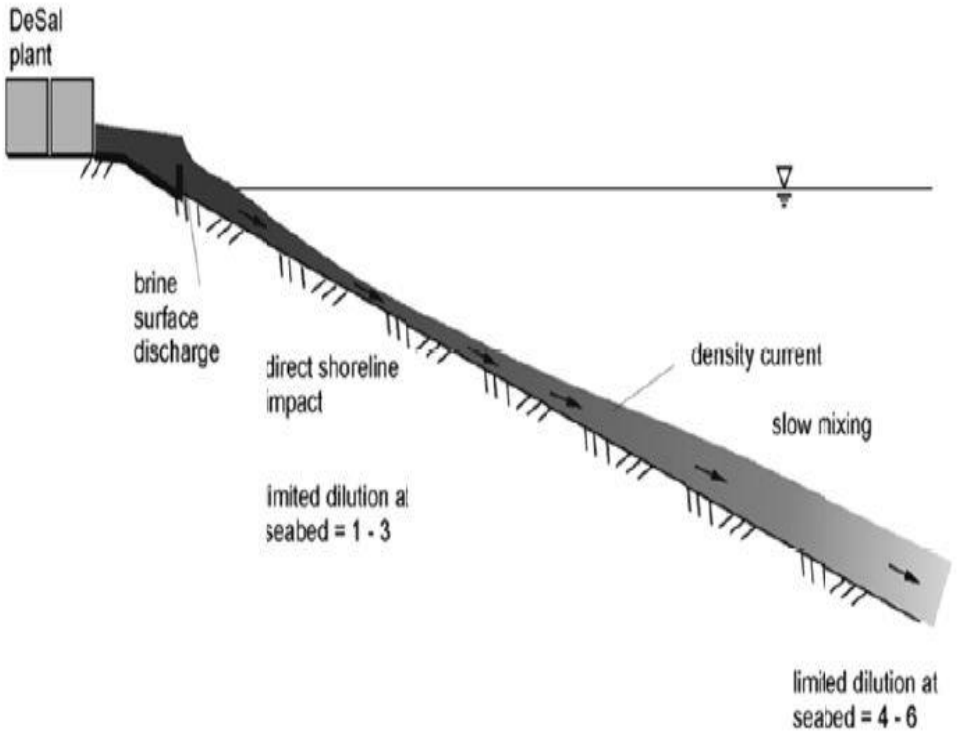

(b)

Figure 2.1: Surface Discharge (a) Ringsend Tank Sewage Discharge into Dublin Bay, Dublin (Source: https://www.irishtimes.com/news/environment/failure-of-ringsend-tank-led-to-sewage-discharge-into-dublin-bay-1.3806086) (b) Surface Discharge's Sketch, From Bleninger and Jirka (2008); Kheirkhah Gildeh (2013)

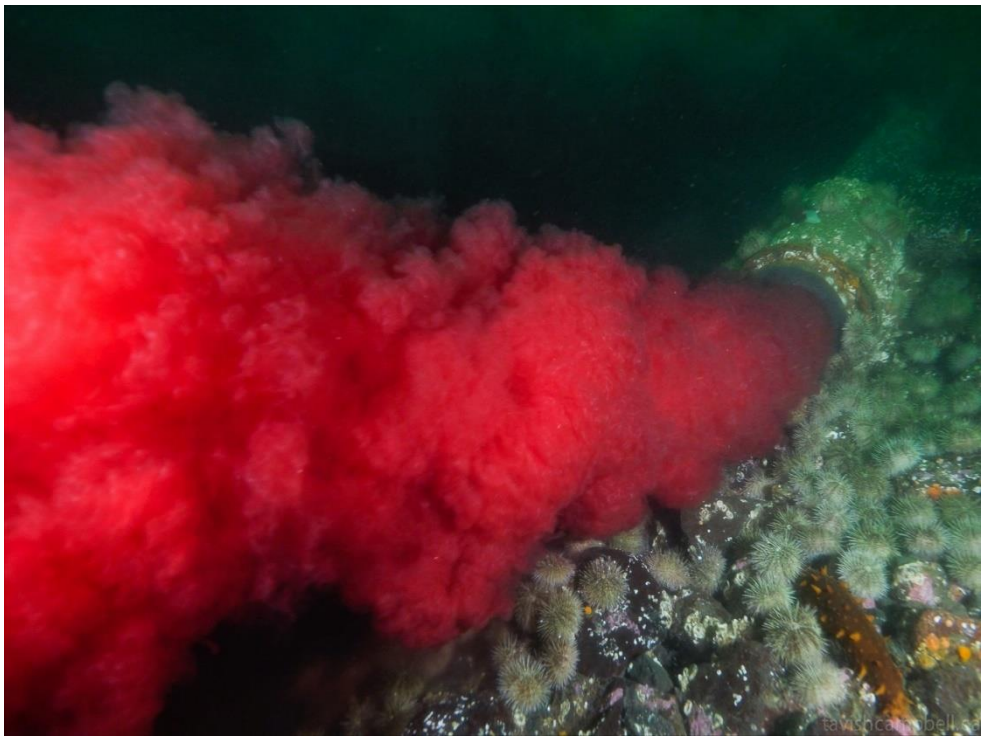

(a)

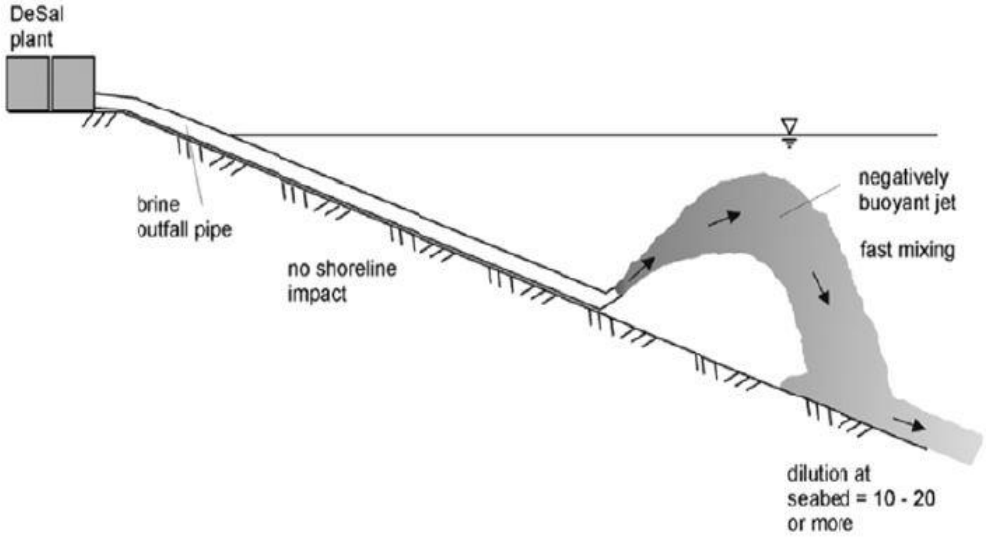
DeSal
plant
brine
outfall pipe
no shoreline
impact
negatively
buoyant jet
fast mixing
dilution at
seabed = 10 - 20
or more

(b)

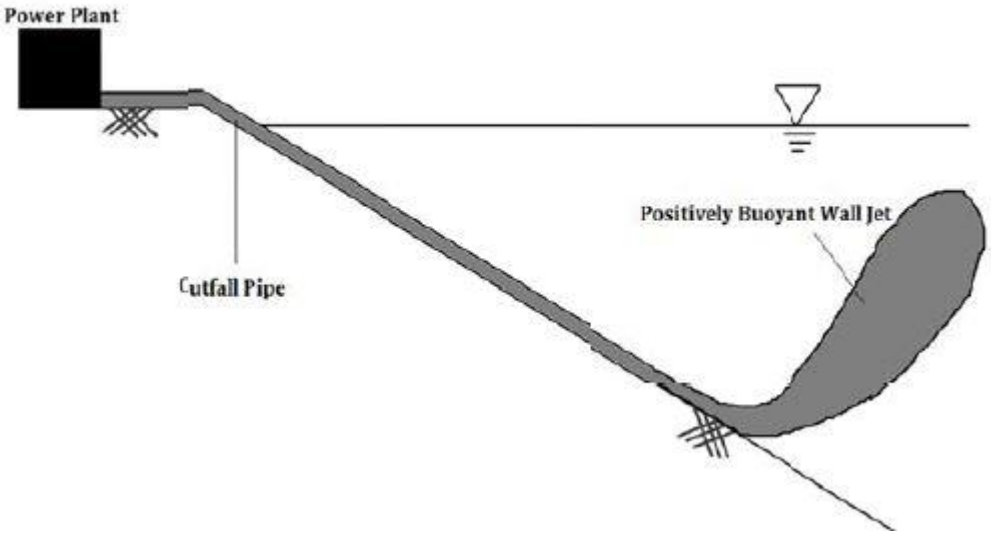

(c)

Figure 2.2:(a) Submerged discharge of effluent in Brown's Bay on Canada's Vancouver Island (Source: https://www.seattletimes.com/seattle-news/environment/video-of-infected-fish-waste-spewing-into-b-c-waters-roils-fish-farming-issue/) (b)Negatively buoyant submerged discharge. From Bleninger and Jirka (2008); Kheirkhah Gildeh (2013) (c) Positively Buoyant Submerged Discharge. From Kheirkhah Gildeh (2013)

As mentioned in chapter 1, the prediction of the salinity would be very beneficial in order to mitigate the marine environmental impacts. Hence, numerical studies are generally conducted to predict the discharge characteristics but with advancement in technology, Artificial Intelligence techniques are coming up as one of the most robust and promising ways for prediction regardless of any particular domain. In the recent years, researchers are adopting AI techniques widely for variety of applications as AI techniques have various advantages which consist of easy integration of physical conditions in the model, handling large amount of data, and determining additional information from the data (Mcgovern et al., 2017). Application of AI is often superior in prediction of the problems which include different types and sources of data or large amount of data.

In the thesis, negatively buoyant jets are considered, and the literature review consists of numerical modelling of the negatively buoyant jets and in the later section

applications of various Artificial intelligence techniques are discussed in different areas of study.

2.2 Numerical Studies

Kikkert et al. (2007) studied the negatively inclined buoyant discharges in which analytical solutions were developed. Later, the assessment of the data obtained from these solutions were compared with the data of the previous studies and the experiments performed by Kikkert et al. (2007). For the experimental studies, light attenuation (LA) and laser induced fluorescence techniques were applied to study the flows. It was found that for angles from 0^0 to 75^0 and Froude number ranging from 14 to 99, analytical solutions predicted the data reasonably well. However, the trajectory predictions of numerical models CorJet and VisJet from the previous studies were similar but lower as compared to the analytical solutions. Also, the dilution prediction of the mentioned numerical models was on the conservative side.

Oliver et al. (2008) investigated *k-ε* model, which is a part of a computational fluid dynamics package (CFX) for the prediction of inclined negatively buoyant discharge. For the study, two sets of simulations were performed. In the first approach, a standard model was used and for the second approach the model was calibrated by adjusting the Schmidt number in the transport equation and making prediction for the positively buoyant discharge followed by utilizing it for negatively buoyant discharge. Schmidt numbers selected for standard model and calibrated model were 0.9 and 0.6, respectively, for inclinations of 15^0, 35^0, 40^0 and 60^0. The configuration of Oliver et al., (2008) study for negatively buoyant jet is shown in Figure 2.3. Comparison between these numerical studies with the previous experimental studies was done and it was deduced that trajectory predictions by numerical models were more accurate compared to integral model and analytical solutions, but *k-ε* model (standard and calibrated) had over-estimated the mean-integrated concentration and effect of density gradients while underestimated the mean integrated dilution. Standard and calibrated models had also made the initial discharge angle essential while it was not relevant in the data. Hence, after comparing the previous studies, it was concluded that these models were sophisticated, but for predicting the bulk flow parameters analytical solutions could be better as they are much simpler to use.

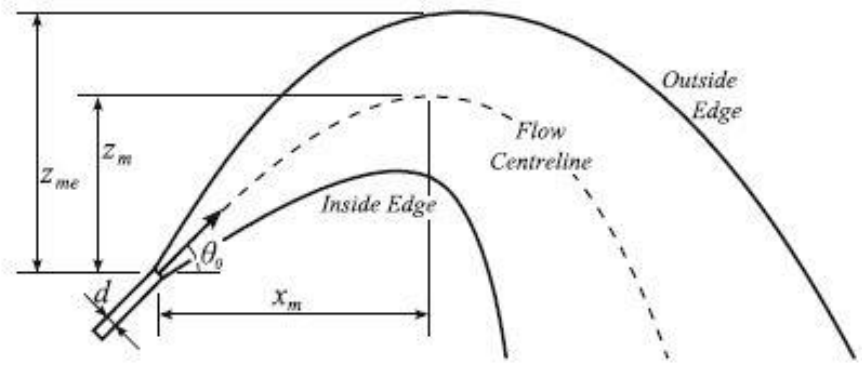

Figure 2.3: Discharge configuration with θ_0 as discharge angle, d as outfall diameter, x_m and z_m as horizontal and vertical distance to centreline and z_{me} as vertical distance to the maximum height for outside edge. From Oliver et al. (2008)

Zhang et al. (2014) studied negatively buoyant jets at 45degree inclination using Smagorinsky and Dynamic Smagorinsky sub-grid scale (SGS) models by implementing large eddy simulation (LES) method to predict the kinematic and mixing behaviour. Later, experiments were conducted and observations from previous studies were compared with the numerical models to validate the results. It was concluded that both the Smagorinsky and Dynamic Smagorinsky models performed well compared to the integral models as these models predicted return point coordinate, horizontal and vertical coordinates for centreline reasonably well with approximately 10 % of over prediction compared to experimental observations. Also, the models predicted return point dilution well because the under-prediction compared to experimental observation was approximately 20%. Hence, overall LES was considered as a superior approach. Palomar et al. (2012a) had analyzed software such as CORMIX, VISUAL PLUMES and VISJET for the near field brine discharges. Palomar et al. (2012b) validated various numerical software such as CORMIX, VISUAL PLUMES and VISJET for brine discharge in near-field. In the study, various experimental data of the previous studies were used. The study had focussed on the single port dense jet and compared the characteristics such as dilution, geometry and velocity of the jet for stagnant and dynamic conditions. CORMIX1, CORJET, UM3 and JetLag models of CORMIX, VISUAL PLUMES and VISJET respectively were considered (Palomar et al., 2012b). It was deduced that commercial tools such as CORJET, UM3 and JetLag performed better for the dense modelling for all the conditions i.e. they were reliable tools but CORMIX1 showed some errors. However, the degree of accuracy, out of these three models i.e. CORJET, UM3 and JetLag in stagnant condition was higher for CORJET

as it had given the fluctuation from 10%-17% for the dilution at the impact point compared to other models which had given deviations from 50%-65%. For dynamic environment, major differences were observed when crossflow direction was considered. Though, the models had followed the experimental observations' trend by increasing the dilution with decrease in the maximum rise height, but overall there was significant difference in the dilution rate.

Bleninger and Jirka (2008) investigated the application of CORJET model for the negatively buoyant jet and used the laboratory data from previous studies. The CORJET model used was developed by Jirka (2004) study as it was validated before and had given good results. The CORJET model was applied for the discharge angles ranging from 0^0 to 90^0 and for different offshore angle, θ_B from 0^0 to 30^0 (Figure 2.4). Parameters such as maximum points of the centreline trajectory i.e. x_{max} and z_{max} along with maximum height of upper jet boundary Z_{max} were considered. It was inferred that there were differences between the experimental observations of different studies but CORJET model could be suitable to examine the parametric study for the negatively buoyant discharges. It was also suggested that better dilution results could be obtained at discharge angles 30^0 to 45^0 as at these angles, highest dilution was produced at maximum height and at impingement point (Figure 2.5). However, due to lack of enough experimental data, requirement of experiments with better mixing characteristics and jet evolution were recommended as existing data predicted that discharge at 60^0 was mostly favoured.

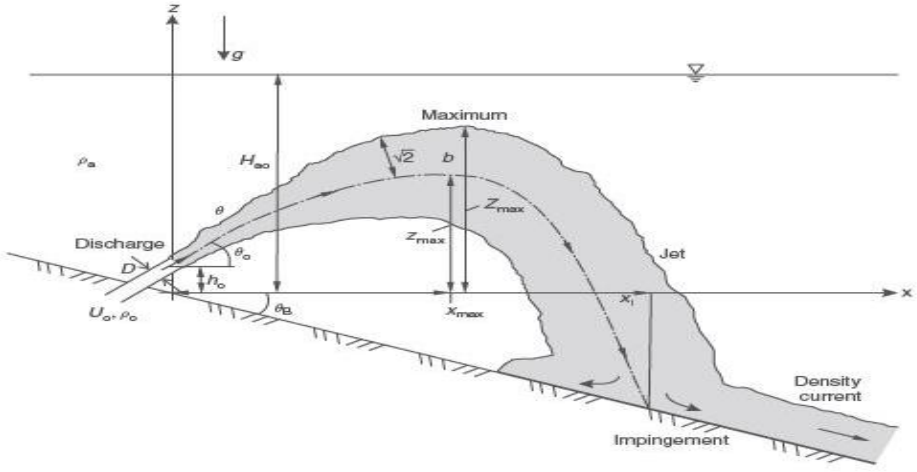

Figure 2.4: Negatively Buoyant Jet discharge with inclined bottom. From Bleninger and Jirka (2008)

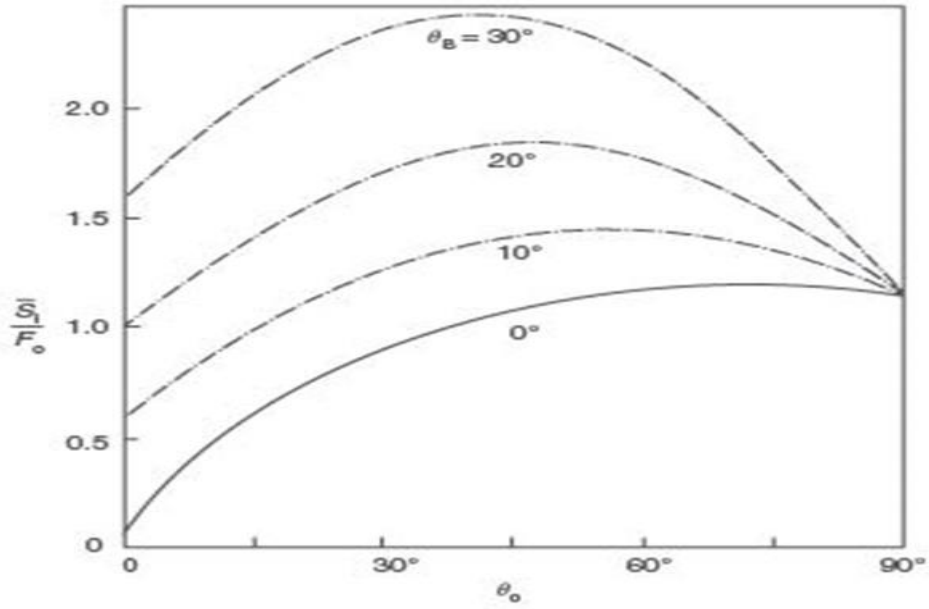

Figure 2.5: Negatively Buoyant Jet for discharge angles $0^0 \leq \theta_0 \leq 90^0$ with offshore slope angle, θ_B ranging from 0^0 to 30^0. From Bleninger and Jirka (2008)

Abou-Elhaggag et al. (2011) conducted experimental and numerical studies for the brine discharge of the dense jet in limited area. The study was divided into two sections, in the first section, experiments were conducted to study the different characteristics of brine discharge and in the second section numerical investigations were done with Fluent CFD package which were later compared with experimental data. The laboratory experiments conducted were based on the new empirical formula comprising of penetration depth, to investigate the jet trajectory and dilution of the negatively buoyant jet for analysing the mixing pattern at a given operating condition. Also, the experimental observations were compared with the previous and current studies which later validated the linear penetration depth function in terms of densimetric Froude number. Different combinations of diameter and concentration of the effluent salinities were examined over a wide range of conditions. The numerical study was done to identify the penetration depth and it had also followed the same empirical pattern which showed good agreement between the numerical and empirical observations. Numerical simulation showed multi-peaks for the concentration of brine which was explained as it was because of the restricted water volume surrounding each port.

Gildeh et al. (2015) investigated the negatively buoyant jet at discharge angles 30^0 and 45^0. Five Reynolds Averaged Navier Stokes turbulence models i.e. RNG $k - \varepsilon$, realizable $k - \varepsilon$; nonlinear $k - \varepsilon$, LRR and Launder–Gibson were examined to determine the suitable numerical model by evaluating the concentration, velocity and geometric characteristics of the jet. As at same angle, for higher Froude number, trajectory and the distance for return point were longer. Hence, in the study it was found that though the nonlinear $k - \varepsilon$ had longer trajectory than rest of the models but overall for both angles, the jet trajectories of all the five turbulence models were in good agreement with previous experimental studies and they were almost close to each other till the maximum terminal rise height. Differences were observed in the descending part of the trajectories as it could be observed from Figures 2.6 and 2.7 that nonlinear $k - \varepsilon$ had the longer trajectory and RNG $k - \varepsilon$ had the shorter descending part. Also, it was deduced that dilution for nonlinear $k - \varepsilon$ was lower compared to the experimental and other numerical models, whereas LRR had almost similar dilution as realizable $k - \varepsilon$ while Launder–Gibson showed similarity with RNG $k - \varepsilon$ model. It was also concluded that the inclinations had the similar trends as the typical jet for the maximum velocity decay and after the point $s/D/Fr <\sim 0.6$ in the centerline maximum decay curve, the maximum velocity decreased linearly. Overall, realizable $k - \varepsilon$ model and LRR models were accurate compared to the other models studied. Though, computational cost for LRR was higher compared to realizable $k - \varepsilon$.

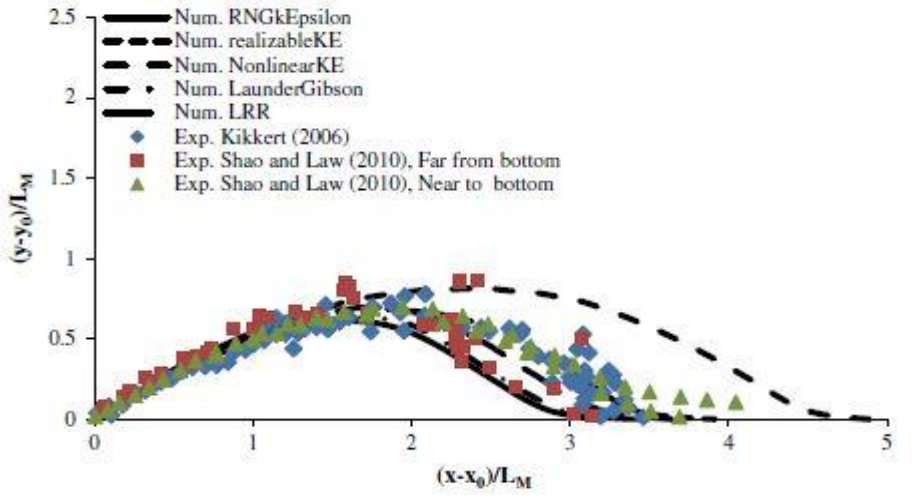

Figure 2.6: Centreline Trajectory for $\theta=30^0$ and Froude number=28.10. From Gildeh et al.(2015)

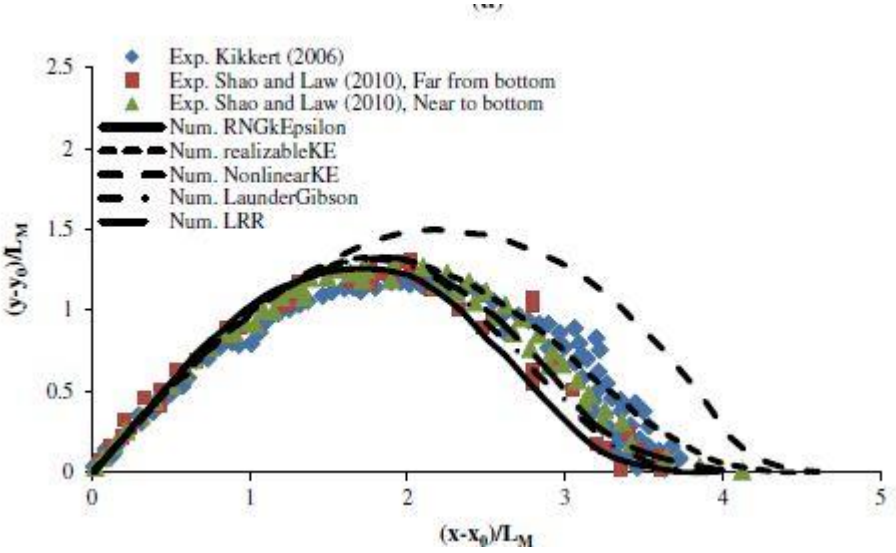

Figure 2.7: Centreline Trajectory for $\theta=45^0$ and Froude number= 34.30. From Gildeh et al.(2015)

2.3 Artificial Intelligence Techniques

Soft computing methods have not been studied so far on negatively buoyant jets. Hence, in this part of the literature review, various selected soft computing methods are put together for different applications. Taghavifar et al. (2015) examined the heat accumulation by hydrogen fueled engine which was influenced by the parameters such as crank angle, hydrogen mass fraction, penetration and equivalence ratio. For the study, computational fluid dynamics (CFD) method was applied to work on the combustion process. Later, CFD results were validated by performing experiments. ANFIS was applied to model the system. It was observed that CFD and experimental data showed good agreement in determining the heat accumulation and hence, the model was validated with the experimental results (Figure 2.8). For the ANFIS model, data were spilt into 50% training set and 50% test set and seven different types of membership functions were practiced. The statistical parameters such as Root-Mean Squared Error (RMSE) and coefficient of determination (R^2) were considered to evaluate the performance of the model. However, the performance of test data were lower compared to train data which was explained by the idea of inclusion of unforeseen data in the developed ANFIS model. Overall, it was elucidated that the ANFIS model with membership function; Trimf yielded the lowest RMSE and highest R^2 values i.e. 0.011527 and 0.999, respectively.

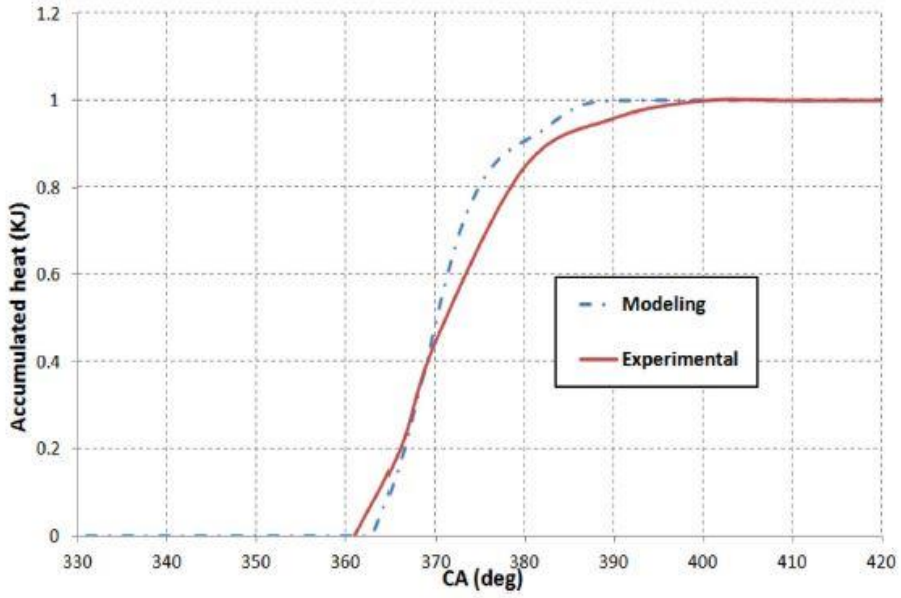

Figure 2.8: Calculated and Measured curve for accumulated heat. From Taghavifar et al. (2015)

Yaghoobi et al. (2016) conducted a study on the application of ANFIS and genetic algorithm (GA) to determine the optimized loading (pressure) path in the hydroforming process in order to save the time and cost from trial and error simulations. In the study, finite element simulations (FES) were run in order to determine the maximum thinning to train the ANFIS model. In total 54 simulations were ran, out of which forty-nine were the training dataset and 5 were the test dataset. The input parameters consisted of six points of the pressure part while maximum thinning in the critical area of the workpiece was the output parameter. For the later part of the study, GA was incorporated with ANFIS to determine the optimum pressure path for the minimum thinning in the critical region of the part. There was a good agreement between model prediction and FES simulation data (Figures 2.9 and 2.10). Hence, ANFIS model was able to predict the maximum thinning output. Also, for ANFIS-GA, there was a good correlation between the ANFIS-GA model data and simulated data. It was concluded that ANFIS-GA approach was suitable in predicting the optimized loading path and could be utilized in place of trial and error simulations.

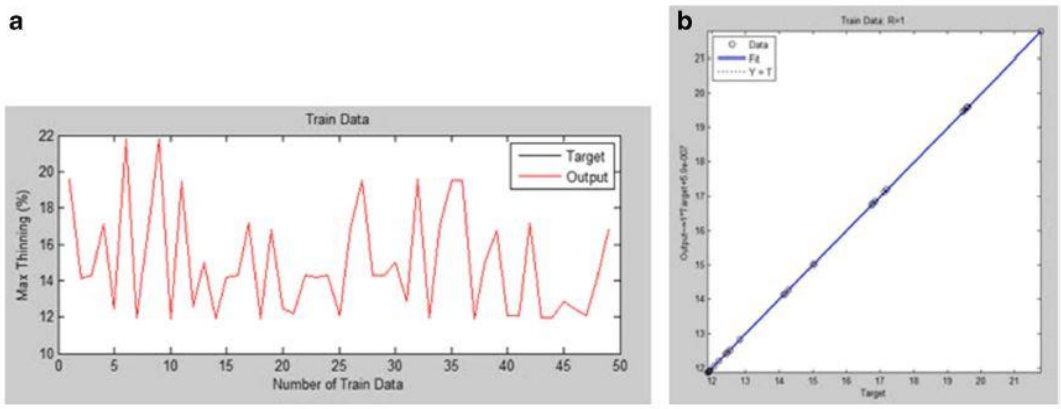

Figure 2.9: a) Predicted and simulated data for training dataset for ANFIS Model

b) Regression for maximum thinning for training dataset. From Yaghoobi et al. (2016)

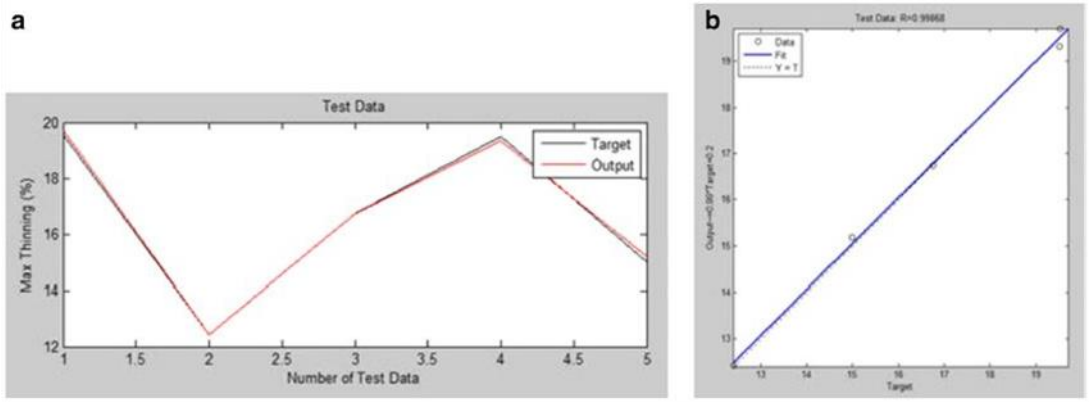

Figure 2.10: a) Predicted and simulated data for test dataset for ANFIS Model

b) Regression for maximum thinning for test dataset. From Yaghoobi et al. (2016)

Rezakazemi et al. (2017) employed ANFIS, ANFIS-GA and ANFIS-PSO to evaluate the performance of hydrogen matrix mixed membranes at various operating conditions. The data were gathered by conducting experiments. For training the ANFIS model, total 216 experimental data were spilt into training set with 151 datapoints and test set with 65 data points. The input parameters in this study were, feed pressure, Nano filter loading and type of gas while the targeted output was H_2/gas selectivity. Gas permeability of CH_4, H_2, C_3H_8 and CO_2 were used for modelling. The computational time for ANFIS model was one minute. Later, ANFIS was incorporated with GA and PSO and the results of ANFIS-GA and ANFIS-PSO were compared with ANFIS model in order to determine the model which had close correlation with the experimental data. The statistical parameters chosen for performance evaluation were R^2 and RMSE. It was found from the results that the model with least error and higher R^2 value is more reliable. Hence, ANFIS-PSO with RMSE value of 0.0135 and R^2

value of 0.9938 was more efficient compared to other models. However, computational time for ANFIS-GA and ANFIS-PSO were observed to be 21 minutes.

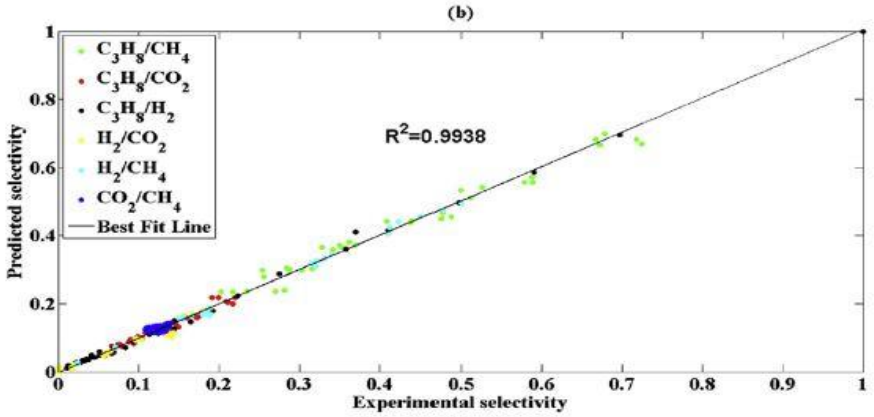

Figure 2.11: Predicted vs. Actual selectivity data for ANFIS-PSO. From Rezakazemi et al. (2017).

Bonakdari and Zaji (2018) investigated ANFIS, ANFIS-DE, ANFIS-GA and ANFIS-PSO to predict the discharge coefficient in designing side weirs. For the study, eight different input combinations were taken into consideration in order to determine appropriate input variables. From first input combination to the eight input combination, the number of input variables in each combinations were 5,4,3,3,3,3,2, and 1 respectively i.e. input variables had decreasing trend towards the end and the complexity was higher than the previous combination. To train the ANFIS models, experimental data from Borghei and Parvaneh (2011) were taken. The performance of the models was evaluated by RMSE statistical parameter. It was observed that, ANFIS-GA had the lowest RMSE value i.e. 0.040 compared to other models of the study, but it was found to be over-fitted. Hence, ANFIS-DE with RMSE value 0.057 was considered as better model than rest of the models. It was also concluded that models performed better with simple variables i.e. number of variables from 5-3 but with increase in complexity, the performance was decreased (Figure 2.12).

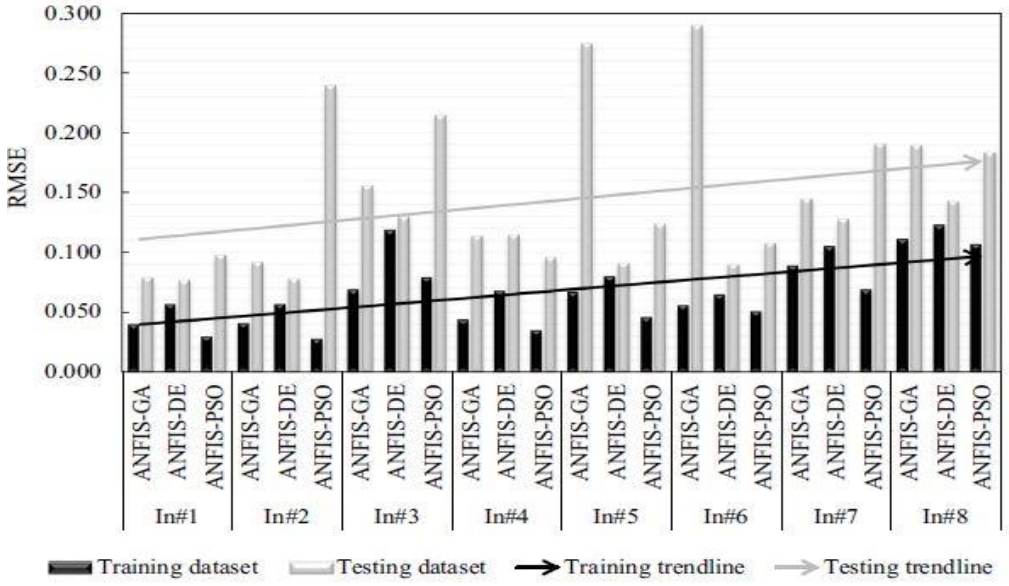

Figure 2.12: ANFIS models' performance. From Bonakdari and Zaji (2018)

Yaseen et al. (2017) worked on ANFIS and the combination of ANFIS with firefly algorithm (FFA) to predict the monthly streamflow. For the study, the monthly flow data of Pahang river was used. Sixteen different types of input combinations were examined with one to five-time lagged variables. The parameters used for evaluating the models were root mean squared error (RMSE), correlation coefficient (r), mean absolute error (MAE). Along with these parameters, other goodness of fit parameters such as Legates and McCabes index (E_{LM}), redefined Willmott's Index ($D_{redefined}$) and Nash- Sutcliffe coefficient (E_{NS}) were used for the evaluation. It was concluded that ANFIS-FFA performed better compared to ANFIS with r, MAE and RMSE as 1, 0.364 and 0.984 and E_{LM}, $D_{redefined}$ and E_{NS} as 0.988, 0.994 and 1 respectively. Also, the study conducted by Azimi et al. (2018) showed that for prediction of the hydraulic roller length models such as ANFIS and ANFIS-Firefly (ANFIS-FFA) with a combination of four different parameters were considered, hence investigation of overall 8 models. In this study the parameters were taken from the study of Carollo et al. (2007), therefore, in the study, the relative roller length (Lr/h_1) shown as a function of Froude number (Fr), ratio of depths (h_2/h_1) and relative roughness (ks/h_1). Also, different combinations of these parameters were used to input the variables for 8 models. The training and test dataset were divided into the ratio of 70:30, where the total datapoints were 368. It was concluded that ANFIS-Firefly in which Lr/h_1 was

taken as a function of h_2/h_1 and ks/h_1 and statistical parameters such as root mean squared error (RMSE), correlation coefficient (r), Mean-absolute relative error (MARE), Bias and scatter index (SI) were considered to evaluate the superior model. It was elucidated that the mentioned ANFIS-Firefly model performed better than the other seven models. Ebtehaj and Bonakdari (2014) evaluated ANFIS model to predict sediment transport by determining the densimetric Froude number. For the study, six different types of models were investigated by using five different parameters. To train the model, dataset from the experiment conducted by Ab. Ghani A (1993) were used and back-propagation and hybrid methods were the training algorithms. The statistical indices used to compare the models were coefficient of determination (R^2), RMSE, MAE, mean relative error (MRE), mean squared relative error (MSRE), mean error (ME), and MARE. To validate the model, the results were compared with different lab experiments and not with the ones utilized for training dataset. It was concluded that ANFIS model whose Froude number was a function of volumetric Froude number (C_v), relative depth flow (R/d), overall sediment friction factor (λ_s) and dimensionless particle number (D_{gr}) showed better results. Pourtousi et al. (2015) compared the CFD model and ANFIS model to determine the hydrodynamics of bubble column reactor in order to find whether ANFIS could be suitable to reduce the computational time of numerical simulation and operational costs of experimental equipment or not. For numerical investigation ANSYS-CFX was used. ANFIS was trained with the measured data from CFD model. In ANFIS model, input parameters were the positions x,y, and z while the output parameters were water liquid velocity in x,y, and z directions, air volume fraction and water liquid turbulence kinetic energy. The statistical indices selected for evaluating the performance of ANFIS model were R^2, RMSE, Pearson correlation coefficient (r) and it was observed that ANFIS had followed the same pattern as CFD for the liquid flow. Also, ANFIS had a good agreement with CFD in predicting the liquid velocity, gas hold up and turbulence kinetic energy. It was also found that gbell membership function had performed better compared to other membership functions in determining the hydrodynamics parameters.

There were other studies conducted in which multiple regression analyses were done along with soft computing methods to select the accurate method for prediction. In a study performed by Esmaeili et al. (2014) to predict the backbreak, an undesirable

effect caused by the breakage behind the last row of the blast holes which could affect the stability of the mine wall or efficiency of the machinery (Konya and Walter 1991; Esmaeili et al. 2014), artificial neural network (ANN), ANFIS, and multiple regression models' performance were assessed. The performance indices selected for the study were R^2, RMSE and mean absolute percentage error (MAPE). For the models seven input parameters and 42 datasets were used, the datasets were taken from the Sangan Iron mine, Iran. It was found that ANFIS performed better than ANN and multiple linear regression model as it had the highest R^2 and lowest RMSE and MAPE values compared to other two models (Figure 2.13). Similarly, a study was done by Bilgili and Sahin (2010) to compare ANN with multiple linear regression and non-linear regression models for the prediction of wind velocity. In the study, data from three different stations were collected and for the regression models, the independent variables were atmospheric pressure, temperature, relative humidity and rainfall. To compare the models, statistical indices such as RMSE, R, Mean Error (BIAS), MAE and MAPE were considered and it was found that ANN performed better compared to the regression models.

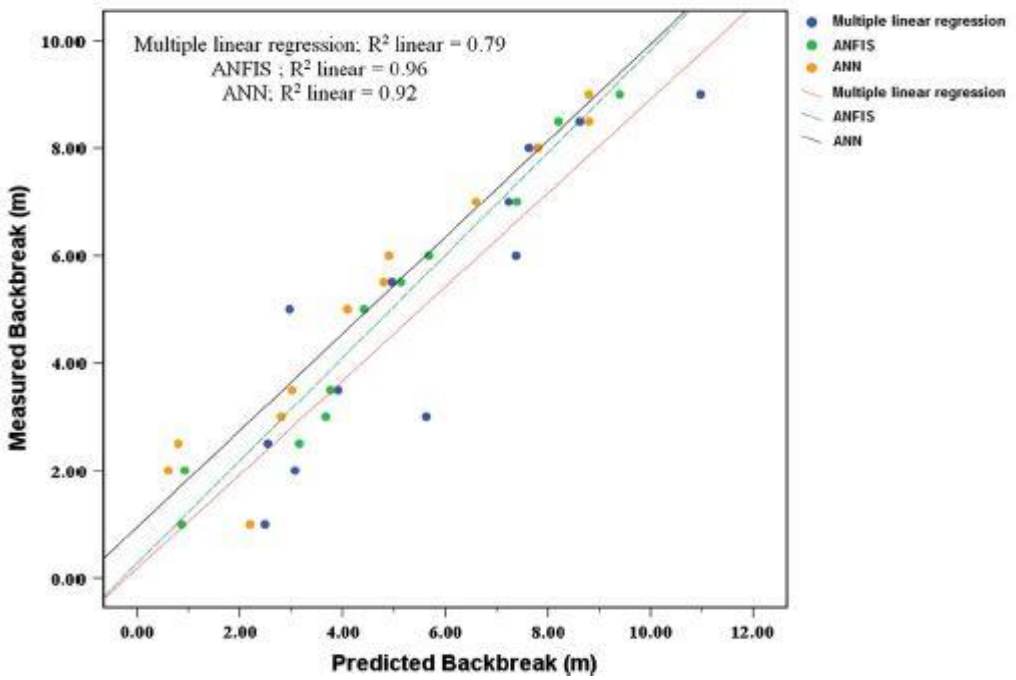

Figure 2.13: Coefficient of Determination for Predicted vs. measured backbreak. From Esmaeili et al. (2014)

In a study conducted by Niazian et al. (2018) to determine the oil content in a medicinal plant, two methods of ANN and Multi Linear Regression (MLR) were examined and 552 datapoints were collected from the field experiments which were performed in the years 2014 and 2015. The collected data were split into 70% training and 30% test data set for ANN model which was processed with 8 different types of transfer functions and various hidden layers to determine the optimal performance of the model. There were four input variables for ANN model which were also taken as independent variables for MLR analysis, computed on SAS software. The performance indices R^2, MAE and RMSE showed that ANN model with Sigmoid Axon transfer function with two hidden layers had performed better than the regression model. Similarly, a study conducted by Chelgani et al. (2011) to identify the suitable method from ANFIS and Multiple regression to determine the Gross Calorific Value (GCV) of organic and inorganic coal. Total 630 datasets were used, out of which over 400 were the training dataset and remaining were test dataset to model ANFIS with sigmoid transfer function. It was deduced that ANFIS was better in prediction of GVC as its R^2 value was higher than multiple regression (Figure 2.14).

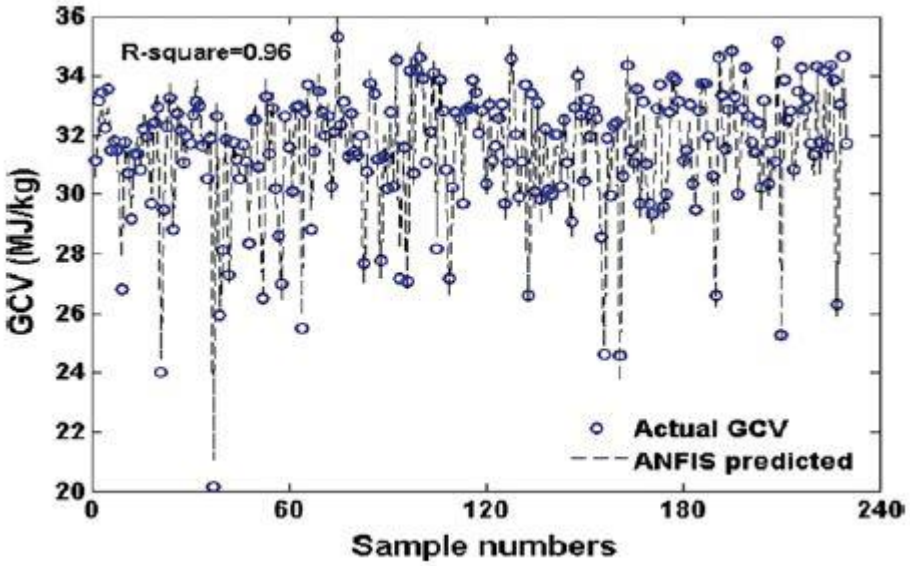

Figure 2.14: Predicted vs. Experimental data for GCV in ANFIS model. From Chelgani et al. (2011)

2.4 Concluding Remarks

It can be observed from the literature review that the studies conducted on numerical modelling for negatively buoyant jets are few. Also, none of the studies are conducted with negatively buoyant jets using soft computing methods, hence the present thesis research is novel. Also, it could be seen from the literature review that comparative studies conducted between computational fluid dynamics models, experimental results and various artificial intelligence models for other studies showed a good agreement between each other. It is also important to note that, data prediction with AI models is not limited to any specific area of study as from literature review it could be observed that all the studies which are conducted using AI algorithms are different from each other. Therefore, AI models could be applied on negatively buoyant jet study, which is the objective of the present thesis.

Chapter 3: Numerical Model

3.1 Introduction

Determination of the concentration of the fluid, could either be done by experimental methods or by numerical methods, experimental methods are often turned out to be expensive due to equipment cost etc. However, scaling up also leads to errors. Hence, numerical investigations are more advantageous compared to experimental methods as numerical investigations are less expensive and both ideal and real conditions can be simulated. Although, sometimes numerical investigations can be disadvantageous due to complexity in the geometry or complexity in the problem, or unavailability of a suitable mathematical model close to the physical conditions.

To develop a numerical model, a suitable mathematical model is required which involves set of Partial differential equations (PDEs) and boundary conditions. Hence, mathematical model needs to be simplified and to approximate the differential equation into algebraic equation, discretization method is applied. Some of the discretization methods are: Finite Volume Method (FVM), Finite Difference Method (FDM) and Finite Element Method (FEM). The numerical model used in this study has used Finite Volume Method (FVM).

Finite Volume method (FVM) is widely used in Fluid mechanics because of its easy to approach, understandability and implementation. It works with integral form of conservation equations and to obtain them, integration over finite volume is done. In finite volume method, generally the domain is divided into finite volumes and variable values present at the surface are represented by the nodal values for which interpolation is applied. When higher order polynomials are used then Finite Element Method would be more precise compared to Finite Volume Method.

3.2 Development of Mathematical Model

This section consists of the equation of conservation of mass, momentum and concentration. For developing a mathematical model, equations mentioned below were used.

3.2.1 Equation of Continuity

The continuity equation is based on the principle of conservation of mass which means that the rate of change of mass in particle is conserved (Malalasekera and Versteeg, 1995; Kheirkhah Gildeh, 2013)

$$\frac{dm}{dt} = 0 \qquad \text{Equation (3.1)}$$

In the form of differential equation, continuity equation can be expressed as:

$$\nabla.\left(\rho \underset{U}{\rightarrow}\right) = 0 \qquad \text{Equation (3.2)}$$

Which in terms of x,y,z direction can be defined as:

$$\frac{\partial(\rho u)}{\partial x} + \frac{\partial(\rho v)}{\partial y} + \frac{\partial(\rho w)}{\partial z} = 0 \qquad \text{Equation (3.3)}$$

The fluid considered in this thesis is incompressible. Hence, Navier-Stokes equations were applied and density is considered to be the function of salinity and temperature. The fluid density was independent of pressure.

The density was calculated using the empirical equations proposed by Millero and Poisson (1981):

$$\rho = \rho_t + AS + BS^{3/2} + CS \qquad \text{Equation (3.4)}$$

Where, ρ is the density of the jet and ρ_t is the density of ambient water.

The density of ambient water is calculated by the following equation:

$$\rho_t = 999.842594 + 6.793952 * 10^{-2}T - 9.095290 * 10^{-3}T^2 + 1.001685 * 10^{-4}T^3 - 1.120083 * 10^{-6}T^4 + 6.536336 * 10^{-9}T^5 \qquad \text{Equation (3.5)}$$

Equations for A, B, C are as follow:

$$A = 8.24493 * 10^{-1} - 4.0899 * 10^{-3}T + 7.6438 * 10^{-5}T^2 - 8.2467 * 10^{-7}T^3 + 5.3875 * 10^{-9}T^4$$

$$B = -5.72466 * 10^{-3} + 1.0227 * 10^{-4}T - 1.6546 * 10^{-6}T^2$$

$$C = 4.8314 * 10^{-4} \qquad \text{Equation (3.6)}$$

3.2.2 Concentration Equation

The concentration equation can be expressed in the following way:

$$\frac{\partial C}{\partial t} + u\frac{\partial C}{\partial x} + v\frac{\partial C}{\partial y} + w\frac{\partial C}{\partial z} = D\left(\frac{\partial^2 C}{\partial x^2} + \frac{\partial^2 C}{\partial y^2} + \frac{\partial^2 C}{\partial z^2}\right)$$

Equation (3.7)

Where, D is the diffusion coefficient C denotes the concentration which is basically salinity.

3.2.3 Momentum Equation

$$\frac{\partial u}{\partial t} + u\frac{\partial u}{\partial x} + v\frac{\partial u}{\partial y} + w\frac{\partial u}{\partial z} = -\frac{1}{\rho}\frac{\partial P}{\partial x} + \frac{\partial}{\partial x}\left(v_{eff}\left(\frac{\partial u}{\partial x}\right)\right) + \frac{\partial}{\partial y}\left(v_{eff}\left(\frac{\partial u}{\partial y}\right)\right) + \frac{\partial}{\partial z}\left(v_{eff}\left(\frac{\partial u}{\partial z}\right)\right)$$

$$\frac{\partial v}{\partial t} + u\frac{\partial v}{\partial x} + v\frac{\partial v}{\partial y} + w\frac{\partial v}{\partial z} = -\frac{1}{\rho}\frac{\partial P}{\partial y} + \frac{\partial}{\partial x}\left(v_{eff}\left(\frac{\partial v}{\partial x}\right)\right) + \frac{\partial}{\partial y}\left(v_{eff}\left(\frac{\partial v}{\partial y}\right)\right) + \frac{\partial}{\partial z}\left(v_{eff}\left(\frac{\partial v}{\partial z}\right)\right) - g\frac{\rho - \rho_o}{\rho}$$

$$\frac{\partial w}{\partial t} + u\frac{\partial w}{\partial x} + v\frac{\partial w}{\partial y} + w\frac{\partial w}{\partial z} = -\frac{1}{\rho}\frac{\partial P}{\partial z} + \frac{\partial}{\partial x}\left(v_{eff}\left(\frac{\partial w}{\partial x}\right)\right) + \frac{\partial}{\partial y}\left(v_{eff}\left(\frac{\partial w}{\partial y}\right)\right) + \frac{\partial}{\partial z}\left(v_{eff}\left(\frac{\partial w}{\partial z}\right)\right)$$

Equation (3.8)

Where, v_{eff} denotes the effective kinematic viscosity, ρ is the fluid density, ρ_o is the reference fluid density and P represents the fluid pressure. Also, the velocity components in x, y and z directions are represented by u, v and w.

3.3 OpenFOAM

The numerical model (Gildeh et al.,2015) used in the thesis was built on OpenFOAM (Open Source Field Operation and Manipulation) platform. OpenFOAM is an open source Computational Fluid Dynamics (CFD) software, implemented in C++ language and launched by OpenCFD Ltd. (www.openfoam.com, OpenFOAM,2011, Kheirkhah Gildeh,2013). OpenFOAM is widely used in many numerical studies comprises of the areas such as heat transfer, coastal engineering, free surface flows, ocean engineering, turbulence modelling etc. (Wang et al.,2019). There are several advantages of using OpenFOAM such as the libraries and solvers in OpenFOAM allow users to solve almost all CFD problems, the dynamic meshes can be used to change the geometry, pre and post processing interfaces are user-friendly, and object-oriented programming language C++ allows the users to incorporate their own models (Chen et al., 2014).

The simulation process priority in OpenFOAM is shown in Figure 3.1

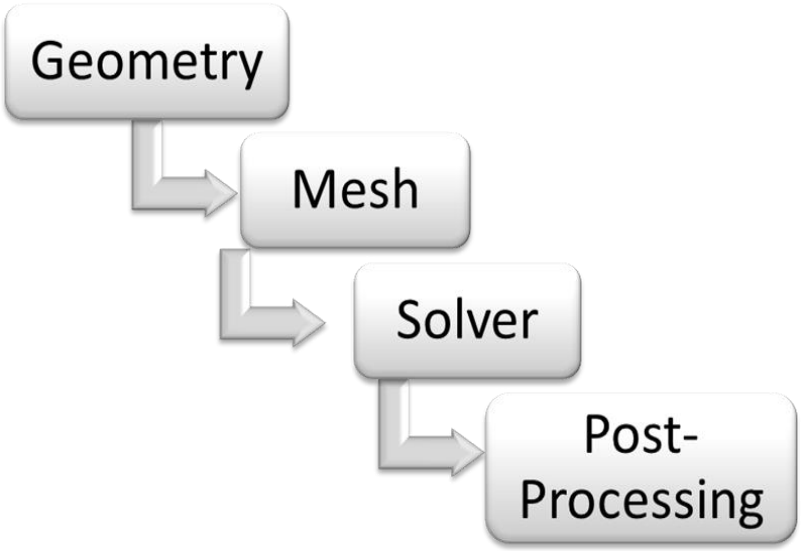

Figure 3.1: Simulation process priority. From Open FOAM (2011), Kheirkhah Gildeh (2013)

The command for geometry and meshing for simulation in the current work was ‘BlockMesh’, and the solver was pisoFoam5.

Chapter 4: Technical Paper - Applications of ANFIS-Type Methods in Simulation of Industrial Outfall Systems

Abstract- ANFIS-type algorithms have been successfully used in various modeling and simulation problems. With the help of algorithms with more accuracy and adaptability, it is possible to obtain better real-life emulating models. A critical environmental problem is the discharge of saline industrial effluents in water bodies. Industries discharge buoyant jets into water bodies. It is important to minimize the effect of effluent discharge on the nearby marine life, by estimating the concentration of the discharge in the ambient water. In this work, submerged discharges, specifically, negatively buoyant jets are modeled. The objective of this study is to compare various artificial intelligence algorithms along with multivariate regression model to find the best fit model emulating effluent discharge. This is done by training and testing the Adaptive Neuro Fuzzy Inference System (ANFIS), ANFIS-Genetic Algorithm (GA), ANFIS-Particle Swarm optimization (PSO) and ANFIS-Firefly Algorithm (FFA) models with input parameters which are obtained by using the realizable *k-ε* turbulence model and simulated parameters which are obtained after modeling the turbulent jet using OpenFoam simulation platform. A comparison of the realizable *k-ε* turbulence model outputs and AI algorithms' outputs is done. Statistical parameters such as least error, coefficient of determination (R^2), Mean absolute error and Average absolute deviation are measured to evaluate the performance of the models. In this work, it is found that ANFIS-PSO performed better compared to the other four models and multivariate regression model.

Index Terms- OpenFOAM, CFD, ANFIS, ANFIS (GA), ANFIS(PSO), ANFIS (FFA)

4.1 Introduction

Due to increase in the population growth and groundwater depletion, the demand for fresh and potable water has led to rising growth of desalination plants, especially in arid and semi-arid regions such as Persian Gulf, Red Sea and the Gulf of Oman (Purnama and Shao, 2015). It has also been estimated that the percentage of water shortage will increase by 60% by the year 2025 (Alameddiene and El-Fadel, 2007).

Hence, considering the fact that about 97.5% of the total volume of the hydrosphere is contained in seas and oceans (Termeh et al., 2019), desalination plants are the most viable solution for today's drinking water problems, but these plants cause many negative impacts. The effluent from desalination plants, called 'brine', is discharged into the sea water and contains concentrated salt which is almost double the salinity of the receiving water and ends up adding this salinity to the sea water (Purnama and Shao, 2015). Along with this, if a desalination plant is using multistage flash (MSF) technique, then the brine could also raise turbidity and temperature (Bleninger and Jirka, 2008). This concentrated brine stream can deteriorate chemical, physical and biological attributes of the receiving water. Hence, the effect of brine is majorly evident on environment especially on flora and fauna. Therefore, many countries like the USA and Europe have made strict regulations for the effluent standards (Bleninger and Jirka, 2008).

To meet the existing regulations, a diffuser can be placed at the end of the outfall system to dilute the concentrated brine since in the absence of dilution, brine plume extends its vicinity and will be harmful for the ecosystem (Purnama and Shao,2015). It has also been reported that the discharge of brine using inclined dense jets has been in use since 1970s in which dilution and geometry are the major parameters to be considered (Christodoulou et al., 2015). Dilution of brine occurs in two steps: a) Primary dilution which appears in the near field due to density difference, between the sea water and effluent as well as due to momentum flux and geometry of the outfall; and b) Natural dilution in the far field due to diffusion and mixing (Malcangio and Petrillo, 2010). The impact can generally be seen in the range of 300 m from the point of discharge, which is generally the near-field region (Alameddiene and El-Fadel, 2007). Hence, it is important to focus on the near-field region to design the outfall system for greater dilution (Marti et al., 2010). Since effluent density varies from the ambient water which makes the jet rise or fall, when the dense effluent is discharged upwards, it is called negatively buoyant jet. As the jet moves upwards its momentum decreases which then returns towards the bottom due to its high density after attaining the maximum height. When the effluent's density is lower than receiving water, and it is discharged downwards, a penetration depth is attained by the jet and hence making the effluent to rise which is called positively buoyant jet (Papakonstantis et al., 2011a,b).

Extensive studies have been conducted on negatively buoyant jets. Marti et al. (2010) conducted research in which an angle of 60 degrees was selected with three different Froude number regime (one-third, two-thirds and full-flow capacity) and it was found that Froude numbers below 20 were giving higher dilution than the predicted extrapolation. Zhang et al. (2016) did the numerical investigation for inclined dense jets at 45^0 angle and for the study, large eddy simulation (LES) method was applied along with Smagorinsky and Dynamic Smagorinsky sub-grid scale (SGS) (Zhang et al., 2016). Later, numerical results including jet trajectory, geometry and dilution were cross validated with the experimental results and it was found that LES was able to regenerate the outputs satisfactorily. Shao and Law (2010) studied the behavior of dense jet for angles 30^0 and 45^0 with different densimetric Froude numbers. For the measurement of velocity and concentration, combined particle image velocimetry (PIV) and planar laser induced fluorescence (PLIF) were applied(Shao and Law,2010). Velocity and concentration profiles were used to find the mixing and diluting parameters as well. It was found that return point dilution, horizontal distance of return point, terminal height, centerline peak location and its dilution were correlated to Froude number. Oliver et al. (2008) investigated the k-ε turbulence model in the standard fluid dynamics package (CFX) and took two approaches which included, one with the standard form of the model and other with the calibrated model by adjusting the Schmidt number. After comparing numerical data, experimental data, along with the data obtained from the studies of previous integral models, it was concluded that the k-ε model was providing better prediction for the trajectory data except the data for the integrated dilution at the centerline as they were over-predicting the density gradient which resulted in under-estimation of the dilution. Palomar at el. (2012) investigated the performances of CORMIX, VISUAL PLUMES and VISJET models for the inclined dense studies and obtained some significant differences in the dilution prediction. Kikkert et al. (2007) investigated the behavior of negatively buoyant jets with angles ranging from 0^0 to 75^0 and Froude number ranging from 14 to 99. The results showed good prediction for outer spread and maximum height of the outer edge. However, inner spread was under-estimated and minimum dilution prediction was conservative. Along with this, previous studies conducted with CorJet and VisJet models were compared with this study and it was found that these numerical models had under-predicted the horizontal and vertical locations of maximum jet height. Also, CorJet and VisJet were not accurate enough for integrated dilution prediction

compared to analytical solutions and the data obtained in a study by Kikkert et al. (2007). Jirka (2008) performed a study with smaller angles like 30^0 and 45^0 based on laboratory experiments and numerical modeling using CorJet model. It was found that the lower angle had given higher dilution when bottom slope was taken into consideration as it had provided better offshore transport of the mixed effluent. Kheirkhah Gildeh et al. (2014 and 2015), Gildeh et al. (2015) performed numerical modeling with 30^0 and 45^0 inclined dense jets. Five CFD models including LRR, RNG *k-ε,* Realizable *k-ε*, non-linear *k-ε*, and Launder Gibson were applied, and it was concluded that LRR and realizable *k-ε* turbulence models were giving better prediction for the mixing and dilution characteristics.

Apart from conventional CFD and experimental measurements, soft computing methods could be applied to minimize the computational time for simulation and investment of money on expensive laboratory equipment. Pourtousi et al. (2015) investigated the combination of computational fluid dynamics (CFD) and ANFIS method for simulation of bubble column hydrodynamics. Previous experimental data were used to validate the CFD model and later these data were used to train the ANFIS model. It was concluded that ANFIS was a promising method for predicting the outputs of bubble column hydrodynamics. Taghavifar et al. (2015) worked on assessment of heat accumulation in hydrogen engine in which the experimental data were compared with the data obtained after CFD modelling to determine the accuracy between the two. Later, CFD data were fed in ANFIS code to train the model and it was concluded that ANFIS model with Trimf membership function had given the highest R^2 and lowest root mean squared error (RMSE) value out of other membership functions and ANFIS was confirmed to be more accurate and simpler than CFD technique in the study. Rezakazemi et al. (2017) evaluated three models, namely ANFIS, ANFIS-PSO and ANFIS-GA, to determine the performance of hydrogen mixed membranes in which input parameters such as feed pressure and Nano filter contents were used to evaluate the output parameter (hydrogen gas selectivity). The criteria for investigation of the better model were R^2 and RMSE values and ANFIS-PSO had given better predictability. Amirkhani et al. (2015) studied the performance of ANN and ANFIS models to estimate the inlet air velocity of the chimney. Three days of experimental data were used to train the models and it was found that ANFIS model's results were closer to the experimental results as its R^2 was higher than ANN.

Bonakdari and Zaji (2018) worked on the modified triangular side weir in which they simulated its discharge coefficient. They studied three different methods of ANFIS, namely ANFIS-GA, ANFIS-PSO and ANFIS-DE, with combinations of eight different input variables and it was found that ANFIS-DE performed better as a it had given lowest RMSE value compared to ANFIS-GA and ANFIS-PSO. Shabanian et al. (2017) studied the ANFIS model with eight types of membership functions to predict the hydrogen yield of the jet fuel and efficiency of conversion for a non-catalytic filtration combustion reactor. Later, imperialist competitive algorithm (ICA) was applied for to get the optimized results for the hydrogen yield which was found to be efficient algorithm for the combustion process optimization.

The aim of this research is to investigate the application and performance of soft computing method with ANFIS, ANFIS-GA, ANFIS-PSO, ANFIS-FFA algorithms for negatively buoyant jets to predict the dilution and mixing characteristics. This is the first study on this topic. Negatively buoyant jets are considered for a wide range of Froude numbers, i.e. 5, 10, 12.5, 15, 17.5, 20, 22.5, 25, 27.5, 30, 32.5, 35, 37.5, 40, 50 and 60 with angles ranging from 20 degrees to 72.5 degrees using realizable *k*-ε model turbulence model in OpenFOAM platform.

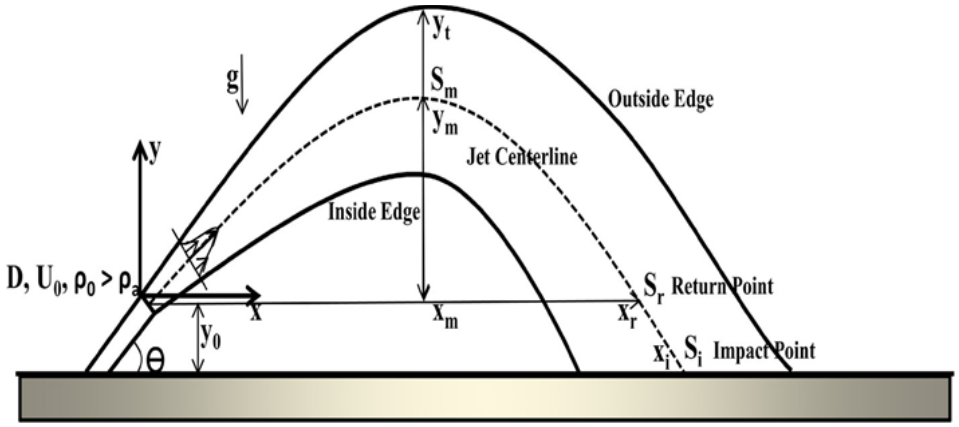

Figure 4.1: Configuration for Negatively Buoyant Jet (Gildeh et al., 2015)

4.2 Dimensional Analysis and Numerical Model

As it can be seen in Figure 4.1, negatively buoyant jets are discharged at an angle Θ and velocity U_o, the density of the ambient water is represented by ρ_a and density of jet is represented by ρ_o. It can be observed that $\rho_o > \rho_a$ which makes the jet to rise. The diameter of the jet is denoted by D. The terminal height is represented by y_t which hits the surface at coordinate x_i while the coordinates of peak centerline are represented by x_m and y_m with peak salinity as S_m. Also, jet concentration is represented by C_o. The return point of the jet is represented by x_r and return salinity value is S_r. For the dimensional analysis densimetric Froude number is used which is denoted by the following equation:

$$Fr_d = \frac{U_O}{\sqrt{g_0' D}} \tag{4.1}$$

$$g_0' = \left(\frac{\Delta\rho_o}{\rho a}\right) \tag{4.2}$$

Where, $\Delta\rho_o = (\rho_o - \rho_a)$ and g_o' is the reduced gravitational acceleration.

The centerline peak salinity is a function of Froude number and angle which can be represented by the following equation:

$$\frac{S_m}{Fr_d} = f(Fr_{d,}\, \theta) \tag{4.3}$$

For numerical modeling the following equations were used by Gildeh et al. (2015)

Continuity Equation:

$$\frac{\partial u}{\partial x} + \frac{\partial v}{\partial y} + \frac{\partial w}{\partial z} = 0 \tag{4.4}$$

Momentum Equations:

$$\frac{\partial u}{\partial t} + u\frac{\partial u}{\partial x} + v\frac{\partial u}{\partial y} + w\frac{\partial u}{\partial z} = -\frac{1}{\rho}\frac{\partial P}{\partial x} + \frac{\partial}{\partial x}\left(v_{eff}\left(\frac{\partial u}{\partial x}\right)\right) + \frac{\partial}{\partial y}\left(v_{eff}\left(\frac{\partial u}{\partial y}\right)\right) + \frac{\partial}{\partial z}\left(v_{eff}\left(\frac{\partial u}{\partial z}\right)\right) \tag{4.5}$$

$$\frac{\partial v}{\partial t} + u\frac{\partial v}{\partial x} + v\frac{\partial v}{\partial y} + w\frac{\partial v}{\partial z} = -\frac{1}{\rho}\frac{\partial P}{\partial y} + \frac{\partial}{\partial x}\left(v_{eff}\left(\frac{\partial v}{\partial x}\right)\right) + \frac{\partial}{\partial y}\left(v_{eff}\left(\frac{\partial v}{\partial y}\right)\right) + \frac{\partial}{\partial z}\left(v_{eff}\left(\frac{\partial v}{\partial z}\right)\right) - g\frac{\rho-\rho_o}{\rho} \quad (4.6)$$

$$\frac{\partial w}{\partial t} + u\frac{\partial w}{\partial x} + v\frac{\partial w}{\partial y} + w\frac{\partial w}{\partial z} = -\frac{1}{\rho}\frac{\partial P}{\partial z} + \frac{\partial}{\partial x}\left(v_{eff}\left(\frac{\partial w}{\partial x}\right)\right) + \frac{\partial}{\partial y}\left(v_{eff}\left(\frac{\partial w}{\partial y}\right)\right) + \frac{\partial}{\partial z}\left(v_{eff}\left(\frac{\partial w}{\partial z}\right)\right) \quad (4.7)$$

Where, v_{eff} denotes the effective kinematic viscosity, ρ is the fluid density, ρ_o is the reference fluid density and P represents the fluid pressure. Also, the velocity components in x, y and z directions are represented by u, v and w.

Concentration Equation:

$$\frac{\partial C}{\partial t} + u\frac{\partial C}{\partial x} + v\frac{\partial C}{\partial y} + w\frac{\partial C}{\partial z} = D\left(\frac{\partial^2 C}{\partial x^2} + \frac{\partial^2 C}{\partial y^2} + \frac{\partial^2 C}{\partial z^2}\right) \quad (4.8)$$

Where, D is the diffusion coefficient and C denotes the concentration which is basically salinity.

For inlet, boundary conditions for velocity in x, y and z directions are defined as $u=U_0*\text{Cos}(\theta)$, $v=U_{0*}\sin(\theta)$ and w= 0. While concentration $C=C_0$ and Temperature $T = T_0$ (Gildeh et al., 2015). The temperature selected to calculate the density for this study is 22 degree Celsius as 'close lid' assumption is made for this study. Also, for the model no stratification and no waves at the surface are assumed.

Simulations were performed on LINUX server and sample results are provided in Figures 4.2 and 4.3

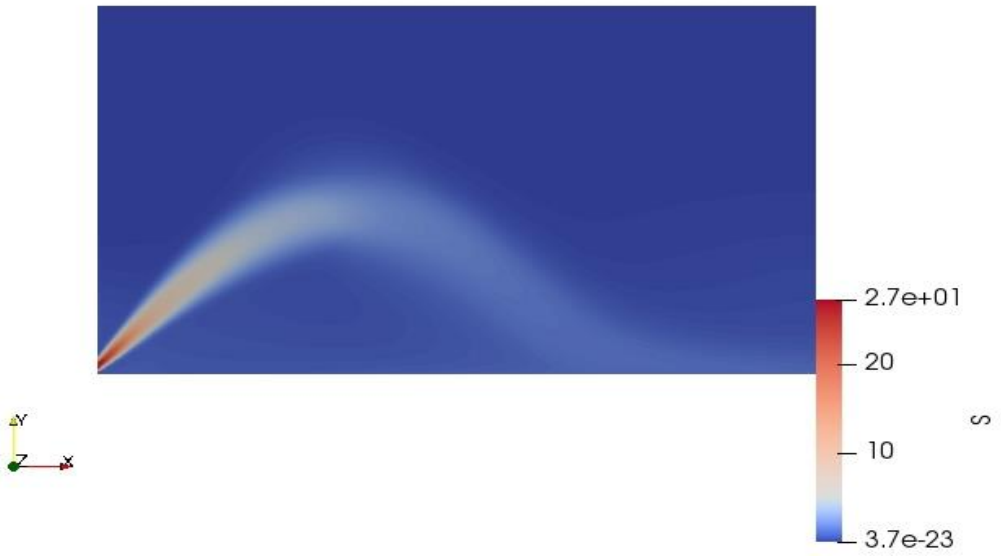

Figure 4.2: Negatively buoyant jet at 45 degrees discharge angle and Froude number 40

Figure 4.3: Negatively buoyant jet for 60 degrees discharge angle Froude number 50

4.3 ANFIS-Type and Multivariate Regression Models

The data generated from the above numerical modelling using realizable k- ε model in the OpenFOAM platform is used in this part, to train and test the ANFIS and hybrid models. For the soft computing method, two input variables, Froude number ranging from 5 to 60 and jet angle ranging from 20 degrees to 72.5, were employed. The data was collected till 72.5 degrees as this is the commonly used range in practice. The aim is to investigate input and output combinations (Table 4.1) to evaluate the performance of ANFIS, ANFIS-GA, ANFIS-PSO, ANFIS-FFA and Multivariate regression model.

The AI modelling was divided into three stages: i) Pre-Processing stage in which data from CFD models were gathered, raw data were converted into usable data ii) Modelling Stage where modelling tools such as ANFIS, ANFIS-GA, ANFIS-PSO and ANFIS-FFA were used to extract the outputs iii)Post-Processing stage where evaluation of the models are done using statistical indices and scatter plots.

In the present study, programming language MATLAB is used to design ANFIS (Jang, 1993; Ebtehaj and Bonakdari, 2014; Bonakdari et al., 2015) and the three hybrid models, ANFIS-GA (Holland 1975; https://yarpiz.com/), ANFIS-PSO (Kennedy and Eberhart, 1995; https://yarpiz.com/) and ANFIS-FFA (Yang 2010; Yaseen et al., 2017; Azimi et al., 2018). These models are built on the fundamental of training and testing which can be seen in Figure 4.4.

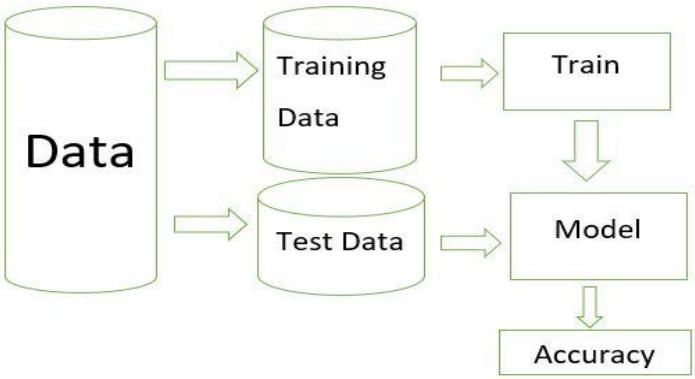

Figure 4.4: Training data and Test data

4.3.1 Adaptive Neuro Fuzzy Inference System (ANFIS)

Adaptive Neuro Fuzzy Inference System (Jang,1993) is an artificial intelligence method, applied to solve nonlinear problems. ANFIS is a combination of ANN and FIS, which works effectively to solve the complex issues. The architecture for ANFIS containing two inputs, one output f and five layers is illustrated in Figure 4.5. In the architecture, Sugeno model with Fuzzy IF-THEN rules are employed. The rules R1 and R2 are shown below:

R1:

If $x_1 = U_1$ and $x_2 = V_1$ (4.9)

Then $f_1 = s_1x_1 + t_1x_2 + r_1$ (4.10)

R2:

If $x_1 = U_2$ and $x_2 = V_2$ (4.11)

Then $f_2 = s_2x_1 + t_2x_2 + r_2$ (4.12)

U_1, U_2 are the membership functions for input x_1 and V_1, V_2 are the membership functions for input x_2, while s_1, s_2, t_1, t_2, r_1 and r_2 are the adjustable parameters determined during training process.

The first layer is the input layer in which input variables are transferred to the next layer and it is formed by the membership functions of the input variables.

$$O_{1,i} = \mu_{Ui}(x_1), \quad i = 1,2 \tag{4.13}$$

$$O_{1,i} = \mu_{Vi}(x_2), \quad i = 1,2 \tag{4.14}$$

The degree of membership functions represented by μ_{Ui} and μ_{Vi-2} for the fuzzy sets U_i and V_i respectively.

In layer two, each node is fixed and non-adaptive, when each node input values are multiplied to each other, weights (w_i) are obtained.

$$O_{2i} = w_i = \mu_{Ui}(x_1) * \mu_{Vi}(x_2), \quad i = 1,2 \tag{4.15}$$

The third layer which is a non-adaptive in nature called as the rule layer. In this layer, the weight function is normalized as follows:

$$O_{3i} = w_i^* = \frac{w_i}{\sum_i w_i} \tag{4.16}$$

The fourth layer which is the layer where defuzzification takes place and output of the previous layer is combined with the Sugeno fuzzy rule's function. However, nodes in this layer are adaptive in nature and contains a node function:

$$O_{4i} = w_i^* f_i = w_i^*(s_i x_1 + t_i x_2 + r_i) \tag{4.17}$$

At layer five, which is the last layer called output layer, the single node will calculate the overall output and it will be the summation of all the inputs from previous layers.

$$O_{5i} = \sum_i w_i^* f_i = \frac{\sum_i w_i f_i}{\sum_i w_i} \tag{4.18}$$

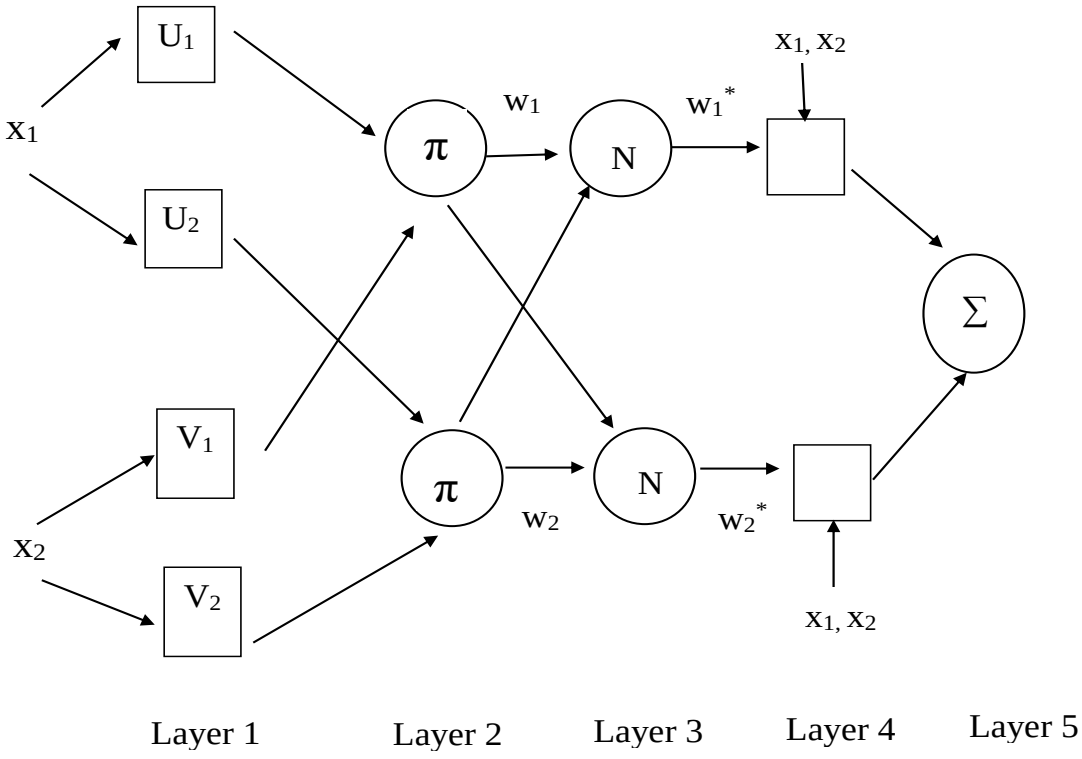

Figure 4.5: ANFIS structure

4.3.2 Genetic Algorithm (GA)

Genetic Algorithm (Holland 1975) is the heuristic search algorithm which comes under the class of evolutionary algorithm (EA) and based on the concept of natural selection and genetics where the idea of inheritance, selection, cross-over, and

mutation are applied. It is commonly used in various domains such as manufacturing, engineering, science, etc. (Yaghoobi et al., 2016). Genetic algorithm (GA) starts the process of optimization with a random initial population (Figure 4.6). In GA, population is a set of individuals which are present in the work space. Each individual has a set of parameters (variables) which are called genes, they are joined together to form chromosome (solution) which could be mutated and altered. These solutions could either be presented in the form of binary coding i.e. 0s and 1s or in other encoding forms. The criteria for determining the goodness of individual is by evaluating through fitness function as the population is initialized through randomly generated individuals, hence, it is an iterative process (Yaghoobi et al.,2016). The best suitable individual with higher fitness value will be chosen from the population to create the new generation and the solutions of this new generation will be used for next iteration in the same algorithm. The algorithm will be terminated, when the produced generations reach to maximum limit or a satisfactory fitness level is achieved (Yaghoobi et al.,2016). In this paper, GA code has been run in MATLAB software and ANFIS model has been trained to find the peak salinity S_m, peak coordinates x_m and y_m, return salinity S_r and return coordinate in x direction x_r.

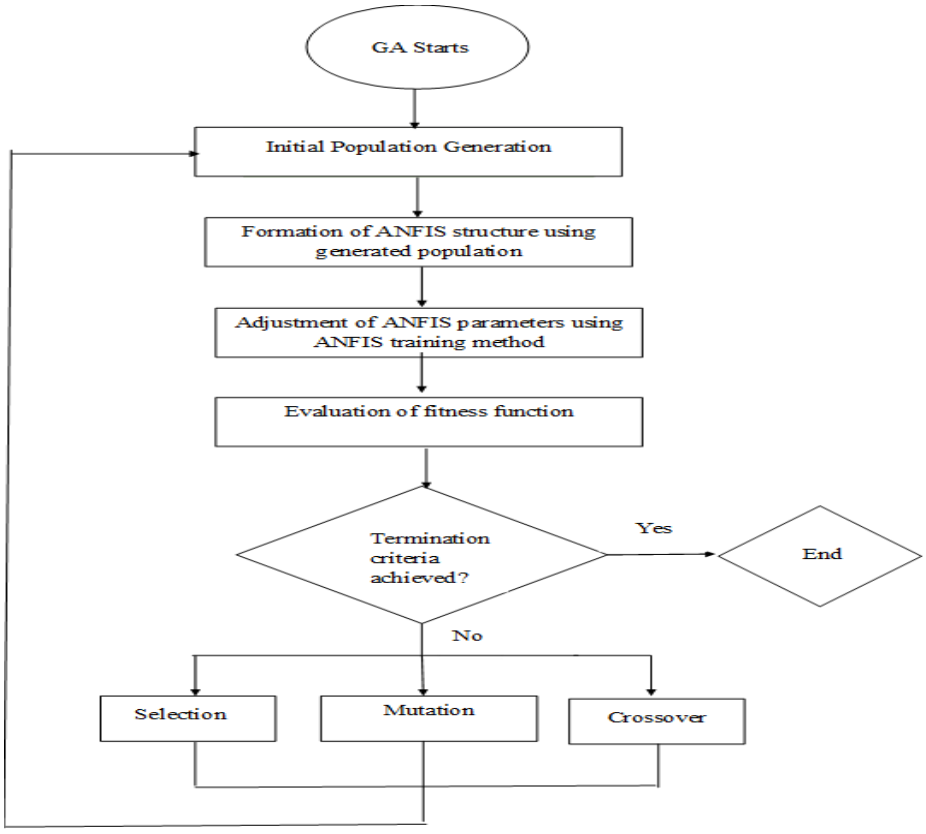

Figure 4.6: GA algorithm

4.3.3 Particle Swarm Optimization (PSO)

Particle swarm optimization (Kennedy and Eberhart,1995) algorithm is a population-based optimization method. PSO, begins with random particles in the search space which looks for optimal solution and each particle is associated with fitness value which is evaluated by fitness function (Figure 4.7). Each particle is affected by its best achieved individual position and the best position achieved among the group and for every iteration, the updating of each particle takes place by these two best values. In every iteration particle chooses new velocities which is based on their current velocity and the two mentioned best values. New velocity and new position can be evaluated by the following equations (Bonakdari and Zaji, 2018):

$$v^i[t+1] = wv^i[t] + c_1 r_1 \left(x^{Pbest}[t] - x^i[t]\right) + c_2 r_2 (x^{Gbest}[t] - x^i[t]) \quad (4.19)$$

$$x^i[t+1] = x^i[t] + v^i[t+1] \quad (4.20)$$

Where, x^i and v^i are the position and velocity vector for particle i and x^{Pbest} and x^{Gbest} are the best individual position and best position achieved in the group respectively. c_1 and c_2 are the learning coefficients and r_1 and r_2 are the random coefficients. Also, w represents the inertia weight.

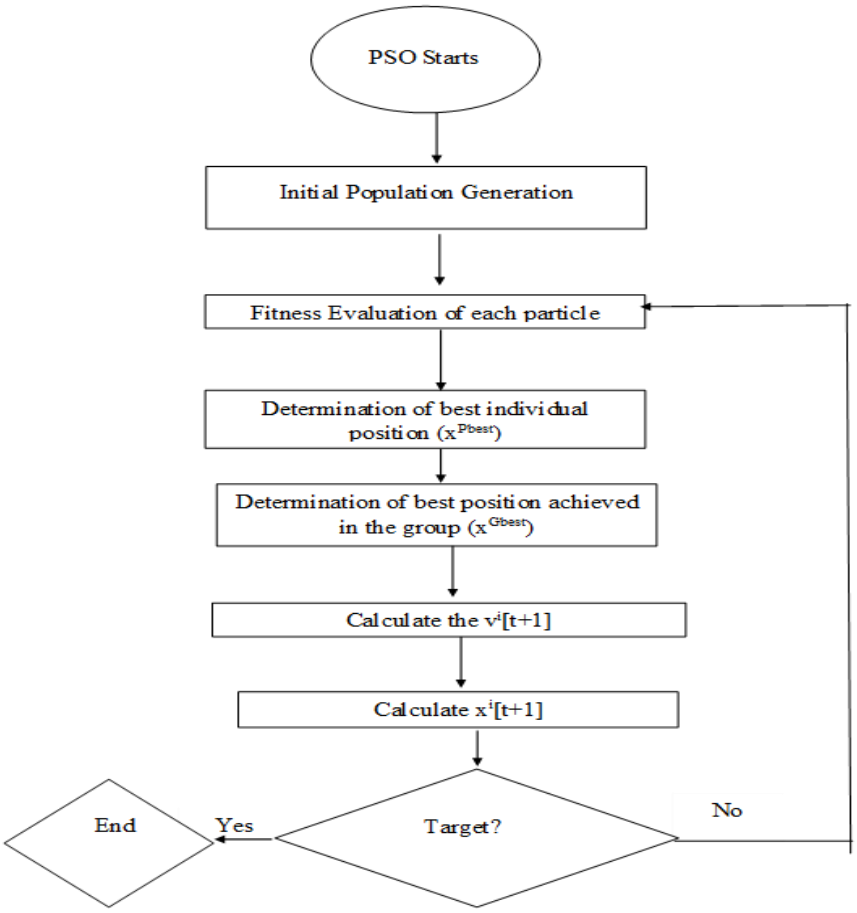

Figure 4.7: PSO Algorithm

4.3.4 Firefly Algorithm (FFA)

Firefly algorithm (FFA) is built on the idea of relationship between light and fireflies (Yang, 2010). The FFA follows three basic rules (Yang, 2010): i) All fireflies are unisexual; hence they have the ability to absorb other fireflies; ii) The intensity of attraction of firefly is directly proportional to the luminosity. As the distance increases, brightness may decrease, and brighter firefly can also move randomly to absorb less bright firefly; and iii) Brightness or Luminosity of the firefly related to the objective function provided in the algorithm. Based on these rules, the attractiveness value is directly proportional to the luminosity, hence, it can be calculated by following equation (Yang, 2010; Yaseen et al., 2018):

$$I = I_o e^{-\gamma r^2} \tag{4.21}$$

$$w(r) = w_0 e^{-\gamma r^2} \tag{4.22}$$

Where, w(r) denotes the attractiveness at distance r from the firefly, I_o is the light intensity at distance r=0, I represents the light intensity, γ denotes the coefficient of light absorption and w_0 is the attractiveness when distance r=0 (Yang, 2010; Yaseen et al., 2018).

The distance between the fireflies i and j is represented by r, can be calculated from the following equation (Yang, 2010; Yaseen et al. 2018):

$$r_{ij} = \|x_i + x_j\| = \sqrt{\sum_{k=1}^{d}(x_{i,k} - x_{j,k})} \quad (4.23)$$

Where, x_i and x_j are fireflies' locations. As firefly is attracted to one another, the movement for firefly from one position to another is represented by the following equation (Yang, 2010; Yaseen et al. 2018):

$$\Delta_{xi} = \beta_0 e^{-\gamma r^2}(x_j - x_i) + \alpha\varepsilon_i \quad (4.24)$$

Where, α denotes the randomization coefficient and ε_i represents the random number vector. Also, α varies from 0 and 1. $\beta_0 e^{-\gamma r^2}$ is attraction term (Yaseen et al. 2018)

The Firefly algorithm is shown in Figure 4.8

In this paper, ANFIS model was integrated with FFA in order to determine the peak salinity S_m, peak coordinates x_m and y_m, return salinity S_r and return coordinate x_r. By trial and error method, the values of light absorption coefficient (γ) is taken as 0.1, attraction coefficient base (β_0) is taken as 4 and movement coefficient (α) is taken as 0.3.

4.3.5 Multivariate Linear Regression Model (MLR)

Multivariate regression analysis is widely used to find a linear relationship between the dependent and multiple independent variables. The data collected from numerical modeling are non-linear data but to determine the closeness of data with the linearity, multivariate regression analysis has been done by using Microsoft excel add-ins which helped in creating a model based on least square methods (Emadi and Mahfoud, 2011). The generalized equation for MLR can be expressed in the following way (Tosun et al.,2016 and Fumo and Biswas, 2015):

$$Y = \beta_o + \beta_1 X_1 + \beta_2 X_2 + \cdots + \beta_n X_n \quad (4.25)$$

Where, X_1, X_2, X_n are the independent variables which are also called predictor variables. Y is the dependent variable also known as response variable and n is the number of variables (Fumo and Biswas, 2015).

For multivariate regression, data collected from numerical modeling were divided into training and test data. The equation obtained for training data set after regression analysis has been used to generate the predicted test output. The statistical parameters to evaluate the multivariate regression model are same as the ones used for ANFIS and hybrid models. The equations mentioned in statistical parameters section are used for the calculation of the values for regression analysis.

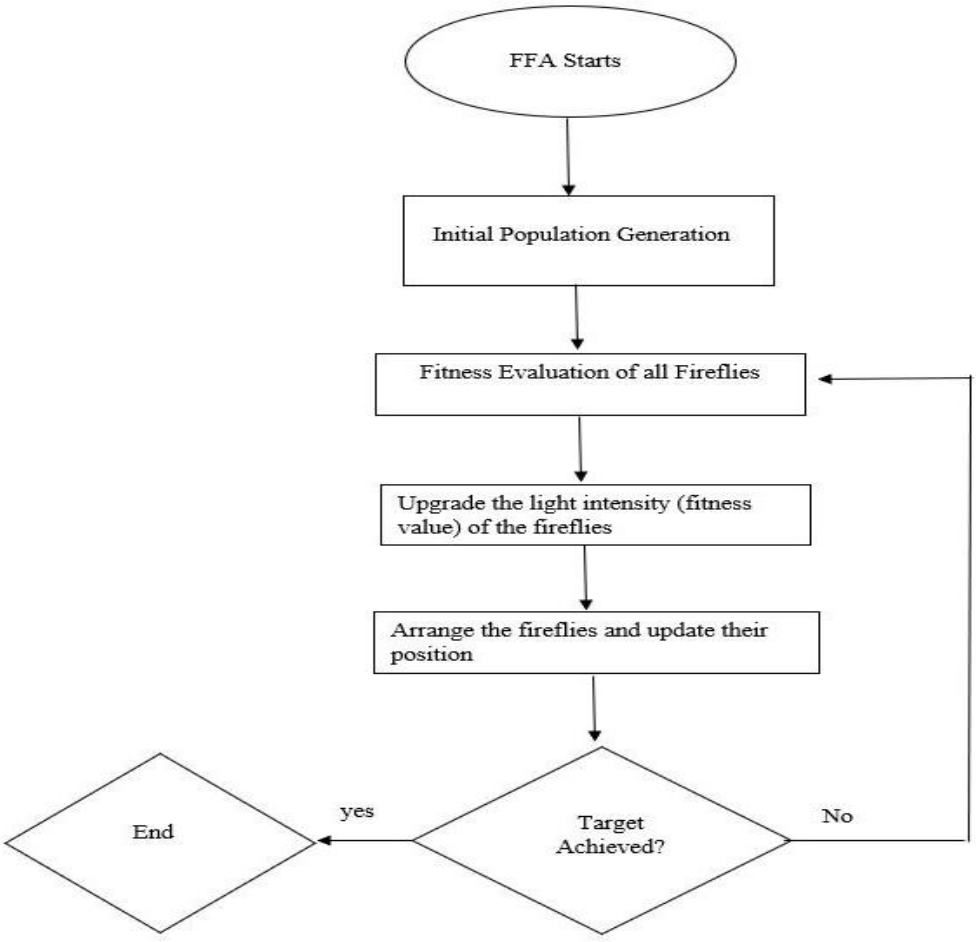

Figure 4.8: FFA Algorithm

4.3.6 Statistical Analysis

To determine the accuracy of ANFIS, ANFIS-GA, ANFIS-PSO, ANFIS-FFA and multivariate regression models discussed above, statistical parameters of all the models are compared, the statistical parameters taken into consideration are coefficient of determination (R^2), root mean squared error (RMSE), mean absolute error (MAE), and average absolute deviation (δ %) i.e. error of the model in percentage (Bonakdari and Zaji, 2018). The mentioned parameters can be measured by the following equations:

$$RMSE = \sqrt{\frac{\sum_{i=1}^{N}(O_i - P_i)^2}{N}} \tag{4.26}$$

$$R^2 = 1 - \frac{\sum_{i=1}^{N}(O_i - P_i)^2}{\sum_{i=1}^{N}(O_i - O_m)^2} \tag{4.27}$$

$$MAE = \frac{1}{N}\sum_{i=1}^{N} |O_i - P_i| \tag{4.28}$$

$$\delta\% = \frac{\sum_{i=1}^{N} |O_i - P_i|}{\sum_{i=1}^{N} O_i} * 100 \tag{4.29}$$

Where, P_i is the predicted value obtained after training the models, O_i is the observed value obtained after numerical modeling on OpenFOAM, O_m is the mean of observed value and N is the number of samples.

4.4 Results

Overall, 1760 data points are obtained from numerical modelling for S_m, S_r, x_m, x_r and y_m outputs and 352 data points belong to each combination set of input and output. The data are divided into two sections, training data and test data where training data contain 272 of the total data and test data contain 80 of the total data test data. For the

models two input variables i.e. Froude number and angle are chosen to obtain one output. The targeted outputs are S, S_r, x_m, y_m, x_r. Hence, 5 sets with different outputs are prepared for all the models as shown in Table 4.1.

Table 4.1: Input-Output combinations

Combinations	Inputs		Output
1	Froude number	Angle	S_m
2	Froude number	Angle	S_r
3	Froude number	Angle	x_m
4	Froude number	Angle	x_r
5	Froude number	Angle	y_m

4.4.1 Performance evaluation for S_m

ANFIS-Type Models

It can be observed from Table 4.2 that all the models' RMSE values for training and test data are almost same which means none of them are trapped in over-fitting. Also, in Figure 4.9(a-h), targets and outputs are reasonably coinciding with each other, that concludes accuracy of the data for ANFIS and hybrid models. From Table 4.2, it can be observed that, out of all the models ANFIS-PSO is giving the highest R^2, and the lowest RMSE, MAE and δ % which are 0.984, 0.589, 0.357 and 5.889%for the test data that make it more accurate out of all.

Multi-variate Regression Model

The equation obtained after training the regression model for salinity (S_m) is shown below:

$$S_m = 13.4212 - (0.23703 * Fr) - (0.01983 * Angle) \quad (4.30)$$

The above equation was used to predict the test outputs and it can be seen from Table 4.2 that the in regression model there is no over-fitted data as the training and test data sets are showing almost similar statistical parameters but overall, regression model had the lowest R^2 value and highest RMSE, MAE and δ % i.e. in both training and test sets

as compared to other models which made regression model incompatible for predicting peak salinity.

Table 4.2: Models' performance evaluation for S_m

Model	Output	Training Database				Test Database			
	S_m	R^2	RMSE	MAE	δ %	R^2	RMSE	MAE	δ %
ANFIS		0.950	0.959	0.726	12.160	0.964	0.890	0.709	11.680
ANFIS-GA		0.947	1.019	0.834	13.974	0.935	1.187	0.866	14.249
ANFIS-PSO		0.985	0.547	0.336	5.631	0.984	0.589	0.357	5.889
ANFIS-FFA		0.979	0.643	0.409	6.866	0.975	0.739	0.447	7.367
Multi-variate Regression		0.594	2.909	2.118	35.482	0.582	3.009	2.245	36.948

ANFIS:

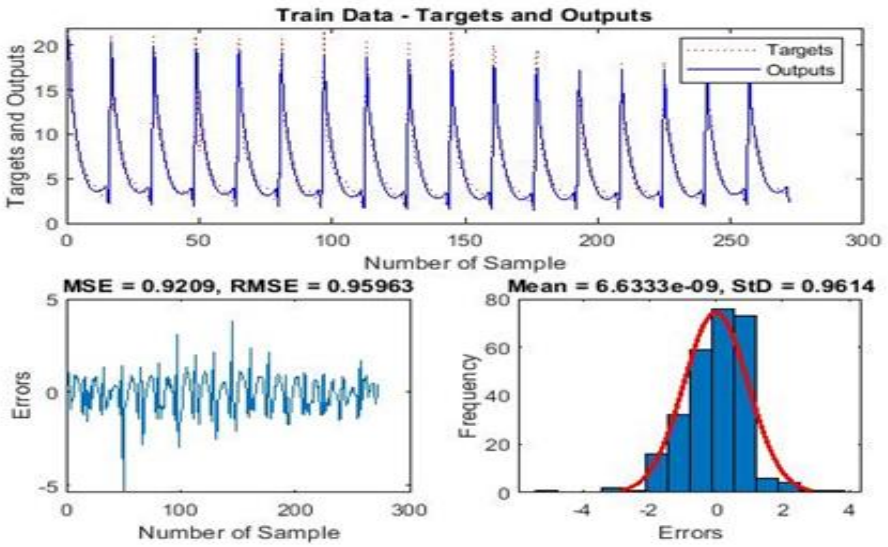

a)

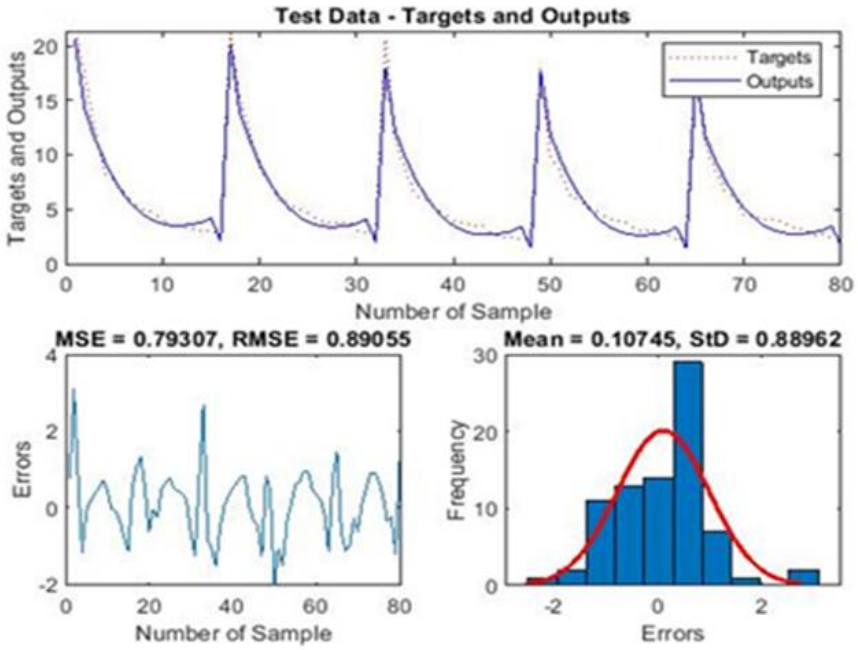
Test Data - Targets and Outputs
Targets
Outputs
Targets and Outputs
Number of Sample
MSE = 0.79307, RMSE = 0.89055
Errors
Number of Sample
Mean = 0.10745, StD = 0.88962
Frequency
Errors

b)

ANFIS-GA

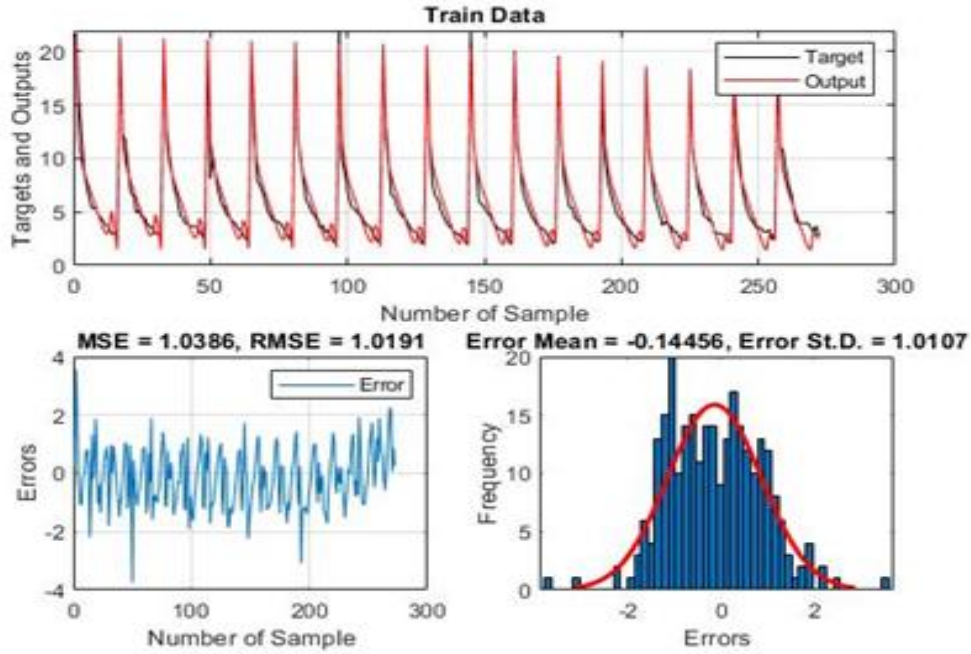
Train Data
Target
Output
Targets and Outputs
Number of Sample
MSE = 1.0386, RMSE = 1.0191
Error
Errors
Number of Sample
Error Mean = -0.14456, Error St.D. = 1.0107
Frequency
Errors

c)

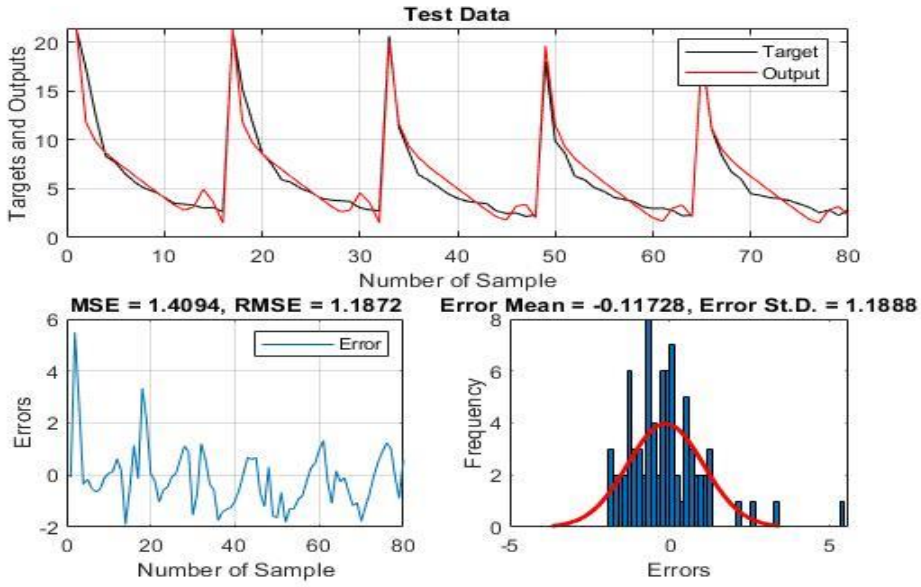
Test Data
Target
Output
Targets and Outputs
Number of Sample
MSE = 1.4094, RMSE = 1.1872
Error Mean = -0.11728, Error St.D. = 1.1888
Error
Errors
Number of Sample
Frequency
Errors

d)

ANFIS-PSO

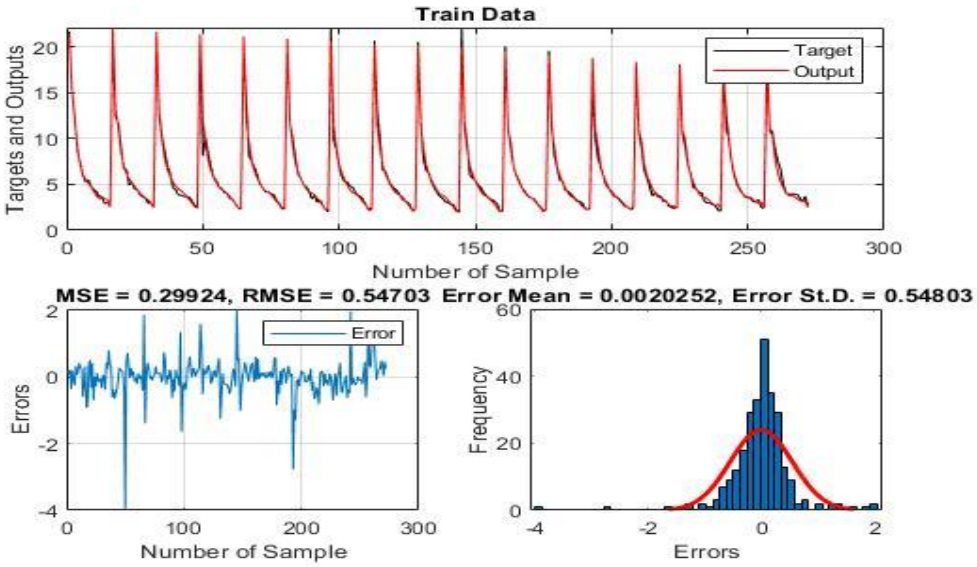
Train Data
Target
Output
Targets and Outputs
Number of Sample
MSE = 0.29924, RMSE = 0.54703
Error Mean = 0.0020252, Error St.D. = 0.54803
Error
Errors
Number of Sample
Frequency
Errors

e)

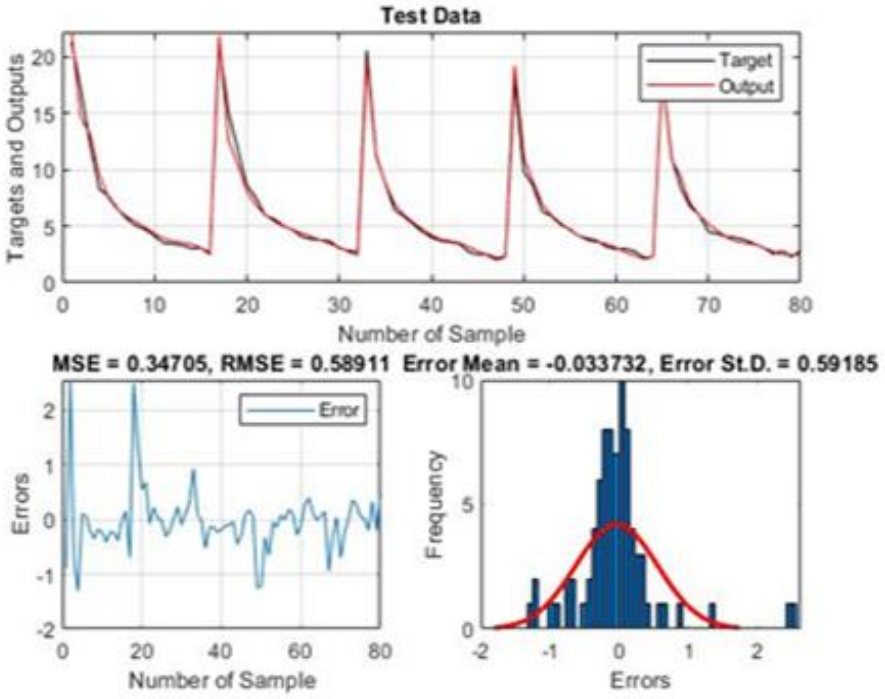
Test Data
Target
Output
Targets and Outputs
Number of Sample
MSE = 0.34705, RMSE = 0.58911 Error Mean = -0.033732, Error St.D. = 0.59185
Error
Errors
Number of Sample
Frequency
Errors

f)

ANFIS-FFA:

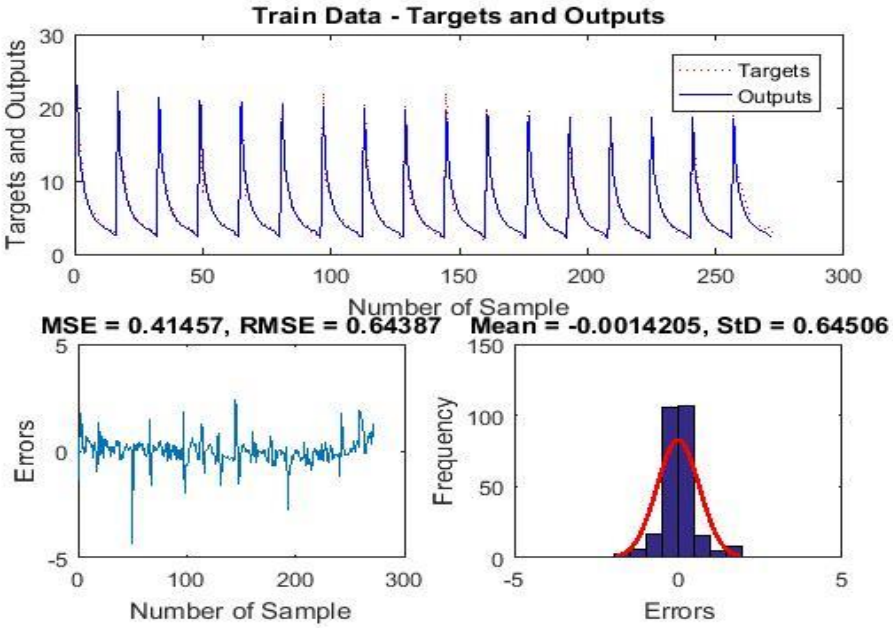
Train Data - Targets and Outputs
Targets
Outputs
Targets and Outputs
Number of Sample
MSE = 0.41457, RMSE = 0.64387 Mean = -0.0014205, StD = 0.64506
Errors
Number of Sample
Frequency
Errors

g)

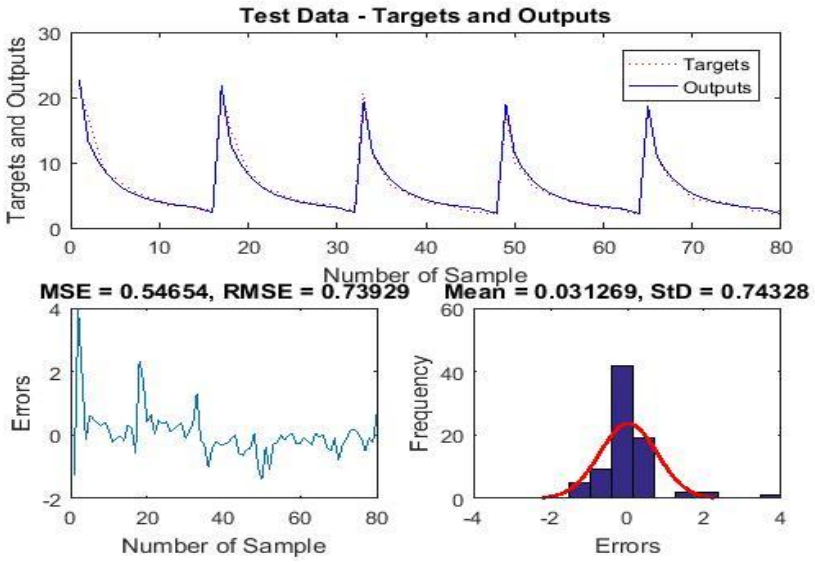

h)

Figure 4.9: ANFIS Model a) targets and outputs, RMSE, MSE values and frequency vs. errors graphs for train data set b) targets and outputs, RMSE, MSE values and frequency vs. errors graphs for test data set. ANFIS-GA: c) targets and outputs, RMSE, MSE values and frequency vs. errors graphs for train data set d) targets and outputs, RMSE, MSE values and frequency vs. errors graphs for test data set. ANFIS-PSO: e) targets and outputs, RMSE, MSE values and frequency vs. errors for train data set f) targets and outputs, RMSE, MSE values and frequency vs. errors for test data set. ANFIS-FFA: g) targets and outputs, RMSE, MSE values and frequency vs. errors for train data set h) targets and outputs, RMSE, MSE values and frequency vs. errors for test data set.

4.4.2 Performance evaluation for S_r

ANFIS-Type Models

Table 4.3, shows the statistical results for S_r and it can be observed that test data for ANFIS-GA, ANFIS-PSO and ANFIS-FFA are showing almost same R^2 value i.e. 0.976, 0.973 and 0.975 but lowest RMSE was observed in ANFIS-GA i.e. 0.471. Hence, ANFIS-GA model can be considered as suitable for predicting the return salinity value. Also, the δ % and MAE are also not high for this model. It is to be mentioned that the RMSE and R^2 values of the test sets are mainly considered in this thesis work for determining the suitable model.

The graphs in figure 4.10(a-h) shows that targets and outputs are following the same pattern which again shows that models are properly trained for output S_r.

Multi-variate Regression Model

The equation obtained after training the regression model for return salinity (S_r) is shown below:

$$S_r = 7.601744 - (0.12495 * Fr) - (0.02693 * Angle) \quad (4.31)$$

It can be observed from the Table 4.3, that the parameters for training and test data are almost same but the regression model's performance compared to other models is very poor as the it has the lowest R^2 value i.e. 0.441 and highest RMSE, MAE values i.e. 2.265 and 1.429 in the test set respectively which shows the model accuracy to predict the data is very low and its test outputs are not near to the outputs obtained from numerical model.

Table 4.3: Models' performance evaluation for output S_r

Model	Output	Training Database				Test Database			
		R^2	RMSE	MAE	δ %	R^2	RMSE	MAE	δ %
ANFIS	S_r	0.893	0.923	0.691	23.870	0.909	0.914	0.684	23.028
ANFIS-GA		0.967	0.510	0.376	12.981	0.976	0.471	0.350	11.803
ANFIS-PSO		0.958	0.579	0.404	13.946	0.973	0.503	0.395	13.304
ANFIS-FFA		0.958	0.573	0.369	12.755	0.975	0.481	0.336	11.331
Multi-variate Regression Model		0.455	2.147	1.394	48.104	0.441	2.265	1.429	48.077

ANFIS:

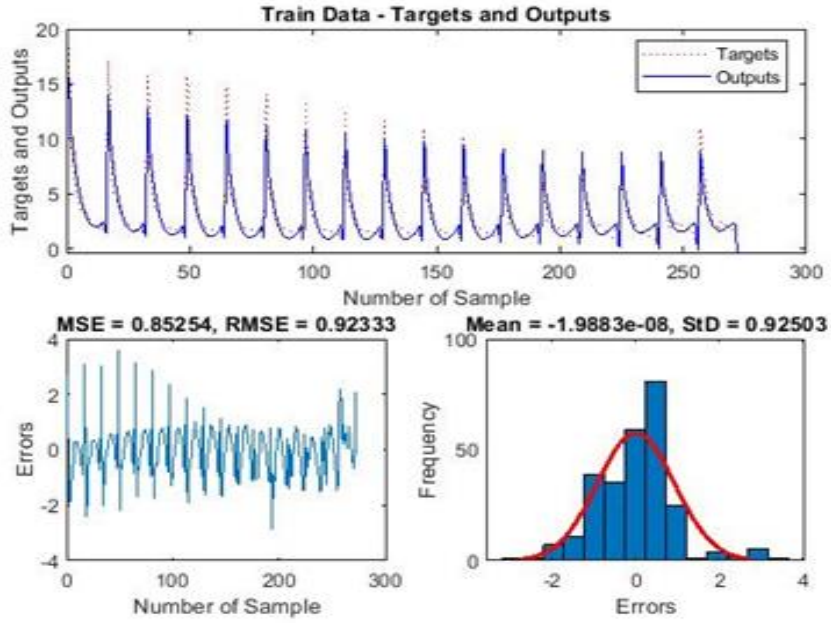
Train Data - Targets and Outputs
Targets
Outputs
Targets and Outputs
Number of Sample
MSE = 0.85254, RMSE = 0.92333
Errors
Number of Sample
Mean = -1.9883e-08, StD = 0.92503
Frequency
Errors

a)

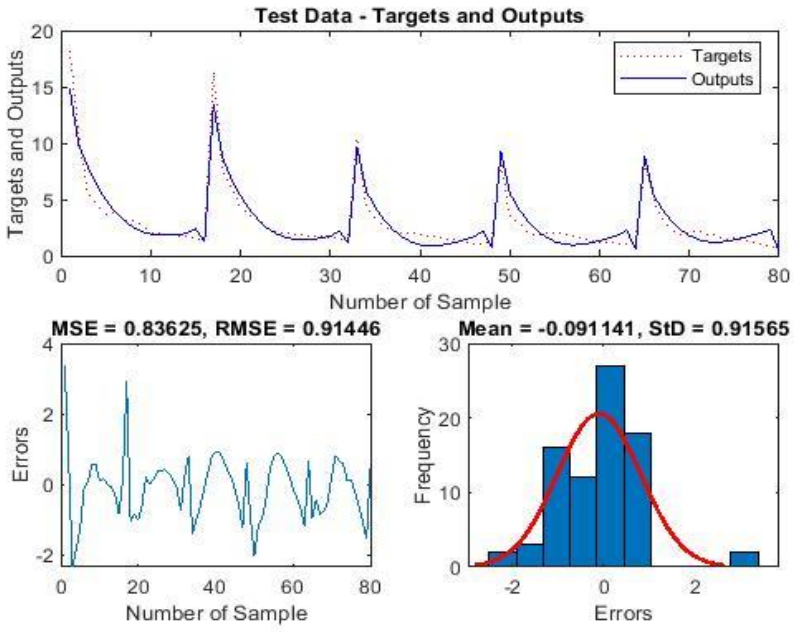
Test Data - Targets and Outputs
Targets
Outputs
Targets and Outputs
Number of Sample
MSE = 0.83625, RMSE = 0.91446
Errors
Number of Sample
Mean = -0.091141, StD = 0.91565
Frequency
Errors

b)

ANFIS-GA:

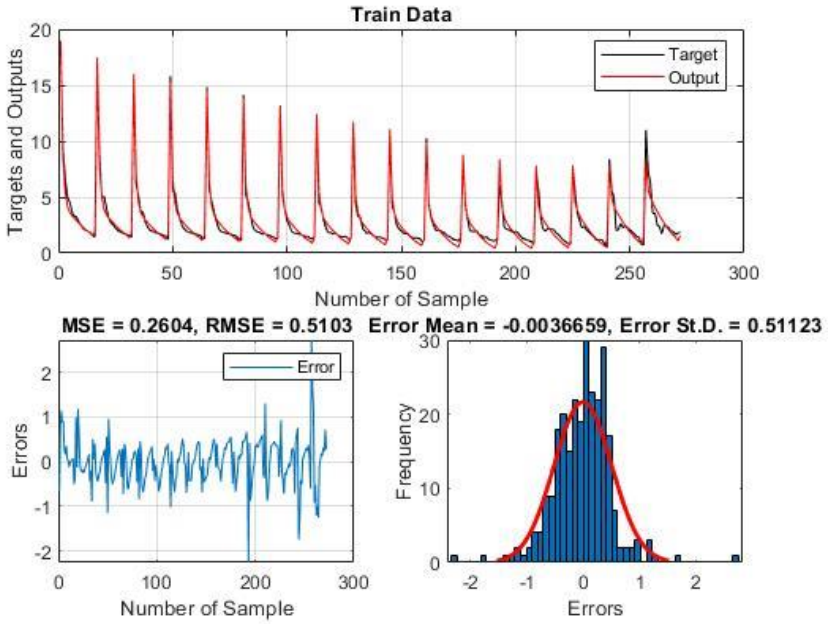
Train Data
Target
Output
Targets and Outputs
Number of Sample
MSE = 0.2604, RMSE = 0.5103 Error Mean = -0.0036659, Error St.D. = 0.51123
Error
Errors
Number of Sample
Frequency
Errors

c)

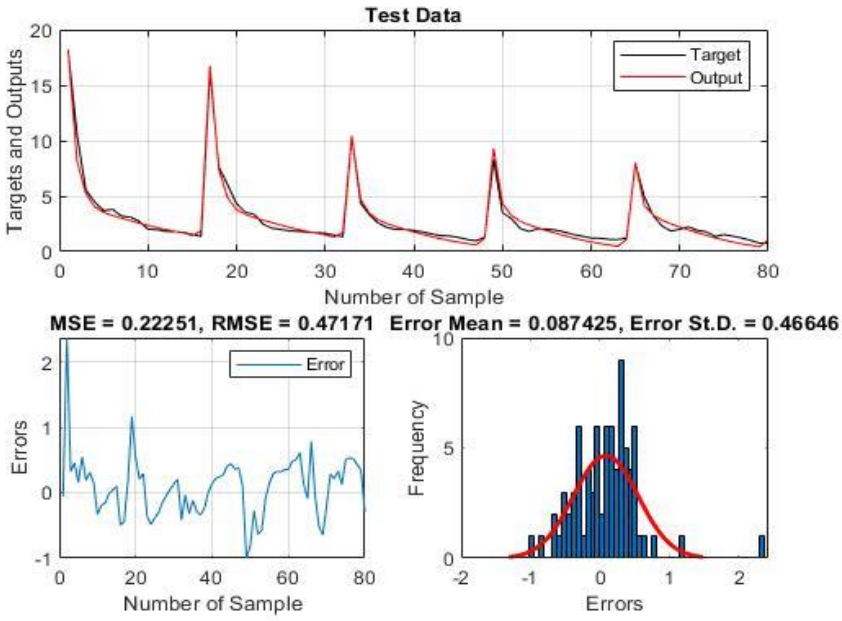
Test Data
Target
Output
Targets and Outputs
Number of Sample
MSE = 0.22251, RMSE = 0.47171 Error Mean = 0.087425, Error St.D. = 0.46646
Error
Errors
Number of Sample
Frequency
Errors

d)

ANFIS-PSO

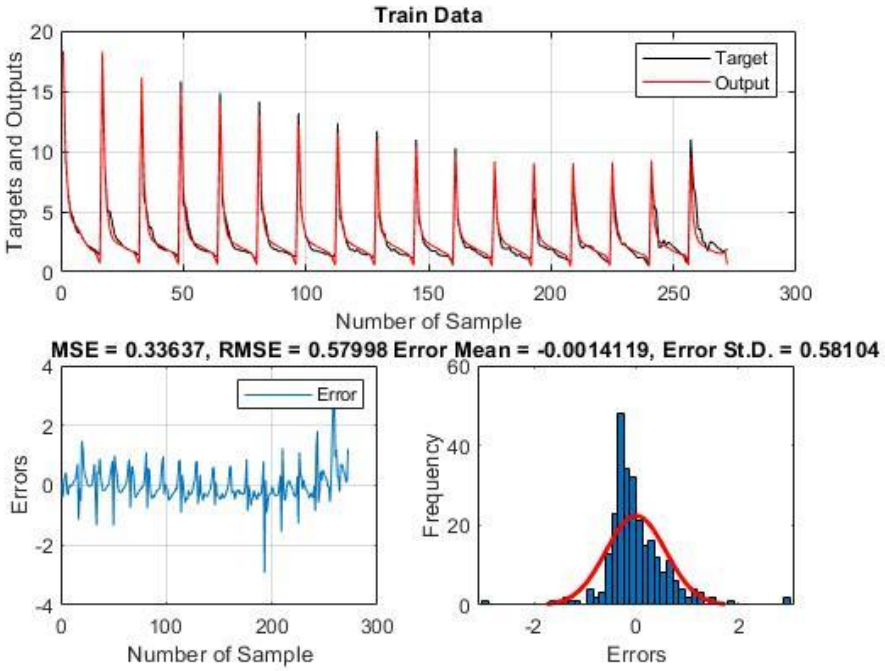
Train Data
Target
Output
Targets and Outputs
Number of Sample
MSE = 0.33637, RMSE = 0.57998 Error Mean = -0.0014119, Error St.D. = 0.58104
Error
Errors
Number of Sample
Frequency
Errors

e)

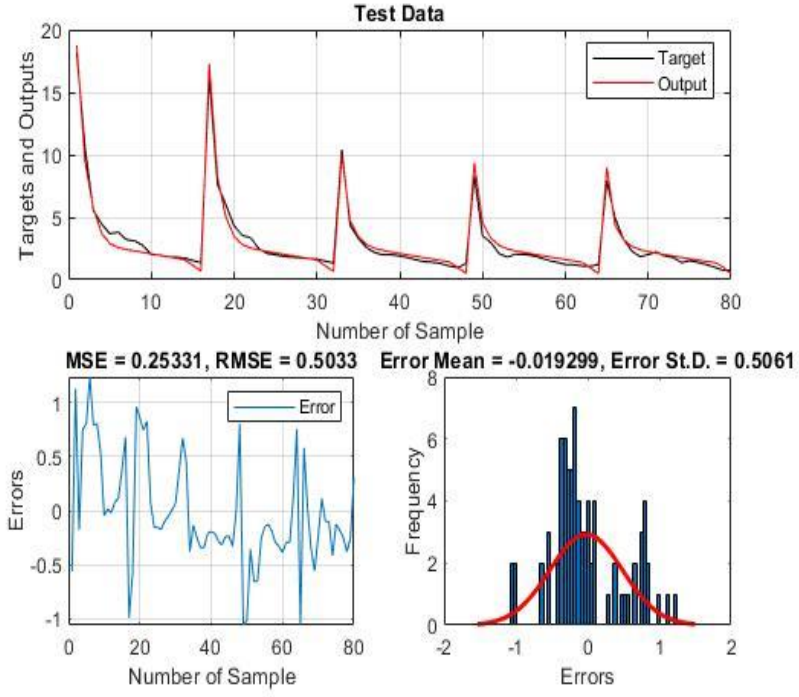
Test Data
Target
Output
Targets and Outputs
Number of Sample
MSE = 0.25331, RMSE = 0.5033 Error Mean = -0.019299, Error St.D. = 0.5061
Error
Errors
Number of Sample
Frequency
Errors

f)

ANFIS-FFA:

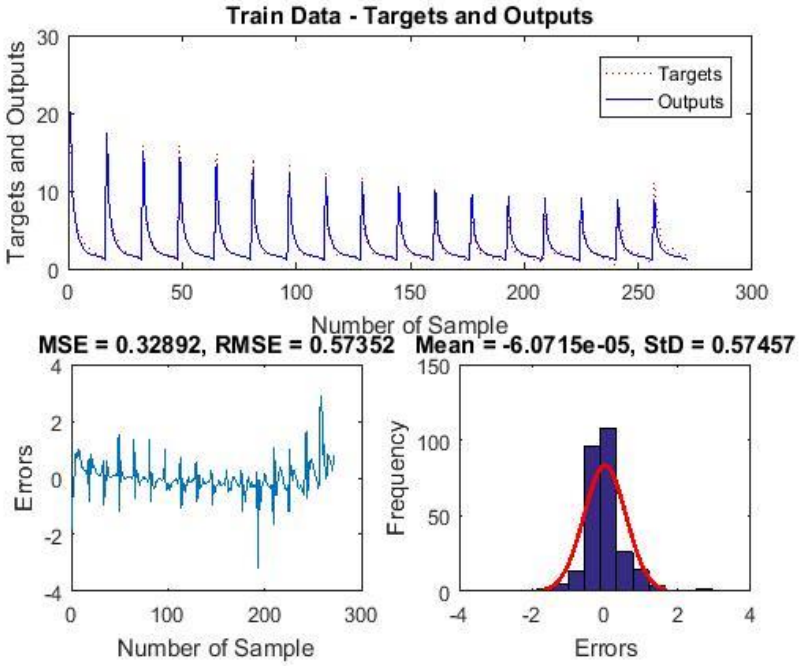

g)

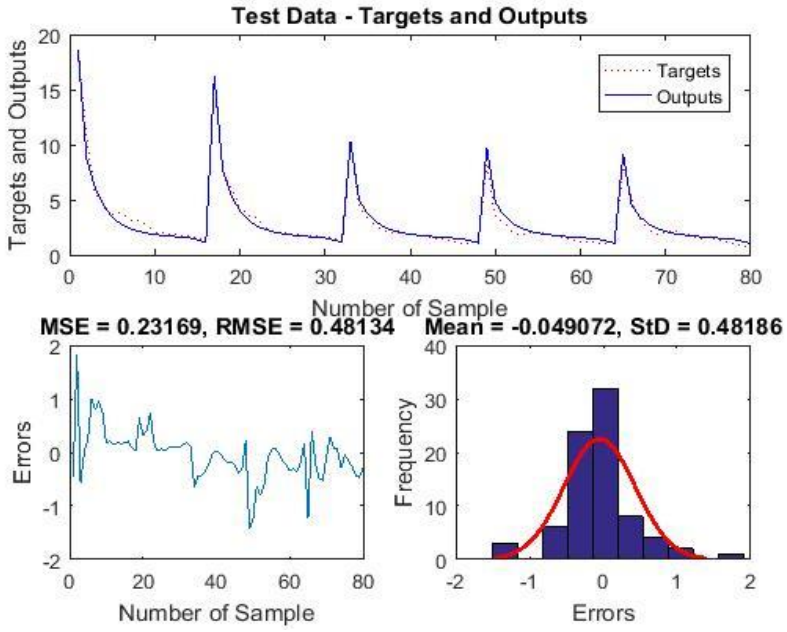

h)

Figure 4.10: ANFIS Model a) targets and outputs, RMSE, MSE values and frequency vs. errors graphs for train data set b) targets and outputs, RMSE, MSE values and frequency vs. errors graphs for test data set. ANFIS-GA: c) targets and outputs, RMSE,

MSE values and frequency vs. errors graphs for train data set d) targets and outputs, RMSE, MSE values and frequency vs. errors graphs for test data set. ANFIS-PSO: e) targets and outputs, RMSE, MSE values and frequency vs. errors for train data set f) targets and outputs, RMSE, MSE values and frequency vs. errors for test data set. ANFIS-FFA: g) targets and outputs, RMSE, MSE values and frequency vs. errors for train data set h) targets and outputs, RMSE, MSE values and frequency vs. errors for test data set.

4.4.3 Performance evaluation for x_m

ANFIS-type Models

From Table 4.4, it can be observed that the statistical parameters for output x_m, are showing good accuracy between training and test which shows none of the models are over-fitted. Though, the percentage deviation for ANFIS-FFA's test data is smaller out of all the models but statistical parameters of ANFIS-PSO's training data are better as compared to its test data which makes the model more reliable. Also, the test sets for ANFIS-GA and ANFIS-FFA have the highest R^2 i.e. 0.987,0.987 with RMSE values, 0.018 and 0.016 respectively. However, considering the RMSE and R^2 values of the test set, it can be seen that ANFIS-FFA is efficient in determining the output x_m as it has the highest R^2 and lowest RMSE, though it also has the lowest MAE and δ %.

Multi-variate Regression Model

To predict, the test output x_m, following equation was obtained from the regression analysis of the training set:

$$x_m = 0.261093 + (0.00818 * Fr) - (0.00515 * Angle) \quad (4.32)$$

Table 4.4, shows that although the performance of regression model was satisfactory but it had the lowest R^2 value and highest RMSE, MAE and δ %in the test set compared to the other models' test sets which show that the predicted outputs from MLR are not close to the observed numerical outputs. The statistical parameters for multivariate regression model are calculated by equations 4.26, 4.27, 4.28 and 4.29.

Table 4.4: Models' performance evaluation for output x_m

Model	Output	Training Database				Test Database			
		R^2	RMSE	MAE	δ %	R^2	RMSE	MAE	δ %
ANFIS	x_m	0.985	0.018	0.013	5.409	0.983	0.018	0.013	5.433
ANFIS-GA		0.981	0.020	0.015	6.251	0.987	0.018	0.014	5.736
ANFIS-PSO		0.989	0.015	0.011	4.637	0.976	0.021	0.016	6.250
ANFIS-FFA		0.987	0.017	0.012	5.011	0.987	0.016	0.011	4.650
Multi-Variate Regression		0.899	0.058	0.043	17.707	0.892	0.047	0.036	14.348

ANFIS:

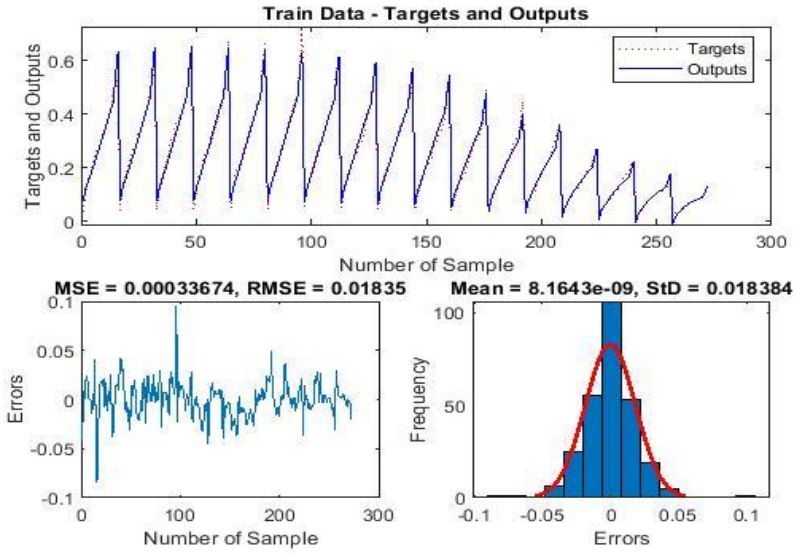

a)

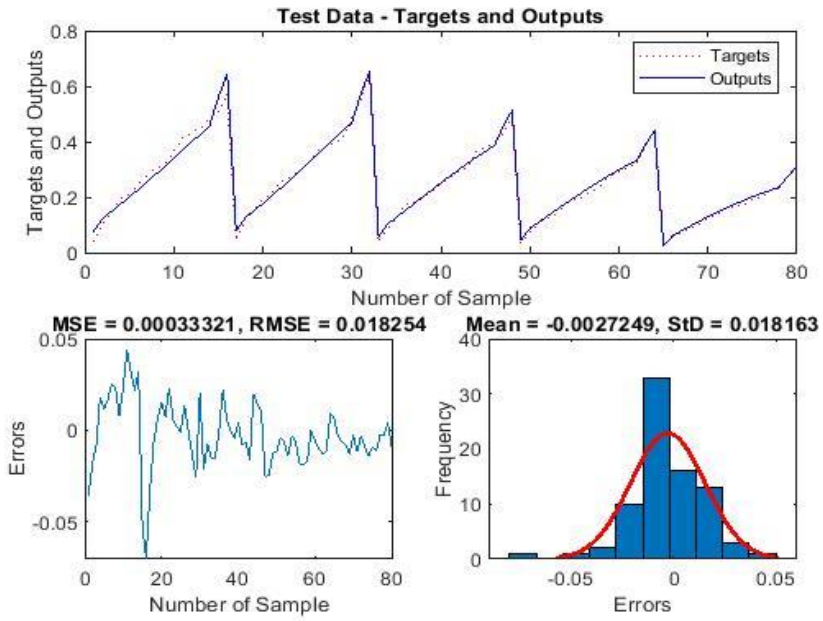
Test Data - Targets and Outputs
Targets
Outputs
Targets and Outputs
Number of Sample
MSE = 0.00033321, RMSE = 0.018254
Mean = -0.0027249, StD = 0.018163
Errors
Number of Sample
Frequency
Errors

b)

ANFIS-GA:

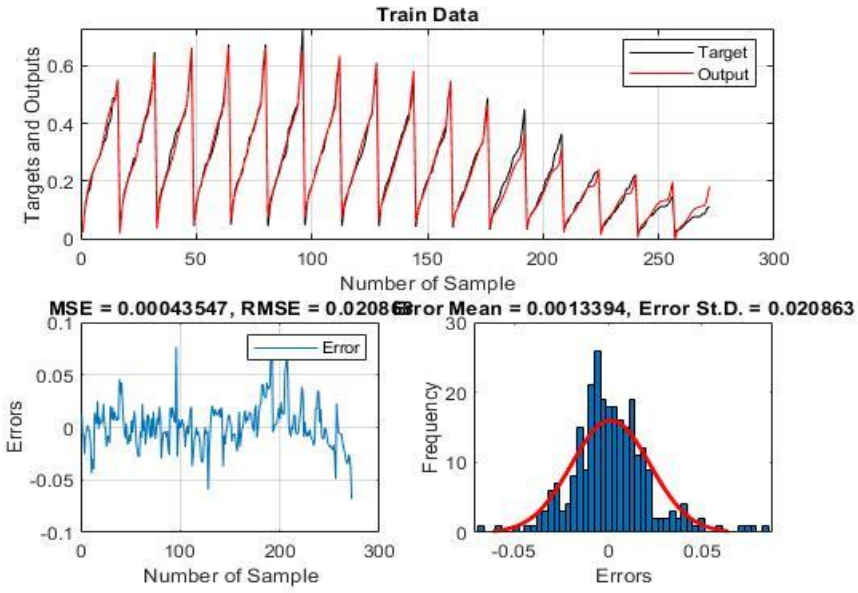
Train Data
Target
Output
Targets and Outputs
Number of Sample
MSE = 0.00043547, RMSE = 0.020863
Error Mean = 0.0013394, Error St.D. = 0.020863
Error
Errors
Number of Sample
Frequency
Errors

c)

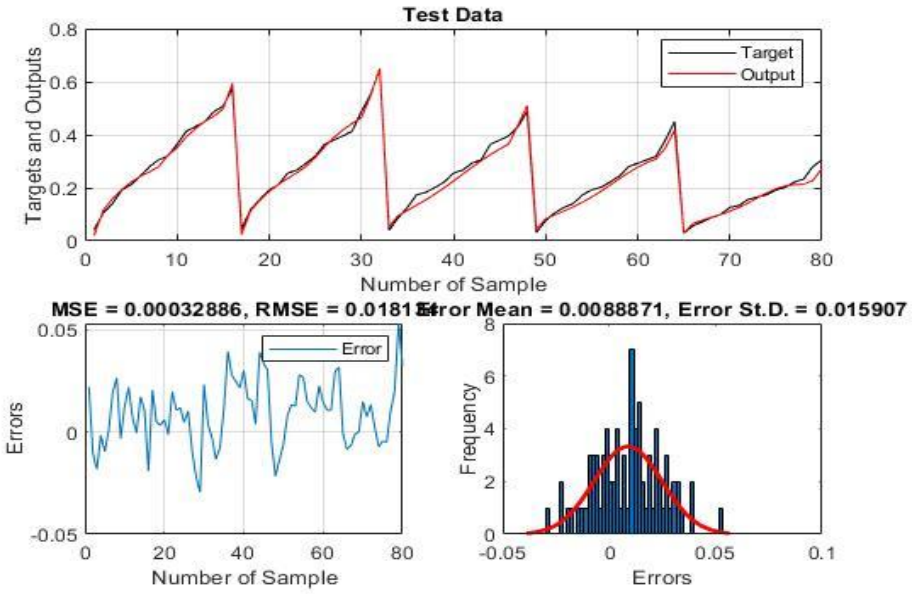
Test Data
Target
Output
Targets and Outputs
Number of Sample
MSE = 0.00032886, RMSE = 0.018134, Error Mean = 0.0088871, Error St.D. = 0.015907
Error
Errors
Number of Sample
Frequency
Errors

d)

ANFIS-PSO:

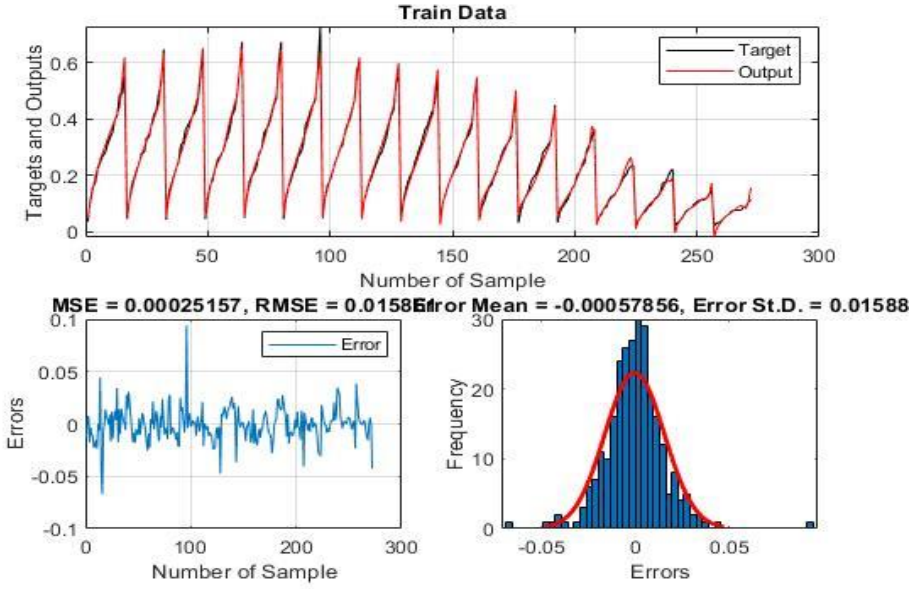
Train Data
Target
Output
Targets and Outputs
Number of Sample
MSE = 0.00025157, RMSE = 0.015861, Error Mean = -0.00057856, Error St.D. = 0.01588
Error
Errors
Number of Sample
Frequency
Errors

e)

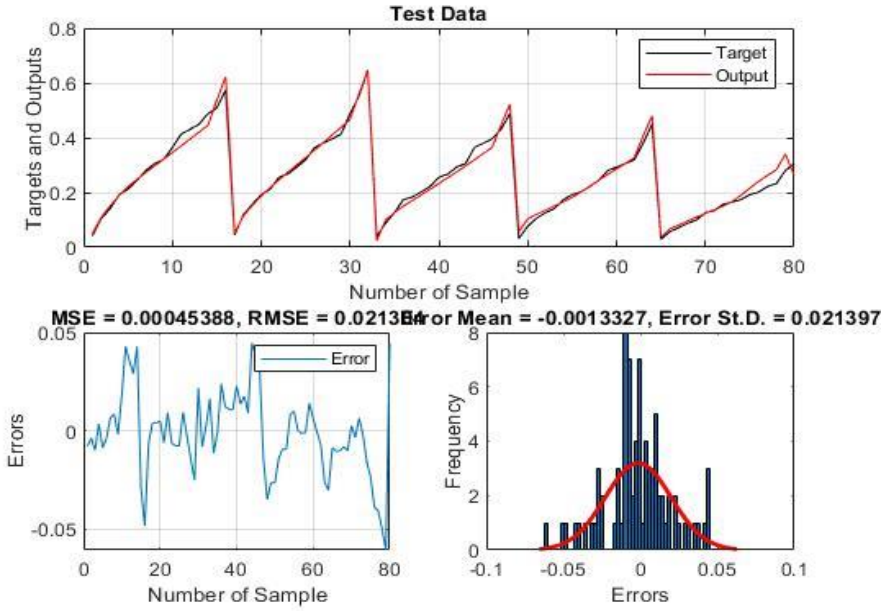
Test Data
Target
Output
Targets and Outputs
Number of Sample
MSE = 0.00045388, RMSE = 0.021304, Error Mean = -0.0013327, Error St.D. = 0.021397
Error
Errors
Number of Sample
Frequency
Errors

f)

ANFIS-FFA:

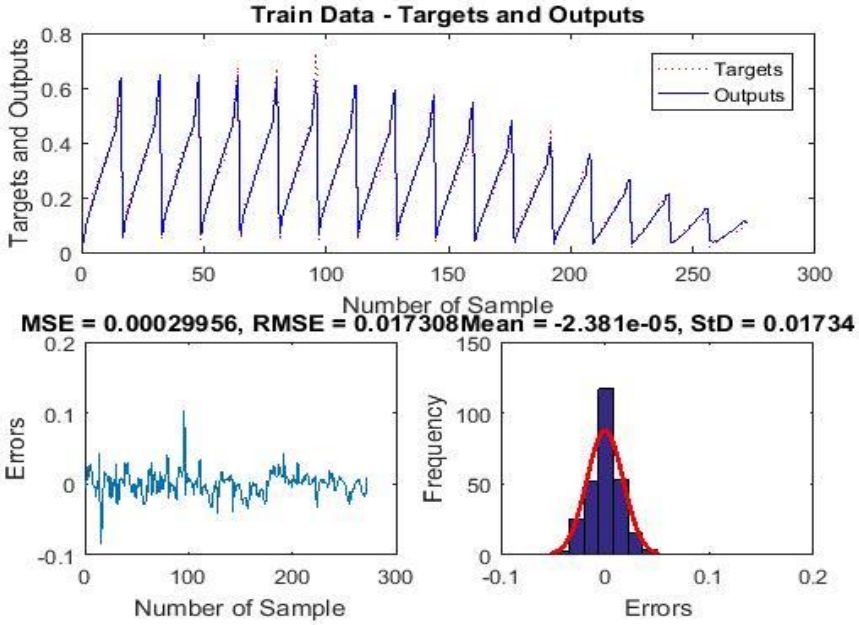
Train Data - Targets and Outputs
Targets
Outputs
Targets and Outputs
Number of Sample
MSE = 0.00029956, RMSE = 0.017308, Mean = -2.381e-05, StD = 0.01734
Errors
Number of Sample
Frequency
Errors

g)

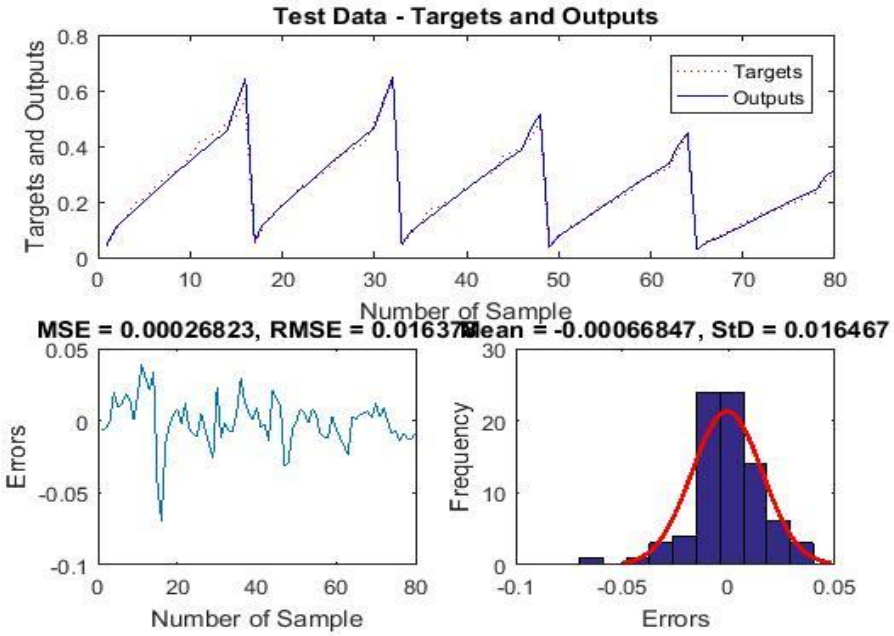

h)

Figure 4.11: ANFIS Model a) targets and outputs, RMSE, MSE values and frequency vs. errors graphs for train data set b) targets and outputs, RMSE, MSE values and frequency vs. errors graphs for test data set. ANFIS-GA: c) targets and outputs, RMSE, MSE values and frequency vs. errors graphs for train data set d) targets and outputs, RMSE, MSE values and frequency vs. errors graphs for test data set. ANFIS-PSO: e) targets and outputs, RMSE, MSE values and frequency vs. errors for train data set f) targets and outputs, RMSE, MSE values and frequency vs. errors for test data set. ANFIS-FFA: g) targets and outputs, RMSE, MSE values and frequency vs. errors for train data set h) targets and outputs, RMSE, MSE values and frequency vs. errors for test data set.

4.4.4 Performance evaluation for x_r

ANFIS-Type Models

For output x_r, Table 4.5 shows, all the models' test data have close performance with training data, in fact statistical parameters of training sets are slightly higher than test sets which again show that models are not over-fitted and they have good predictability. Out of all the models, ANFIS-PSO had given better results as its test set had higher R^2 value i.e. 0.985 and lower RMSE, MAE and δ %i.e. 0.032, 0.021 and 4.639% in the test data respectively.

Multi-variate Regression Model

For output x_r, multivariate regression model showed quite good results with R^2 as 0.904, and RMSE, MAE values as 0.079 and 0.065 respectively. The percentage deviation between the observed and predicted test output was 13.93%. The equation used for the predicted output was:

$$x_r = 0.399753 + (0.015318 * Fr) - (0.00804 * Angle) \quad (4.33)$$

Table 4.5: Performance Evaluation for all the models for output x_r

Model	Output	Training Database				Test Database			
	x_r	R^2	RMSE	MAE	δ %	R^2	RMSE	MAE	δ %
ANFIS		0.989	0.028	0.021	4.745	0.981	0.035	0.024	5.119
ANFIS-GA		0.966	0.051	0.039	8.827	0.953	0.056	0.041	8.832
ANFIS-PSO		0.993	0.022	0.016	3.634	0.985	0.032	0.021	4.639
ANFIS-FFA		0.986	0.031	0.023	5.258	0.980	0.035	0.026	5.717
Multi-variate Regression		0.917	0.099	0.076	17.297	0.904	0.079	0.065	13.933

ANFIS:

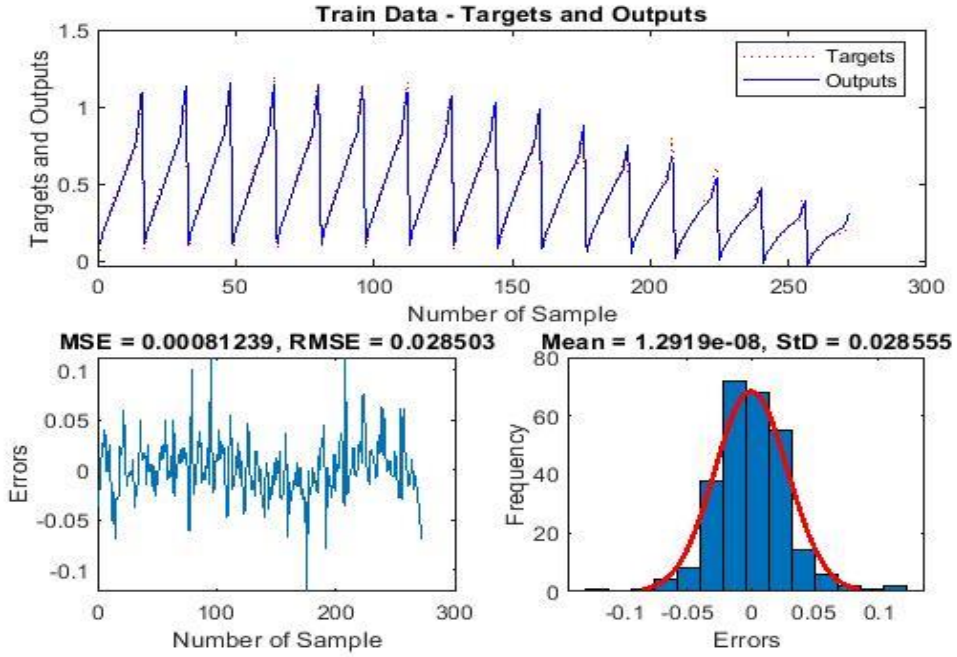
Train Data - Targets and Outputs
Targets
Outputs
Targets and Outputs
Number of Sample
MSE = 0.00081239, RMSE = 0.028503
Errors
Number of Sample
Mean = 1.2919e-08, StD = 0.028555
Frequency
Errors

a)

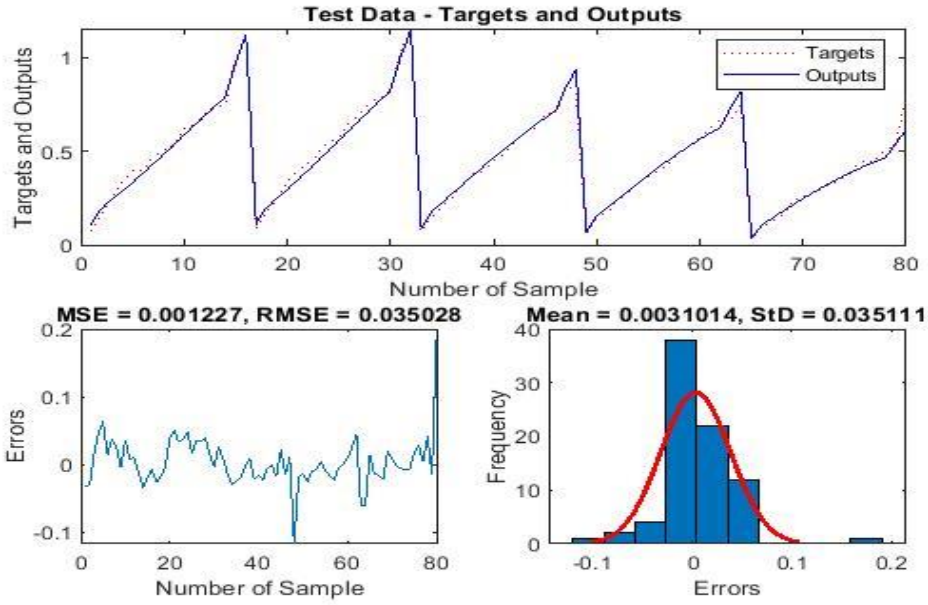
Test Data - Targets and Outputs
Targets
Outputs
Targets and Outputs
Number of Sample
MSE = 0.001227, RMSE = 0.035028
Errors
Number of Sample
Mean = 0.0031014, StD = 0.035111
Frequency
Errors

b)

ANFIS-GA:

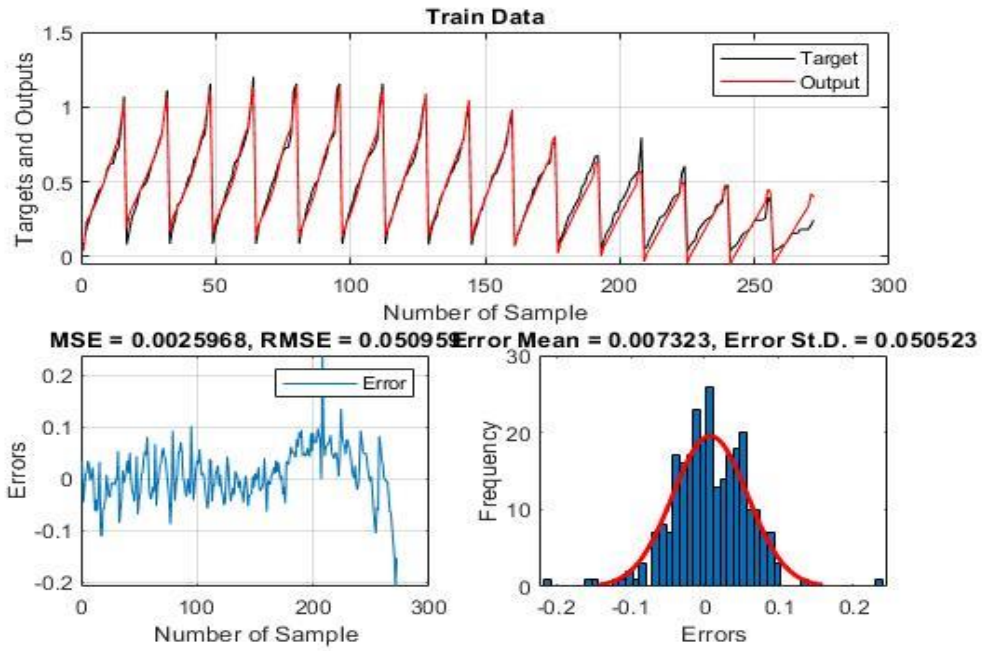
Train Data
Target
Output
Targets and Outputs
Number of Sample
MSE = 0.0025968, RMSE = 0.050959
Error Mean = 0.007323, Error St.D. = 0.050523
Error
Errors
Number of Sample
Frequency
Errors

c)

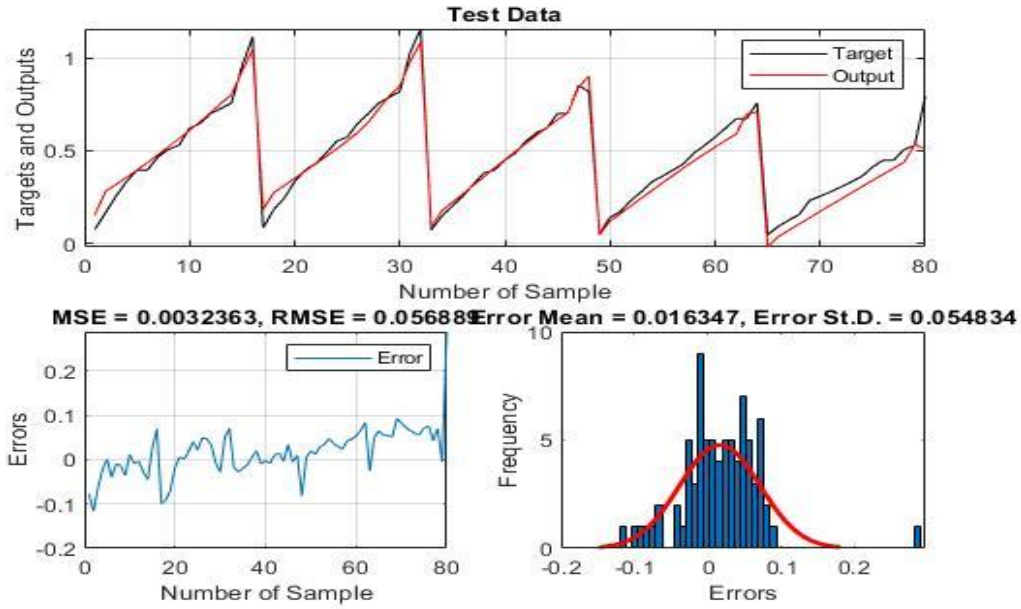
Test Data
Target
Output
Targets and Outputs
Number of Sample
MSE = 0.0032363, RMSE = 0.056889
Error Mean = 0.016347, Error St.D. = 0.054834
Error
Errors
Number of Sample
Frequency
Errors

d)

ANFIS-PSO:

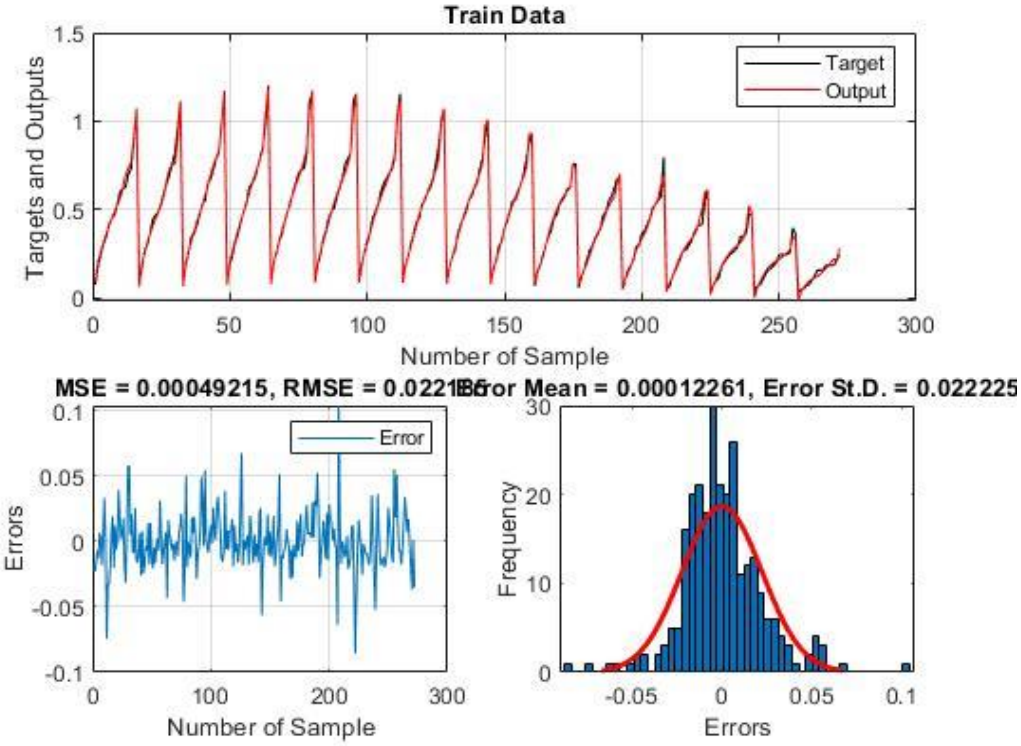
Train Data
Target
Output
Targets and Outputs
Number of Sample
MSE = 0.00049215, RMSE = 0.022186, Error Mean = 0.00012261, Error St.D. = 0.022225
Error
Errors
Number of Sample
Frequency
Errors

e)

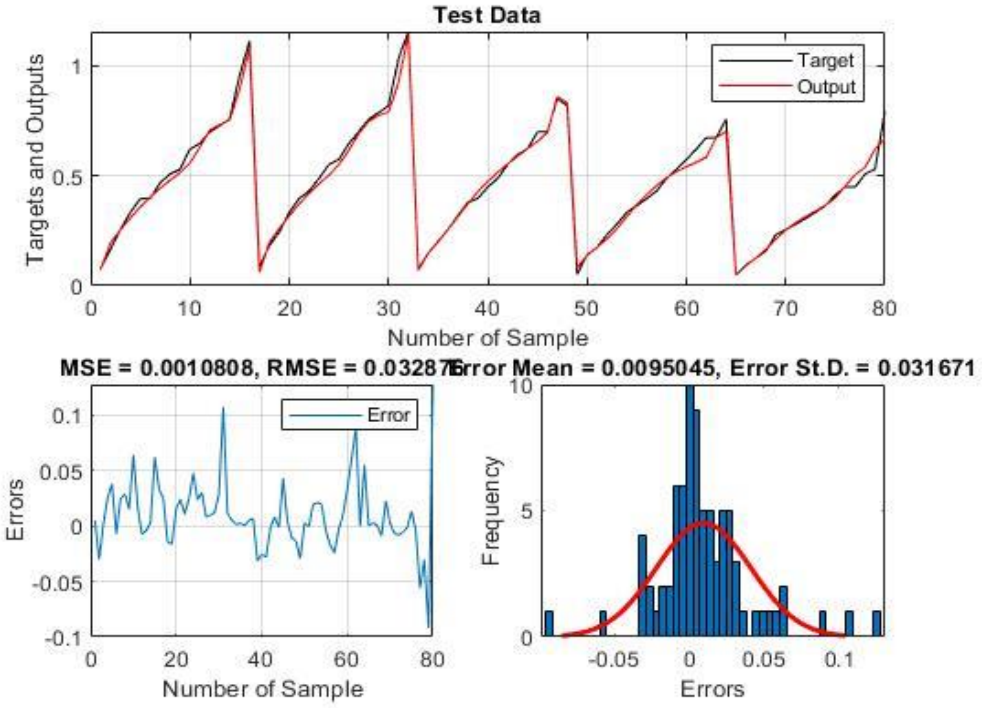
Test Data
Target
Output
Targets and Outputs
Number of Sample
MSE = 0.0010808, RMSE = 0.032876, Error Mean = 0.0095045, Error St.D. = 0.031671
Error
Errors
Number of Sample
Frequency
Errors

f)

ANFIS-FFA

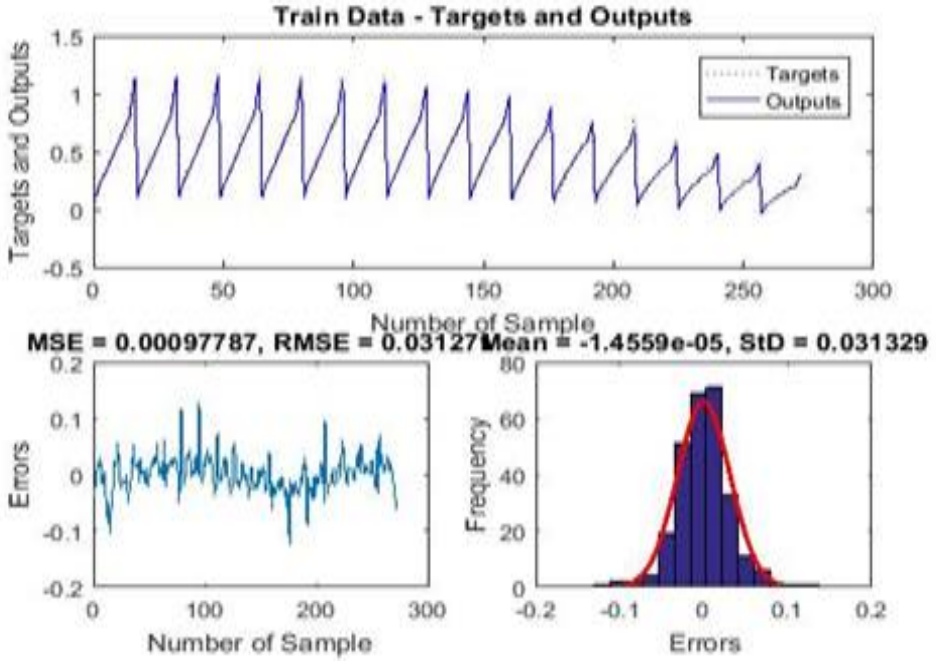

g)

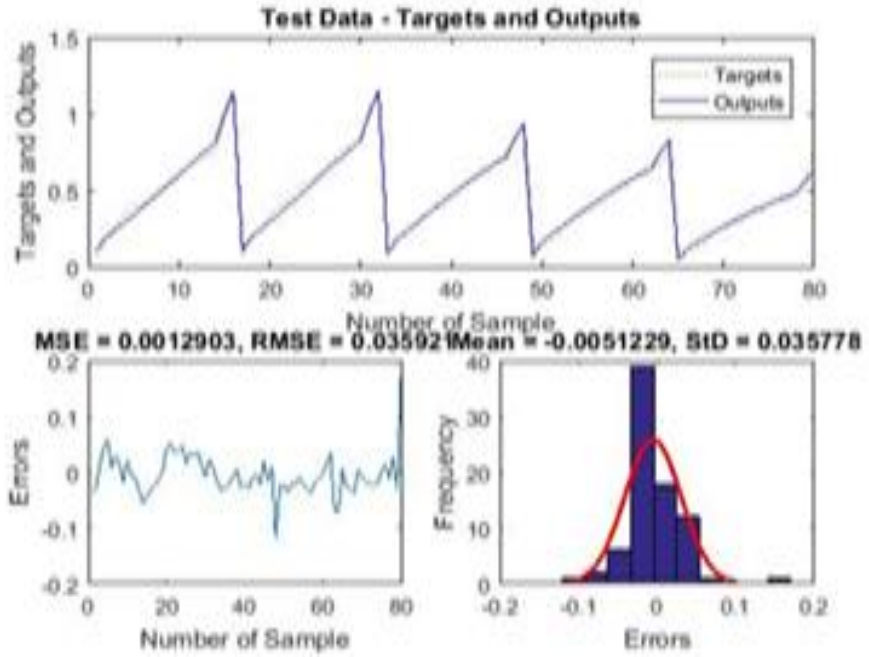

h)

Figure 4.12: ANFIS Model a) targets and outputs, RMSE, MSE values and frequency vs. errors graphs for train data set b) targets and outputs, RMSE, MSE values and frequency vs. errors graphs for test data set. ANFIS-GA: c) targets and outputs, RMSE, MSE values and frequency vs. errors graphs for train data set d) targets and outputs, RMSE, MSE values and frequency vs. errors graphs for test data set. ANFIS-PSO: e)

targets and outputs, RMSE, MSE values and frequency vs. errors for train data set f) targets and outputs, RMSE, MSE values and frequency vs. errors for test data set. ANFIS-FFA: g) targets and outputs, RMSE, MSE values and frequency vs. errors for train data set h) targets and outputs, RMSE, MSE values and frequency vs. errors for test data set.

4.4.5 Performance evaluation for y_m

ANFIS-Type Models

From the Table 4.6, it can be seen the percentage deviation for both the data sets in ANFIS-GA are 6.093% and 7.472% which are higher than all the ANFIS-type models. However, ANFIS, ANFIS-PSO and ANFIS-FFA had given similar R^2 values i.e. 0.989,0.986,0.986 respectively for their test data sets which are highest in the test data for all the models. Also, their test sets R^2 value is comparable to their respective training set which shows the models are trained properly. Along with this, the RMSE values for ANFIS, ANFIS-PSO, ANFIS-FFA are 0.013,0.014,0.014 respectively with same MAE value, 0.010. Hence, they can be considered for prediction of y_m.

Multivariate Regression

The equation obtained after regression analysis on training set to obtain the predicted test outputs is:

$$y_m = -0.13746 + (0.007027 * Fr) + (0.003153 * Angle) \quad (4.34)$$

It can be deduced from table 4.6, that training and test sets are showing good similarity with each other which proves that the data is not over-fitted but statistical parameters' values are lower as compared to ANFIS and hybrid ANFIS models. The gap between the predicted test output and observed test output can be visible by the percentage deviation of 19.735%. in the test set. However, the statistical parameters for MLR are lower than the ANFIS and hybrid models.

Table 4.6: Models' performance evaluation for output y_m

Model	Output	Training Database				Test Database			
	y_m	R^2	RMSE	MAE	δ %	R^2	RMSE	MAE	δ %
ANFIS		0.985	0.014	0.010	5.014	0.989	0.013	0.010	5.157
ANFIS-GA		0.979	0.017	0.012	6.093	0.979	0.019	0.014	7.472
ANFIS-PSO		0.990	0.011	0.008	3.900	0.986	0.014	0.010	5.285
ANFIS-FFA		0.981	0.016	0.011	5.4363	0.986	0.014	0.010	5.475
Multivariate Regression		0.855	0.040	0.030	15.016	0.846	0.049	0.038	19.735

ANFIS:

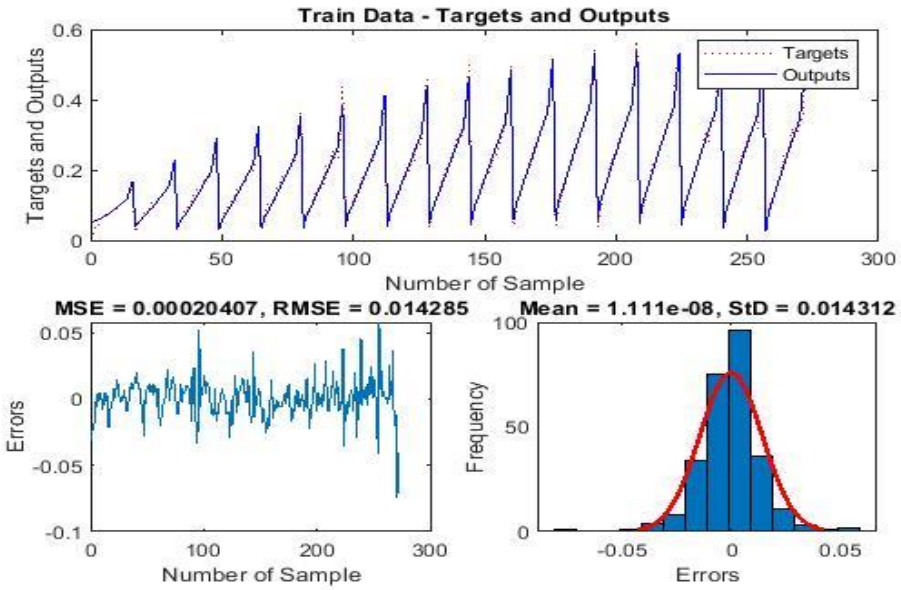

a)

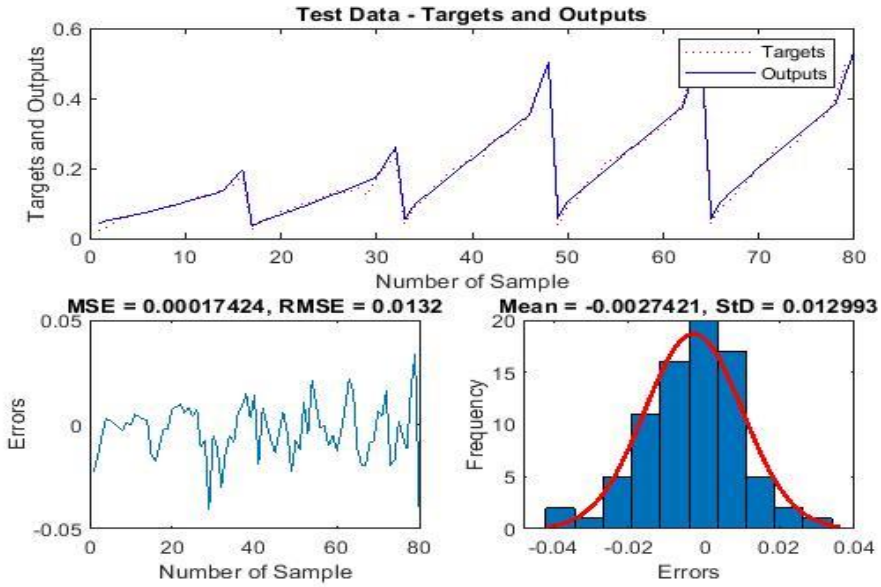
Test Data - Targets and Outputs
Targets and Outputs
Number of Sample
Targets
Outputs
MSE = 0.00017424, RMSE = 0.0132
Errors
Number of Sample
Mean = -0.0027421, StD = 0.012993
Frequency
Errors

b)

ANFIS-GA:

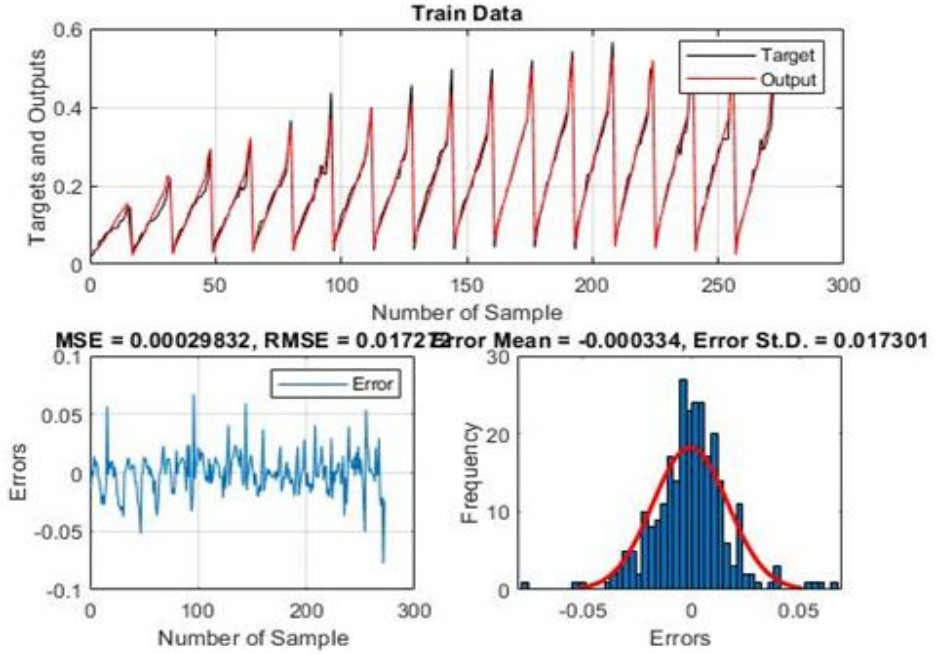
Train Data
Targets and Outputs
Number of Sample
Target
Output
MSE = 0.00029832, RMSE = 0.017272
Errors
Number of Sample
Error
Error Mean = -0.000334, Error St.D. = 0.017301
Frequency
Errors

c)

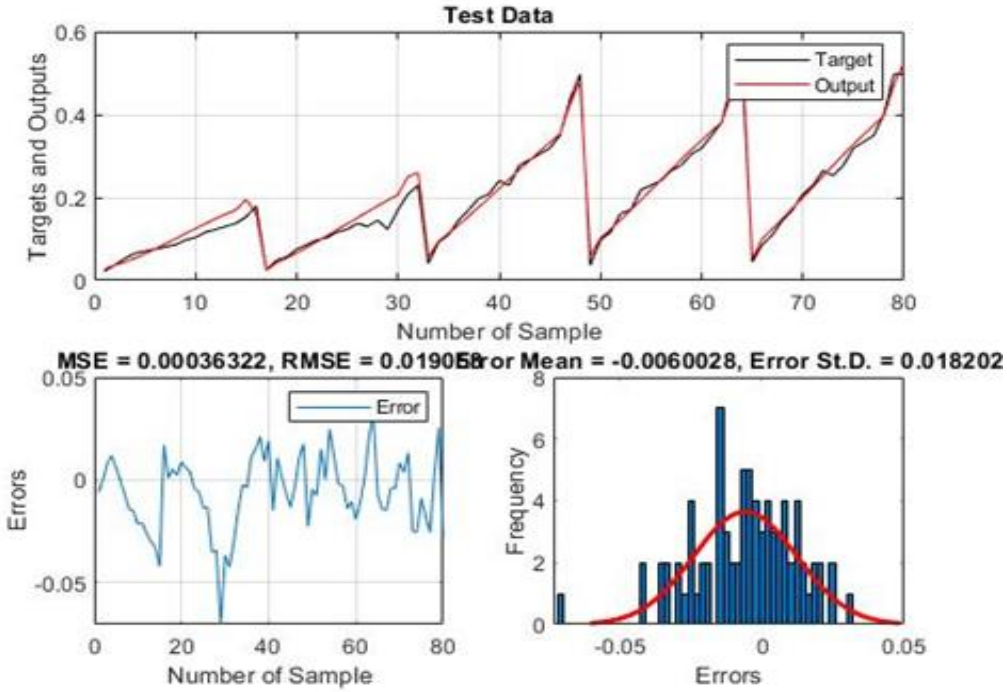
Test Data
Target
Output
Targets and Outputs
Number of Sample
MSE = 0.00036322, RMSE = 0.019058, Error Mean = -0.0060028, Error St.D. = 0.018202
Error
Errors
Number of Sample
Frequency
Errors

d)

ANFIS-PSO:

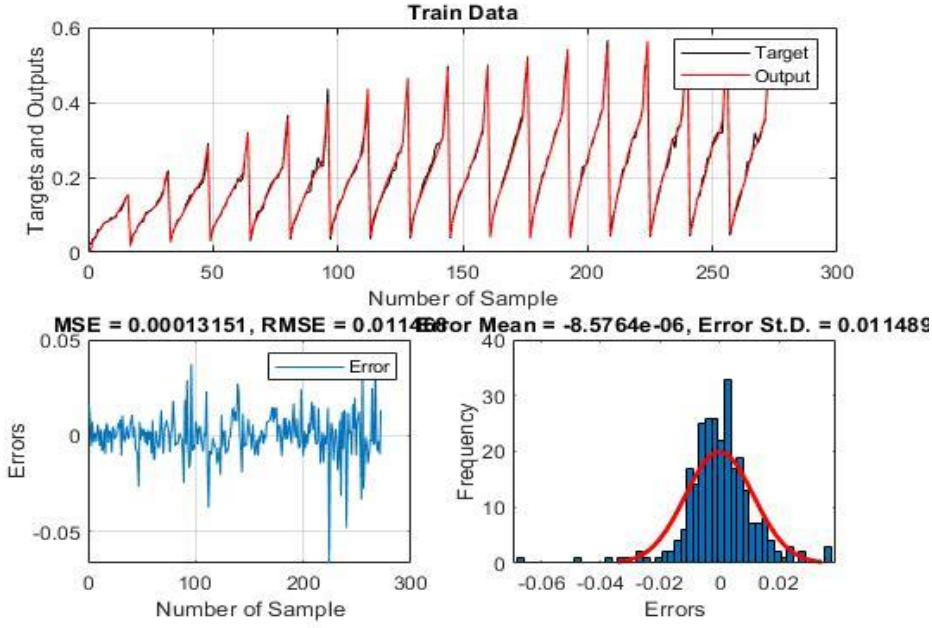
Train Data
Target
Output
Targets and Outputs
Number of Sample
MSE = 0.00013151, RMSE = 0.011468, Error Mean = -8.5764e-06, Error St.D. = 0.011489
Error
Errors
Number of Sample
Frequency
Errors

e)

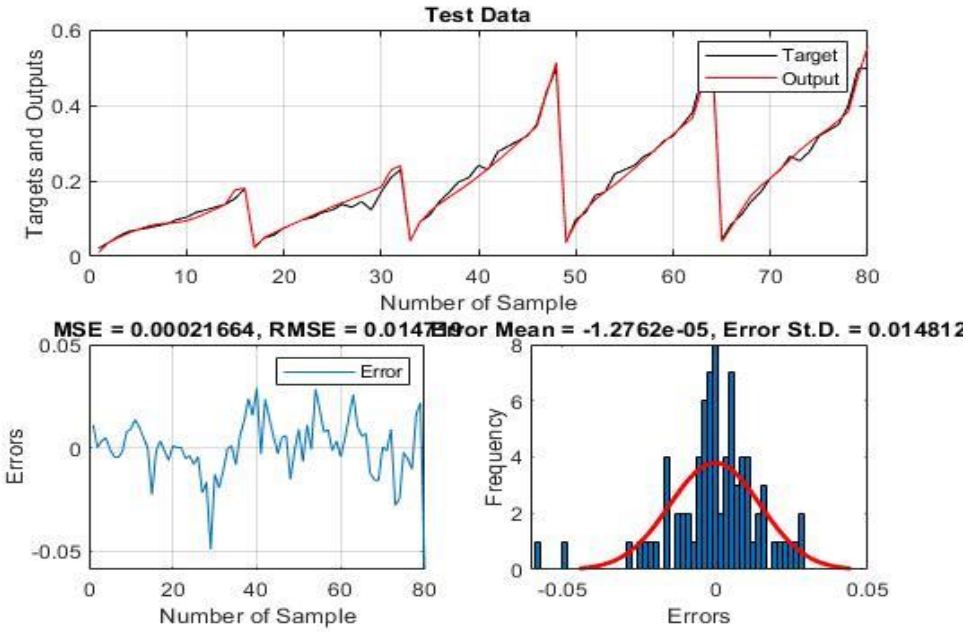
Test Data
Target
Output
Targets and Outputs
Number of Sample
MSE = 0.00021664, RMSE = 0.014718
Error Mean = -1.2762e-05, Error St.D. = 0.014812
Error
Errors
Number of Sample
Frequency
Errors

f)

ANFIS-FFA:

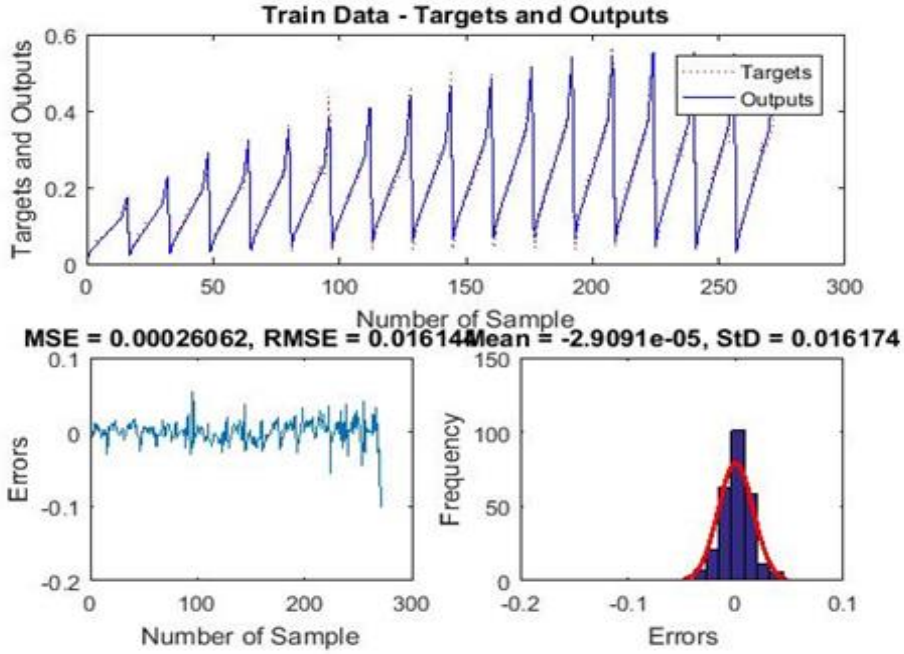
Train Data - Targets and Outputs
Targets
Outputs
Targets and Outputs
Number of Sample
MSE = 0.00026062, RMSE = 0.016144
Mean = -2.9091e-05, StD = 0.016174
Errors
Number of Sample
Frequency
Errors

g)

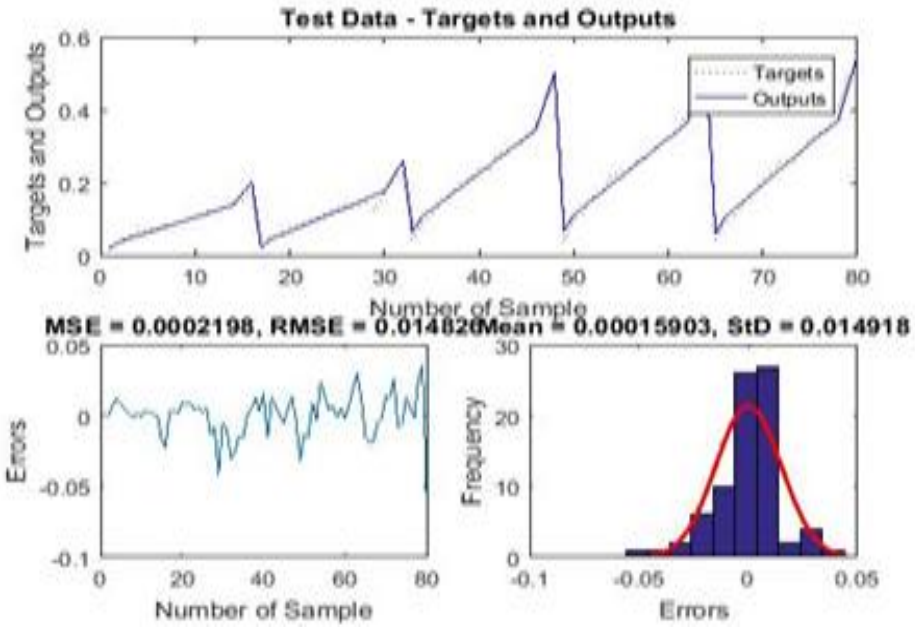

h)

Figure 4.13: ANFIS Model a) targets and outputs, RMSE, MSE values and frequency vs. errors graphs for train data set b) targets and outputs, RMSE, MSE values and frequency vs. errors graphs for test data set. ANFIS-GA: c) targets and outputs, RMSE, MSE values and frequency vs. errors graphs for train data set d) targets and outputs, RMSE, MSE values and frequency vs. errors graphs for test data set. ANFIS-PSO: e) targets and outputs, RMSE, MSE values and frequency vs. errors for train data set f) targets and outputs, RMSE, MSE values and frequency vs. errors for test data set. ANFIS-FFA: g) targets and outputs, RMSE, MSE values and frequency vs. errors for train data set h) targets and outputs, RMSE, MSE values and frequency vs. errors for test data set.

4.5 Conclusion

ANFIS model alone and different hybrid models such as ANFIS-GA, ANFIS-PSO and ANFIS-FFA along with multivariate regression were investigated for the prediction of industrial outfall discharges. The results showed that ANFIS and hybrid models were trained properly which could be seen from targets and outputs graphs in figures 4.9-4.13 as they almost coincided with each other. However, the results showed that multi-variate regression model was not successful in interpreting the relationship between independent and dependent variables especially because of the non-linearity of the data. Hence, ANFIS and hybrid models are the suitable choice to predict the discharge

characteristics of outfall systems. To determine the efficient model to predict all the outputs mentioned in the previous section, it can be deduced from Table 4.7, which is generated by averaging all the outputs that ANFIS-PSO has the highest R^2 value, lowest RMSE and lowest MAE i.e. 0.980 and 0.231 and 0.159 respectively. The other model which showed same R^2value to ANFIS-PSO is ANFIS-FFA but its RMSE value and MAE value are 0.257 and 0.166 respectively which are a little higher than ANFIS-PSO. Also, the difference observed between ANFIS-PSO and ANFIS-FFA was in their computational time which was more for ANFIS-FFA compared to ANFIS-PSO. Therefore, these two models can be considered as suitable for predicting the effluent discharge but ANFIS-PSO would be better, considering the computational time as one of the factors.

Table 4.7: Overall performance evaluation for all the test data outputs

Model	Training Set				Test Set			
	R^2	RMSE	MAE	δ %	R^2	RMSE	MAE	δ %
ANFIS	0.960	0.388	0.292	10.239	0.965	0.374	0.288	10.083
ANFIS-GA	0.968	0.323	0.255	9.625	0.966	0.350	0.257	9.618
ANFIS-PSO	0.983	0.234	0.155	6.349	0.980	0.231	0.159	7.073
ANFIS-FFA	0.978	0.256	0.164	7.065	0.980	0.257	0.166	6.908
Multivariate Regression	0.744	1.051	0.732	26.721	0.733	1.090	0.762	26.608

Chapter 5: Conclusions and Suggestions for Future work

5.1 Conclusion

Negatively buoyant submerged jets have been considered for this study. Prediction of their outfall discharge was done as submerged discharge has higher efficiency of mixing compared to surface discharge, hence, it was preferred for the study. The turbulence model considered was realizable *k-ε* turbulence model as in a previous study (Gildeh et al., 2015) it was observed that realizable *k-ε* turbulence model performed well for negatively buoyant jets compared to other turbulence models.

Numerical simulations were conducted on OpenFOAM platform over a wide range of Froude number and discharge angles in order to collect the data to train and test the ANFIS-types models. Four different models were investigated: Adaptive-Neuro Fuzzy Inference System (ANFIS), ANFIS-Genetic Algorithm (ANFIS-GA), ANFIS-Particle Swarm Optimization (ANFIS-PSO) and ANFIS-Firefly Algorithm (ANFIS-FFA). To check the closeness to the linearity of the data, multivariate linear regression model was also examined. Overall, 1760 data points were collected after simulating negatively buoyant jet over a wide range of Froude number and discharge angles which were the input parameters for the ANFIS-type models. Five combinations of input and output were considered. The output parameters considered for the study were peak salinity (S_m), return salinity (S_r), peak coordinate for peak salinity in x direction (x_m), peak coordinate in y direction (y_m) and return coordinate in x direction (x_r). The statistical parameters used for evaluating the models' performance were Coefficient of determination (R^2), Root Mean Squared Error (RMSE), Mean Absolute Error (MAE) and Average absolute deviation in percentage (δ %). However, R^2 and RMSE values of the test sets are mainly emphasized on determining the efficient model.

For the prediction of S_m, it was concluded that for all the ANFIS-type models, training and testing sets were almost coinciding with each other, which showed that all the models were trained properly and the δ % between predicted and observed value in training and test sets for all the models were almost same. Also, the statistical

parameters of training and test data were almost same, which proved that there was no case of over-fitting. The best performing model would be the one which has highest R^2 value and lowest RMSE, MAE values in the test set. It was observed that for peak salinity, ANFIS-PSO performed well with highest R^2 value i.e. 0.984 and lowest RMSE, MAE values i.e. 0.589 and 0.357, respectively.

For prediction of return salinity (S_r), the graphs showed that test dataset followed the pattern of training dataset and also, closeness of statistical indices between their training and test set showed that the models were trained properly and models were also not over-fitted. The model which performed better out of all the ANFIS-type models was ANFIS-GA had highest R^2 value i.e. 0.976 in the test set. Also, this model had the lowest RMSE value i.e. 0.471. Hence, it would be more accurate in the prediction of return salinity compared to other models.

For prediction of x_m, it was observed that R^2 in the test set for ANFIS-GA and ANFIS-FFA were higher out of all the models, i.e. 0.987 but ANFIS-FFA showed lowest RMSE value in the test set i.e. 0.016. However, the difference between RMSE values of ANFIS-GA and ANFIS-FFA were not much. Therefore, both the models are suitable for predicting x_m. Also, the training set of ANFIS-PSO showed higher R^2 i.e. 0.985 and lowest RMSE i.e. 0.0159 compared to its test dataset values which are R^2=0.976 and RMSE=0.0213, that shows ANFIS-PSO was trained more accurately and hence, it can also be considered as a reliable model for predicting x_m.

For predicting x_r, it was observed that ANFIS-PSO had the highest R^2 and lowest RMSE values i.e.0.0985 and 0.032 respectively out of all the ANFIS-type models. It was also observed from the graphs that test data set had followed the same trend as of train data for all the ANFIS-type models. Hence, models were trained properly.

For predicting y_m, it was found that, though ANFIS had the highest R^2 value (0.989) and lowest RMSE value (0.013) in the test set but its training set R^2 (0.985) and RMSE (0.014) values were minutely lower than the test sets. The models, ANFIS-PSO and ANFIS-FFA with R^2 values, 0.986 for both and RMSE values 0.014 could also be considered as suitable models as the training and test sets of the individual models had almost same values of statistical parameters.

Overall, all the models were trained properly and were not over-fitted. The model which was close to numerical model and suitable for predicting the discharge characteristics was ANFIS-PSO as it could be observed from the average values of the statistical indices that R^2 value for ANFIS-PSO was 0.980. Also, the model had the lowest RMSE, MAE and δ % for ANFIS-PSO were 0.231, 0.159 and 7.073 % respectively. However, ANFIS-FFA had similar R^2 value as ANFIS-PSO but its RMSE and MAE were 0.257 and 0.0166 respectively which were slightly higher than ANFIS-PSO. Along with this, if the computational time has been considered as one of the parameters for selecting the model, then out of both models, ANFIS-PSO took less computational time compared to ANFIS-FFA. It needs to be mentioned that all ANFIS type models except ANFIS-FFA had taken approximately 10 to 15 minutes to run whereas ANFIS-FFA had taken approximately 3.5 hours. Also, the computational time for CFD model was approximately 3.5 days which shows ANFIS-type models take less computational time. Hence, considering the computational time, ANFIS-PSO would be more efficient and suitable.

Multivariate Regression analysis was also conducted for the individual outputs and it was found that multi-variate regression model had poor statistical parameters compared to ANFIS-type models. When average was done, for all the outputs, Multivariate regression model had R^2, RMSE, MAE and δ % values, 0.773, 1.090, 0.762 and 26.608% which were not good as compared to ANFIS-type models. Hence, it showed that the data were not close to linearity and linear model cannot predict the discharge characteristics.

5.2 Suggestions for future work

The following recommendations are proposed for using AI techniques for prediction of industrial discharges:

- There are several other algorithms such as Differential Evolution (DE), Cuckoo Optimization Algorithm (COA), Ant Colony (ACO), etc., which could be merged with ANFIS to get a wider range of study on negatively buoyant jet discharge prediction.
- Experimental data can also be used to train and test the ANFIS-type models.
- Temperature can also be considered as a parameter.

- Other CFD turbulence models can also be studied to check the impact on AI model.
- Other statistical parameters such as Scatter Index (SI), BIAS, Nash, VAF can also be considered for the performance evaluation.
- Artificial Neural Network (ANN) merged with various algorithms such as GA, PSO etc. to predict the outfall discharge.
- Positively buoyant jets could also be considered for predicting the discharge in order to know whether AI techniques could work on Positively buoyant jets or not.
- Positive and negative Jets in crossflow can be examined using various AI methods such as ANFIS-type procedures.
- Other applications of AI techniques in the field of outfall systems include negative jets over a sloping bed, density current, rosette diffusers, various types of jets under wave effect, or under current-only effect, combined effect of wave and current, effect of stratification on various types of discharges with and without current, discharges in shallow water versus deep water, effect of secondary flows and discharges in rivers under the ice.

References

Abou-Elhaggag, M. E., El-Gamal, M. H., & Farouk, M. I. (2011). Experimental and numerical investigation of desalination plant outfalls in limited disposal areas. *Journal of Environmental Protection*, *2*(06), 828.

Ab. Ghani A (1993) Sediment Transport in Sewers. Ph.D Thesis, University of Newcastle Upon Tyne, UK

Alameddine, I., & El-Fadel, M. (2007). Brine discharge from desalination plants: a modeling approach to an optimized outfall design. *Desalination*, *214*(1-3), 241-260.

Amirkhani, S., Nasirivatan, S., Kasaeian, A. B., & Hajinezhad, A. (2015). ANN and ANFIS models to predict the performance of solar chimney power plants. *Renewable Energy*, *83*, 597-607.

Azimi, H., Bonakdari, H., Ebtehaj, I., & Michelson, D. G. (2018). A combined adaptive neuro-fuzzy inference system–firefly algorithm model for predicting the roller length of a hydraulic jump on a rough channel bed. *Neural Computing and Applications*, *29*(6), 249-258.

Bilgili, M., & Sahin, B. (2010). Comparative analysis of regression and artificial neural network models for wind speed prediction. *Meteorology and Atmospheric Physics*, *109*(1-2), 61-72.

Bleninger, T., & Jirka, G. H. (2008). Modelling and environmentally sound management of brine discharges from desalination plants. *Desalination*, *221*(1-3), 585-597.

Bleninger, T., Niepelt, A., & Jirka, G. (2010). Desalination plant discharge calculator. Desalination and Water Treatment, 13(1-3), 156-173.

Bonakdari, H., & Zaji, A. H. (2018). New type side weir discharge coefficient simulation using three novel hybrid adaptive neuro-fuzzy inference systems. *Applied water science*, *8*(1), 10.

Bonakdari, H., Zaji, A. H., Shamshirband, S., Hashim, R., & Petkovic, D. (2015). Sensitivity analysis of the discharge coefficient of a modified triangular side weir by adaptive neuro-fuzzy methodology. *Measurement*, *73*, 74-81.

Borghei, S. M., & Parvaneh, A. (2011). Discharge characteristics of a modified oblique side weir in subcritical flow. *Flow Measurement and Instrumentation*, *22*(5), 370-376.

Carollo, F. G., Ferro, V., & Pampalone, V. (2007). Hydraulic jumps on rough beds. *Journal of Hydraulic Engineering*, *133*(9), 989-999.

Chelgani, S. C., Hart, B., Grady, W. C., & Hower, J. C. (2011). Study relationship between inorganic and organic coal analysis with gross calorific value by multiple regression and ANFIS. *International Journal of Coal Preparation and Utilization*, *31*(1), 9-19.

Chen, G., Xiong, Q., Morris, P. J., Paterson, E. G., Sergeev, A., & Wang, Y. (2014). OpenFOAM for computational fluid dynamics. *Not. AMS*, *61*(4), 354-363.

Christodoulou, G. C., Papakonstantis, I. G., & Nikiforakis, I. K. (2015). Desalination brine disposal by means of negatively buoyant jets. *Desalination and Water Treatment*, *53*(12), 3208-3213.

Ebtehaj, I., & Bonakdari, H. (2014). Performance evaluation of adaptive neural fuzzy inference system for sediment transport in sewers. *Water resources management*, *28*(13), 4765-4779.

Einav, R., Harussi, K., & Perry, D. (2003). The footprint of the desalination processes on the environment. Desalination, 152(1-3), 141-154.

Emadi, D., & Mahfoud, M. (2011). Comparison of Artificial Neural Network and Multiple Regression Analysis Techniques in Predicting the Mechanical Properties of A3 56 Alloy. *Procedia Engineering*, *10*, 589-594.

Esmaeili, M., Osanloo, M., Rashidinejad, F., Bazzazi, A. A., & Taji, M. (2014). Multiple regression, ANN and ANFIS models for prediction of backbreak in the open pit blasting. *Engineering with computers*, *30*(4), 549-558.

Fumo, N., & Biswas, M. R. (2015). Regression analysis for prediction of residential energy consumption. *Renewable and sustainable energy reviews*, *47*, 332-343.

Ghani, A. A. (1993). *Sediment transport in sewers* (Doctoral dissertation, Newcastle University).

Gildeh, H. K., Mohammadian, A., Nistor, I., & Qiblawey, H. (2015). Numerical modeling of $ $30^{\circ} $$ and $ $45 {^\circ} $ $45∘ inclined dense turbulent jets in stationary ambient. *Environmental Fluid Mechanics*, *15*(3), 537-562.

Holland, 1. H., Adaptation in natural and artificial systems. University of Miehigan Press, Ann Arbor, MI, (1975).

Jang, J. S. (1993). ANFIS: adaptive-network-based fuzzy inference system. *IEEE transactions on systems, man, and cybernetics*, *23*(3), 665-685.

Jirka, G. H. (2004). Integral model for turbulent buoyant jets in unbounded stratified flows. Part I: Single round jet. *Environmental Fluid Mechanics*, *4*(1), 1-56.

Jirka, G. H. (2008). Improved discharge configurations for brine effluents from desalination plants. *Journal of Hydraulic Engineering*, *134*(1), 116-120.

Kanu, I., & Achi, O. K. (2011). Industrial effluents and their impact on water quality of receiving rivers in Nigeria. *Journal of applied technology in environmental sanitation*, *1*(1), 75-86.

Kennedy, J., & Eberhart, R. (1995, November). Particle swarm optimization (PSO). In *Proc. IEEE International Conference on Neural Networks, Perth, Australia* (pp. 1942-1948).

Kheirkhah Gildeh H, Mohammadian A, Nistor I, Qiblawey H., (2015) "Inclined Negatively Buoyant Jets: A Numerical Approach", Journal of Applied Water Engineering and Research, IAHR, Taylor and Francis, 4, 2015, 112-127

Kheirkhah Gildeh, H. (2013). *Numerical Modeling of Thermal/Saline Discharges in Coastal Waters* (Master's Thesis, Université d'Ottawa/University of Ottawa).

Kheirkhah Gildeh, H., Mohammadian, A., Nistor, I., & Qiblawey, H. (2014). Numerical modeling of turbulent buoyant wall jets in stationary ambient water. *Journal of Hydraulic Engineering*, *140*(6), 04014012.

Kikkert, G. A., Davidson, M. J., & Nokes, R. I. (2007). Inclined negatively buoyant discharges. *Journal of Hydraulic engineering*, *133*(5), 545-554.

Konya, C. J., & Walter, E. J. (1991). *Rock blasting and overbreak control* (No. FHWA-HI-92-001; NHI-13211). United States. Federal Highway Administration.

Lattemann, S., & Höpner, T. (2008). Environmental impact and impact assessment of seawater desalination. *Desalination*, *220*(1-3), 1-15.

Malalasekera W, Versteeg HK (1995) Computational Fluid Dynamics. Longman Scientific, England

Malcangio, D., & Petrillo, A. F. (2010). Modeling of brine outfall at the planning stage of desalination plants. *Desalination*, *254*(1-3), 114-125.

Marti, C. L., Antenucci, J. P., Luketina, D., Okely, P., & Imberger, J. (2010). Near-field dilution characteristics of a negatively buoyant hypersaline jet generated by a desalination plant. *Journal of Hydraulic Engineering*, *137*(1), 57-65.

McGovern, A., Elmore, K.L., Gagne, D.J., Haupt, S.E., Karstens, C.D., Lagerquist, R., Smith, T. and Williams, J.K. (2017). Using artificial intelligence to improve real-time decision-making for high-impact weather. *Bulletin of the American Meteorological Society*, *98*(10), 2073-2090.

Millero FJ, Poisson A (1981) International one-atmosphere equation of state of sea water, J Deep-Sea Research 28A(6): 625 to 629

Niazian, M., Sadat-Noori, S. A., & Abdipour, M. (2018). Artificial neural network and multiple regression analysis models to predict essential oil content of ajowan (Carum copticum L.). *Journal of applied research on medicinal and aromatic plants*, *9*, 124-131.

Oliver, C. J., Davidson, M. J., & Nokes, R. I. (2008). *k-ε* Predictions of the initial mixing of desalination discharges. *Environmental Fluid Mechanics*, *8*(5-6), 617.

OpenCFD Limited. OpenFOAM - Programmer's Guide, May 2012. Version 2.1.1

OpenCFD Limited. OpenFOAM - User Guide, May 2012. Version 2.1.1

Palomar, P., Lara, J. L., Losada, I. J., Rodrigo, M., & Alvárez, A. (2012a). Near field brine discharge modelling part 1: Analysis of commercial tools. *Desalination*, *290*, 14-27.

Palomar, P., Lara, J. L., & Losada, I. J. (2012b). Near field brine discharge modeling part 2: Validation of commercial tools. *Desalination*, *290*, 28-42.

Papakonstantis, I. G., Christodoulou, G. C., & Papanicolaou, P. N. (2011a). Inclined negatively buoyant jets 1: geometrical characteristics. *Journal of Hydraulic Research*, *49*(1), 3-12.

Papakonstantis, I. G., Christodoulou, G. C., & Papanicolaou, P. N. (2011b). Inclined negatively buoyant jets 2: concentration measurements. *Journal of Hydraulic Research*, *49*(1), 13-22.

Pourtousi, M., Sahu, J. N., Ganesan, P., Shamshirband, S., & Redzwan, G. (2015). A combination of computational fluid dynamics (CFD) and adaptive neuro-fuzzy system (ANFIS) for prediction of the bubble column hydrodynamics. *Powder Technology*, *274*, 466-481.

Purnama, A., & Shao, D. (2015). Modeling brine discharge dispersion from two adjacent desalination outfalls in coastal waters. *Desalination*, *362*, 68-73

Rezakazemi, M., Dashti, A., Asghari, M., & Shirazian, S. (2017). H2-selective mixed matrix membranes modeling using ANFIS, PSO-ANFIS, GA-ANFIS. *International Journal of Hydrogen Energy*, *42*(22), 15211-15225.

Roberts, D. A., Johnston, E. L., & Knott, N. A. (2010). Impacts of desalination plant discharges on the marine environment: A critical review of published studies. *Water research*, *44*(18), 5117-5128.

Shabanian, S. R., Edrisi, S., & Khoram, F. V. (2017). Prediction and optimization of hydrogen yield and energy conversion efficiency in a non-catalytic filtration combustion reactor for jet A and butanol fuels. *Korean Journal of Chemical Engineering*, *34*(8), 2188-2197.

Shao, D., & Law, A. W. K. (2010). Mixing and boundary interactions of 30 and 45 inclined dense jets. *Environmental fluid mechanics*, *10*(5), 521-553.

Taghavifar, H., Khalilarya, S., & Jafarmadar, S. (2015). Adaptive neuro-fuzzy system (ANFIS) based appraisal of accumulated heat from hydrogen-fueled engine. *International Journal of Hydrogen Energy*, *40*(25), 8206-8218.

Termeh, S. V. R., Khosravi, K., Sartaj, M., Keesstra, S. D., Tsai, F. T. C., Dijksma, R., & Pham, B. T. (2019). Optimization of an adaptive neuro-fuzzy inference system for groundwater potential mapping. *Hydrogeology Journal*, 1-24.

Tosun, E., Aydin, K., & Bilgili, M. (2016). Comparison of linear regression and artificial neural network model of a diesel engine fueled with biodiesel-alcohol mixtures. *Alexandria Engineering Journal*, *55*(4), 3081-3089.

Wang, J. H., Zhao, W. W., & Wan, D. C. (2019). Development of naoe-FOAM-SJTU solver based on OpenFOAM for marine hydrodynamics. *Journal of Hydrodynamics*, *31*(1), 1-20.

Yarpiz Evolutionary Algorithms, (2019), https://yarpiz.com/477/ypea-yarpiz-evolutionary-algorithms

Yaghoobi, A., Bakhshi-Jooybari, M., Gorji, A., & Baseri, H. (2016). Application of adaptive neuro fuzzy inference system and genetic algorithm for pressure path optimization in sheet hydroforming process. *The International Journal of Advanced Manufacturing Technology*, *86*(9-12), 2667-2677.

Yang, X. S. (2010). Firefly algorithm, stochastic test functions and design optimisation. *arXiv preprint arXiv:1003.1409*.

Yaseen, Z.M., Ebtehaj, I., Bonakdari, H., Deo, R.C., Mehr, A.D., Mohtar, W.H.M.W., Diop, L., El-Shafie, A. and Singh, V.P. (2017). Novel approach for streamflow forecasting using a hybrid ANFIS-FFA model. *Journal of Hydrology*, *554*, 263-276.

Yaseen, Z.M., Ghareb, M.I., Ebtehaj, I., Bonakdari, H., Siddique, R., Heddam, S., Yusif, A.A. and Deo, R. (2018). Rainfall pattern forecasting using novel hybrid intelligent model based ANFIS-FFA. *Water resources management*, *32*(1), 105-122.

Zhang, S., Jiang, B., Law, A. W. K., & Zhao, B. (2016). Large eddy simulations of 45 inclined dense jets. *Environmental Fluid Mechanics*, *16*(1), 101-121

Appendix A: Coefficient of Determination (R^2) Graphs

Figure A1: Coefficient of Determination (R^2) Graphs for the Outputs of ANFIS Model a)S_m b)S_r c)x_m d)x_r e)y_m

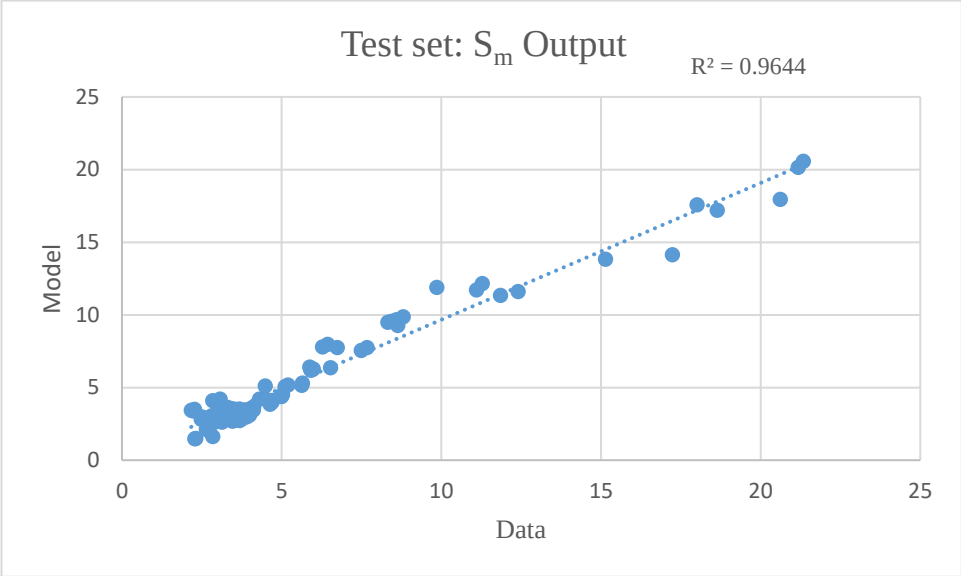

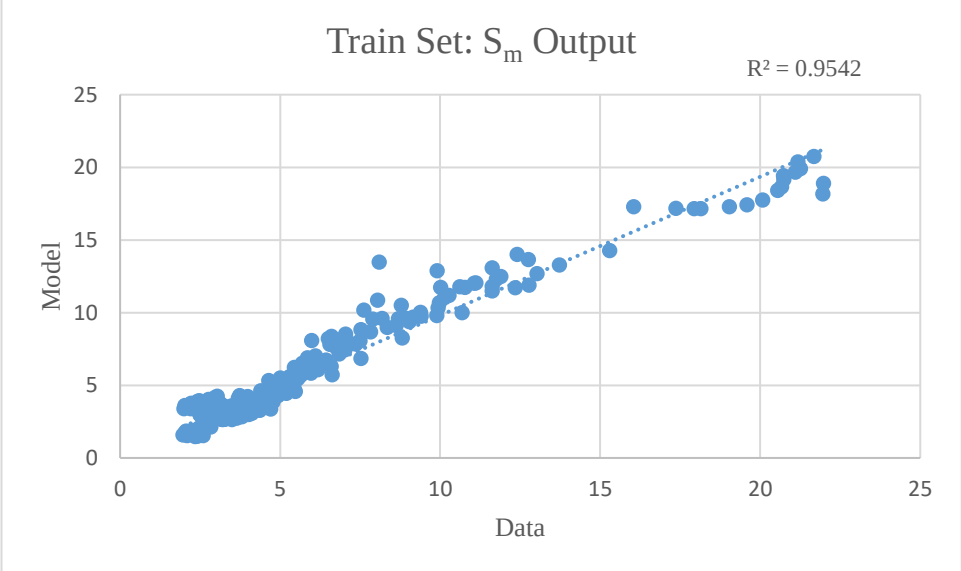

a)

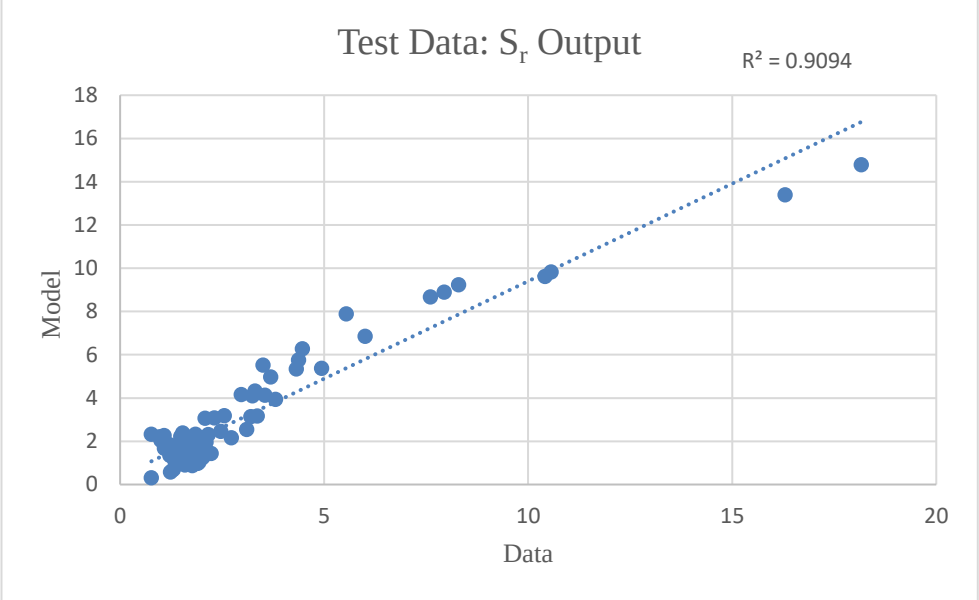
Test Data: S_r Output
R^2 = 0.9094
Model
Data
0
2
4
6
8
10
12
14
16
18
0
5
10
15
20

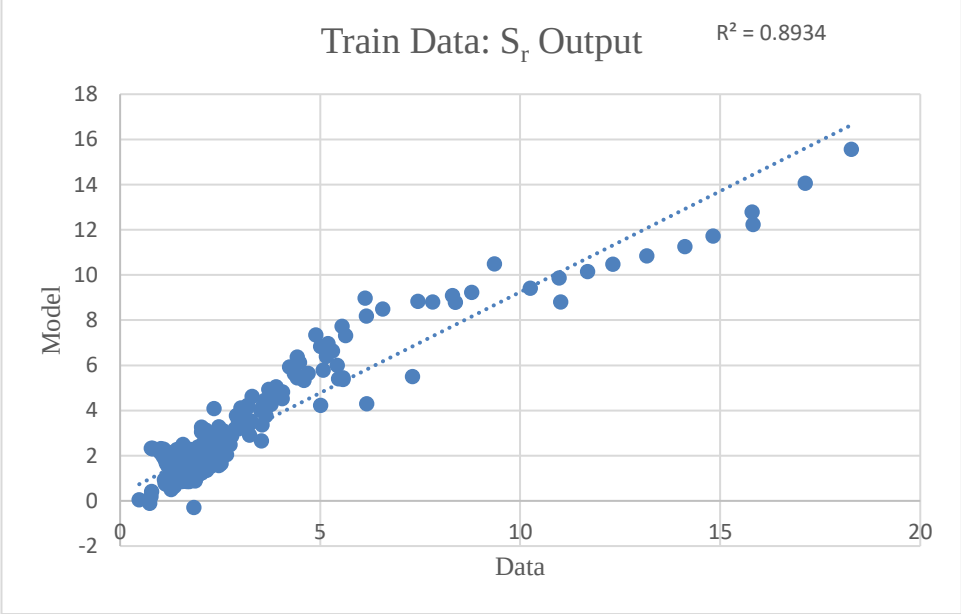
Train Data: S_r Output
R^2 = 0.8934
Model
Data
-2
0
2
4
6
8
10
12
14
16
18
0
5
10
15
20

b)

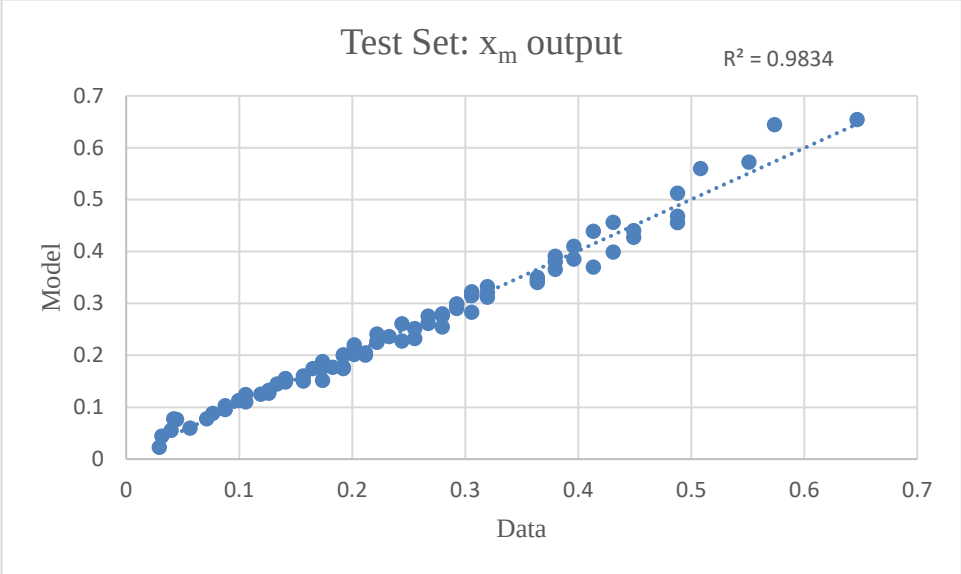
Test Set: x_m output
R² = 0.9834
Model
Data
0
0.1
0.2
0.3
0.4
0.5
0.6
0.7

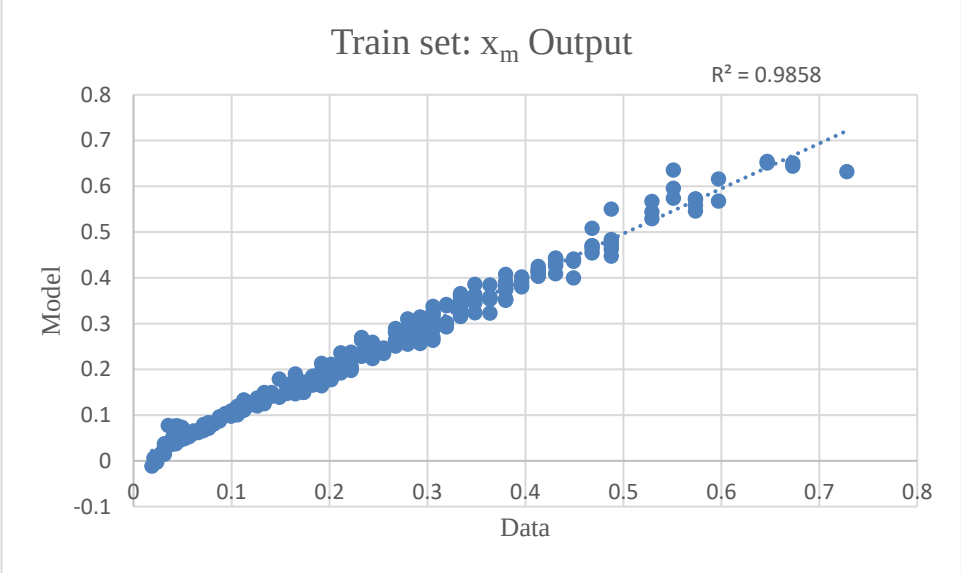
Train set: x_m Output
R² = 0.9858
Model
Data
-0.1
0
0.1
0.2
0.3
0.4
0.5
0.6
0.7
0.8

c)

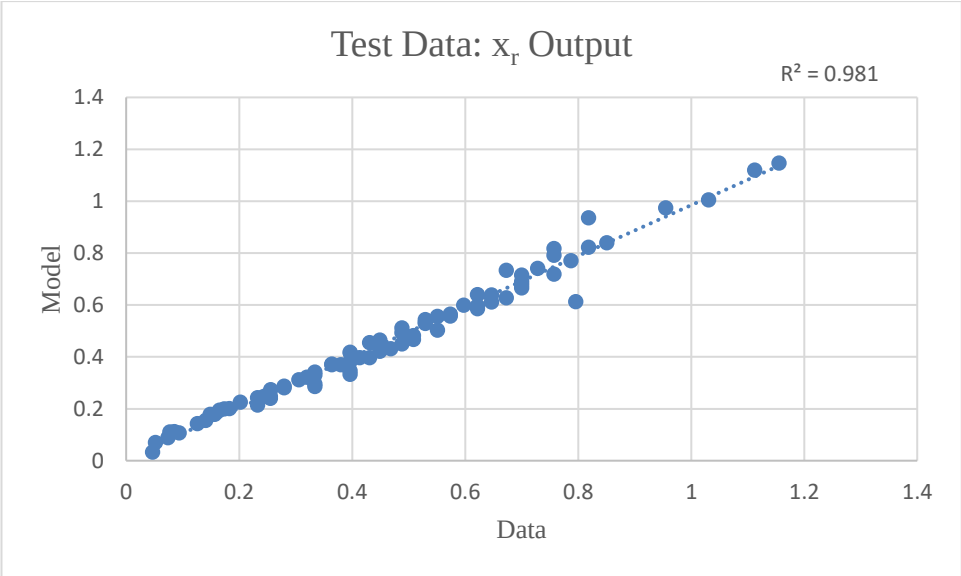
Test Data: x_r Output
R^2 = 0.981
Model
Data
0
0.2
0.4
0.6
0.8
1
1.2
1.4

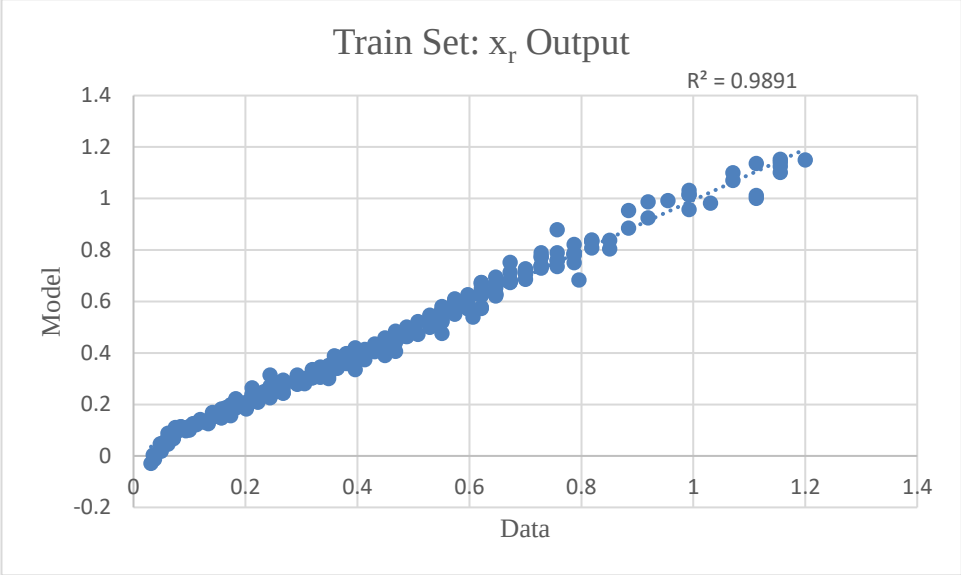
Train Set: x_r Output
R^2 = 0.9891
Model
Data
-0.2
0
0.2
0.4
0.6
0.8
1
1.2
1.4

d)

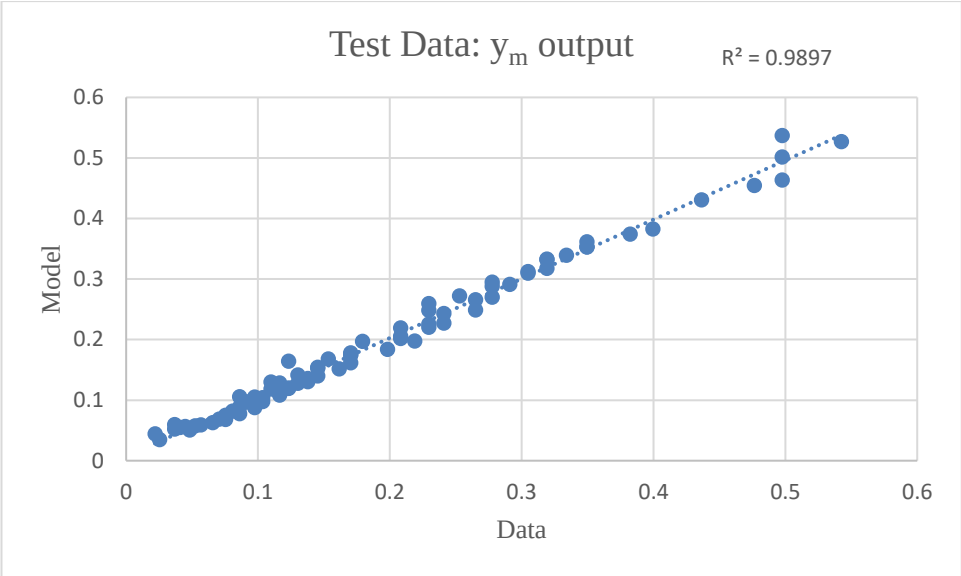
Test Data: y_m output
R^2 = 0.9897
Model
Data
0
0.1
0.2
0.3
0.4
0.5
0.6

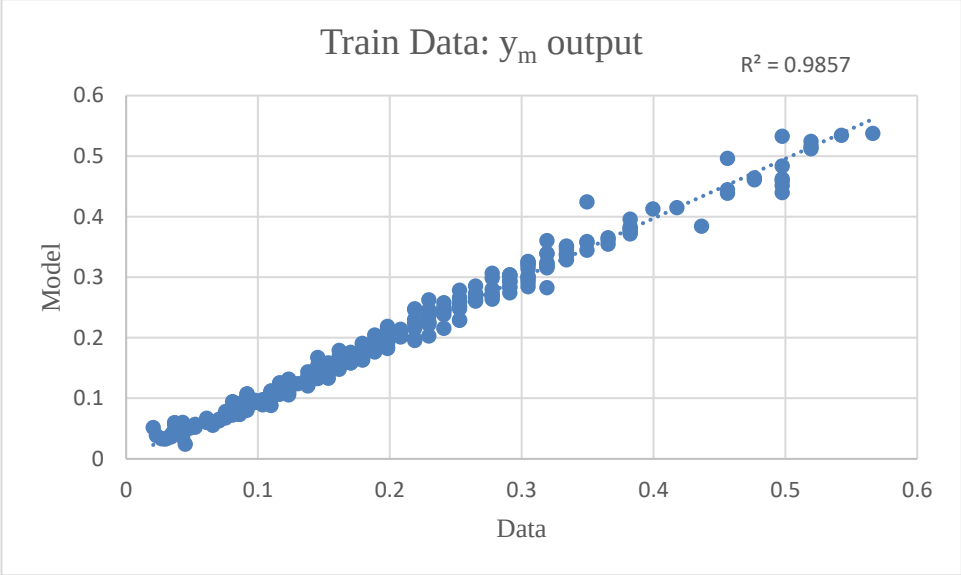
Train Data: y_m output
R^2 = 0.9857
Model
Data
0
0.1
0.2
0.3
0.4
0.5
0.6

e)

Figure A2: Coefficient of Determination (R^2) Graphs for the Outputs of ANFIS-GA Model a)S_m b)S_r c)x_m d)x_r e)y_m

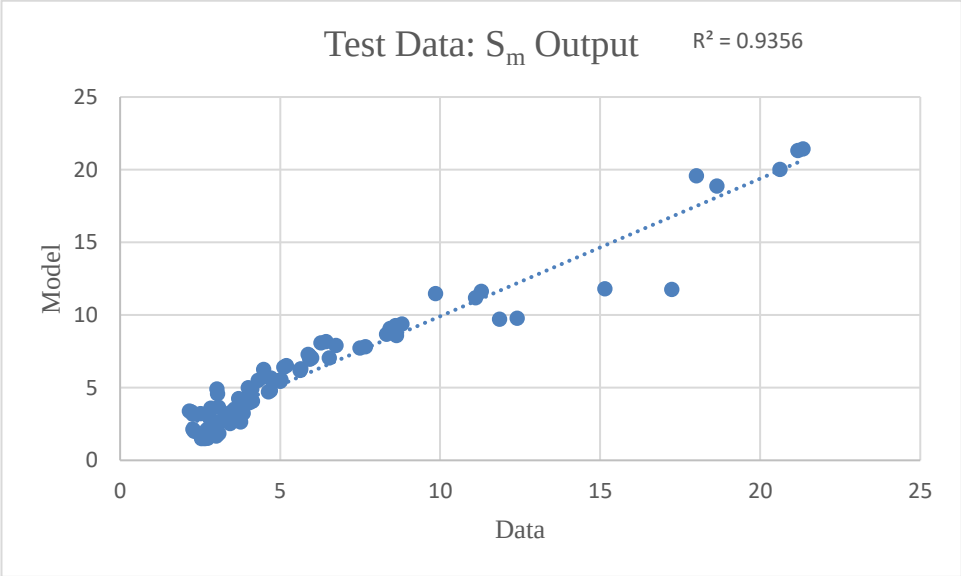

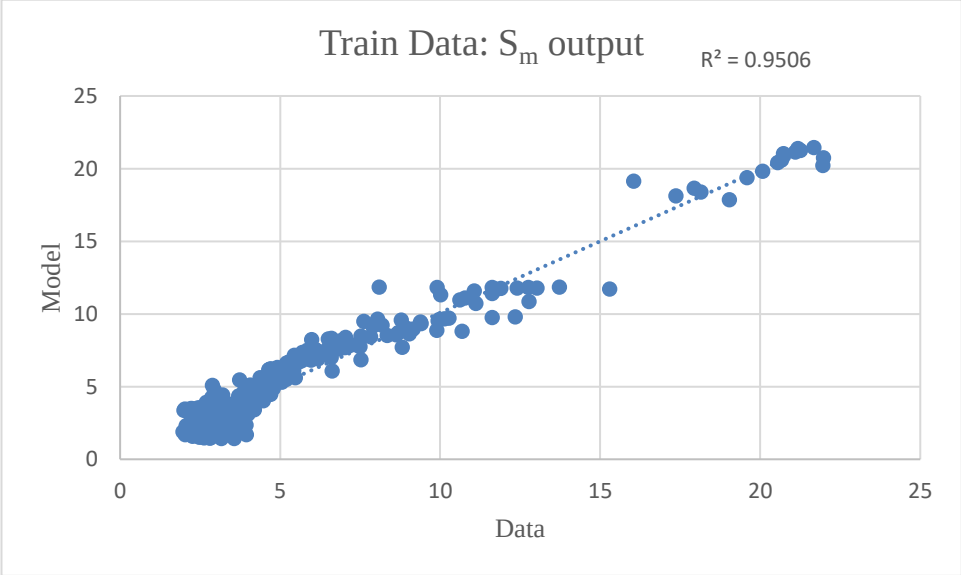

a)

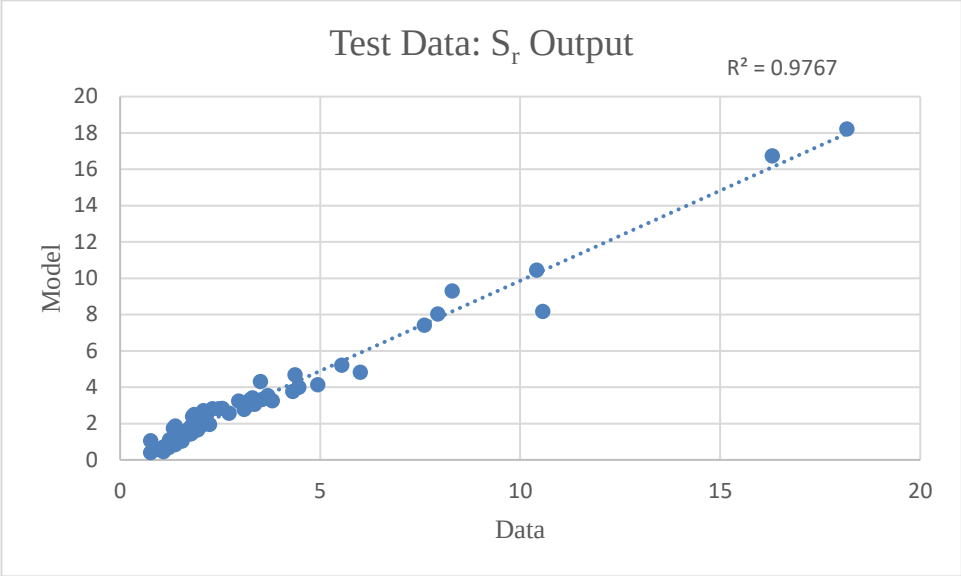
Test Data: S_r Output
R^2 = 0.9767
Model
Data
0
2
4
6
8
10
12
14
16
18
20
0
5
10
15
20

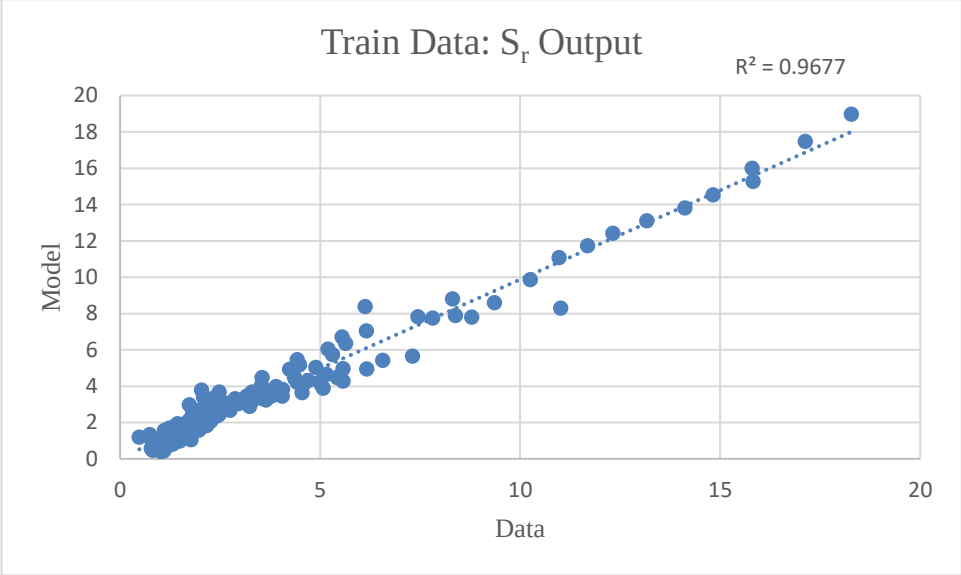
Train Data: S_r Output
R^2 = 0.9677
Model
Data
0
2
4
6
8
10
12
14
16
18
20
0
5
10
15
20

b)

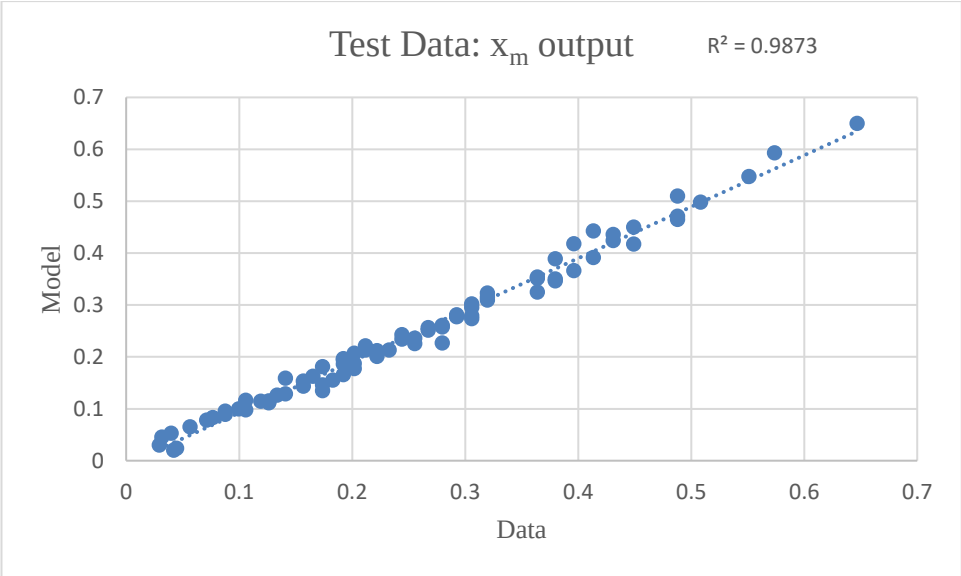
Test Data: x_m output
R^2 = 0.9873
Model
Data
0
0.1
0.2
0.3
0.4
0.5
0.6
0.7

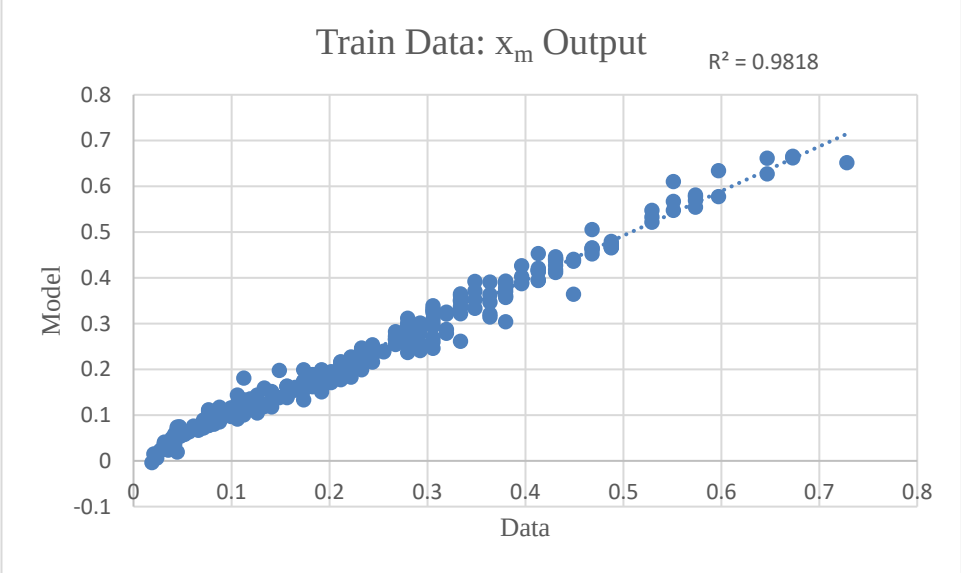
Train Data: x_m Output
R^2 = 0.9818
Model
Data
-0.1
0
0.1
0.2
0.3
0.4
0.5
0.6
0.7
0.8

c)

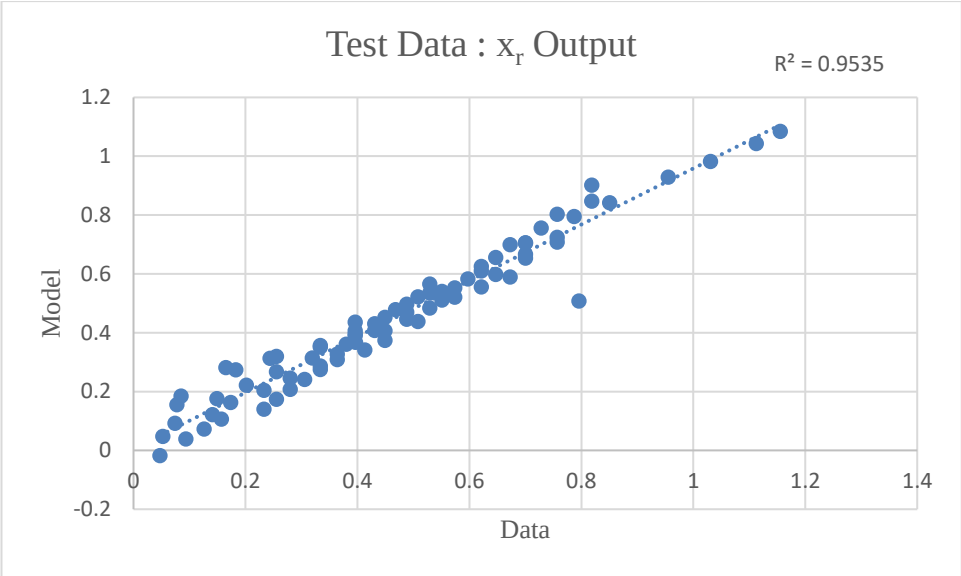
Test Data : x_r Output
R^2 = 0.9535
Model
Data
1.2
1
0.8
0.6
0.4
0.2
0
-0.2
0
0.2
0.4
0.6
0.8
1
1.2
1.4

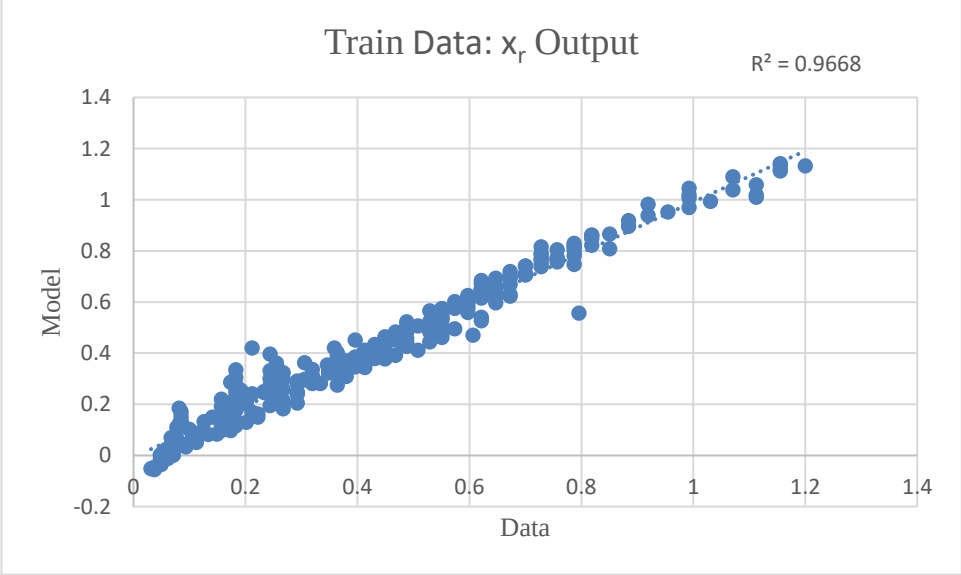
Train Data: x_r Output
R^2 = 0.9668
Model
Data
1.4
1.2
1
0.8
0.6
0.4
0.2
0
-0.2
0
0.2
0.4
0.6
0.8
1
1.2
1.4

d)

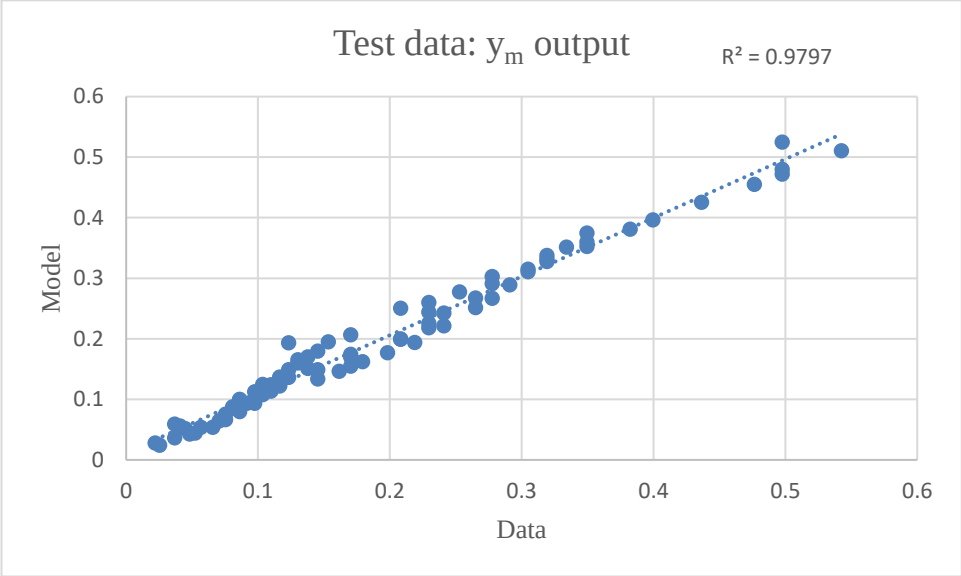
Test data: y_m output
R² = 0.9797
Model
Data
0
0.1
0.2
0.3
0.4
0.5
0.6

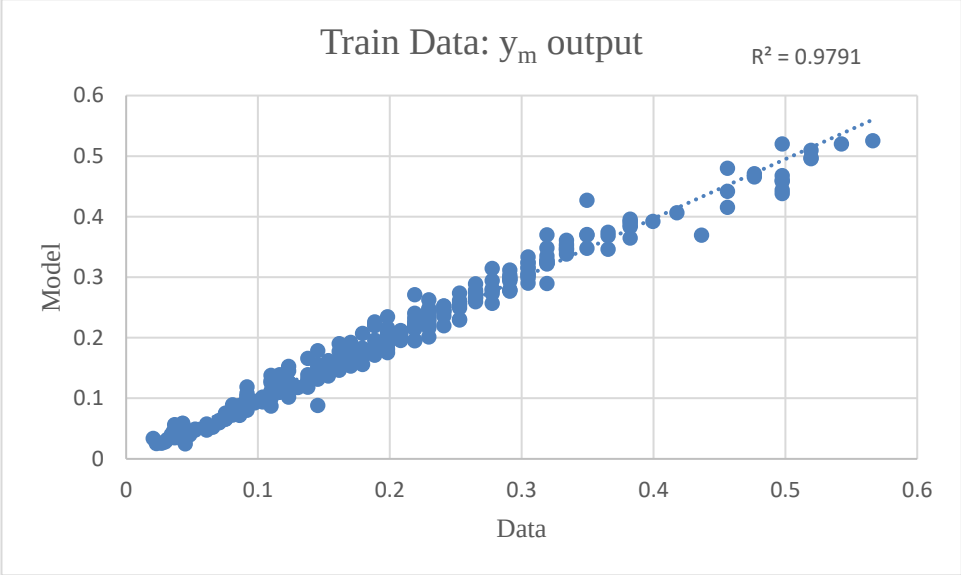
Train Data: y_m output
R² = 0.9791
Model
Data
0
0.1
0.2
0.3
0.4
0.5
0.6

e)

Figure A3: Coefficient of Determination (R^2) Graphs for the Outputs of ANFIS-PSO Model a)S_m b)S_r c)x_m d)x_r e)y_m

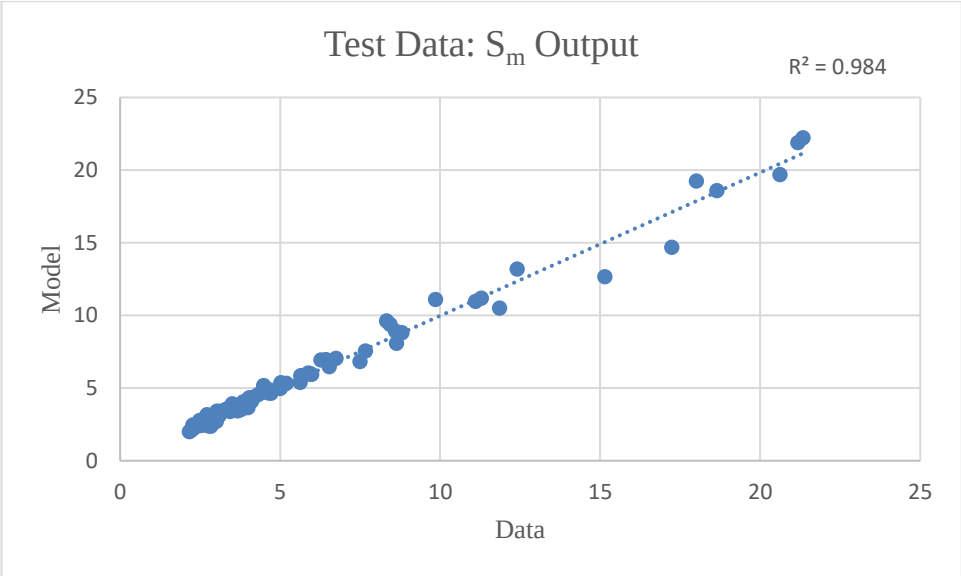

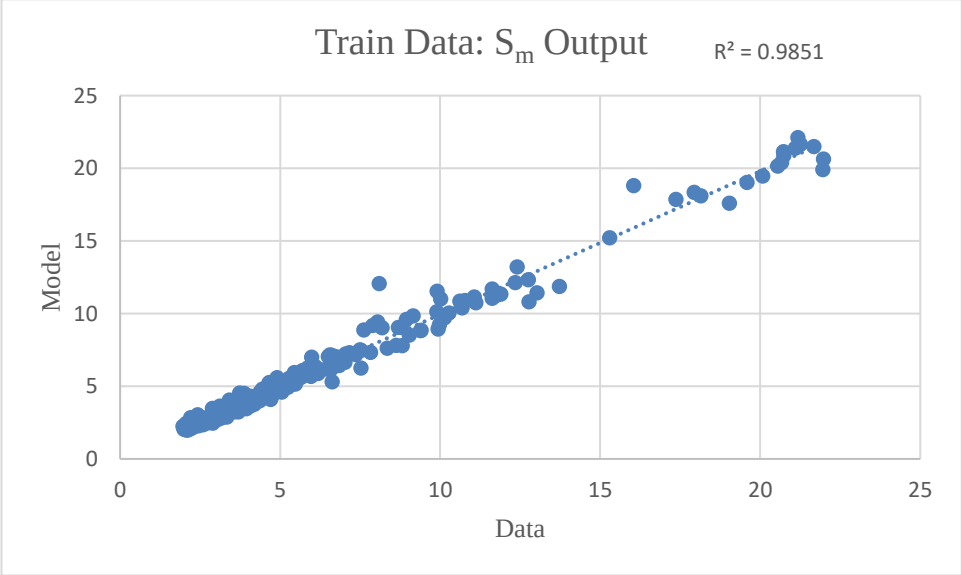

a)

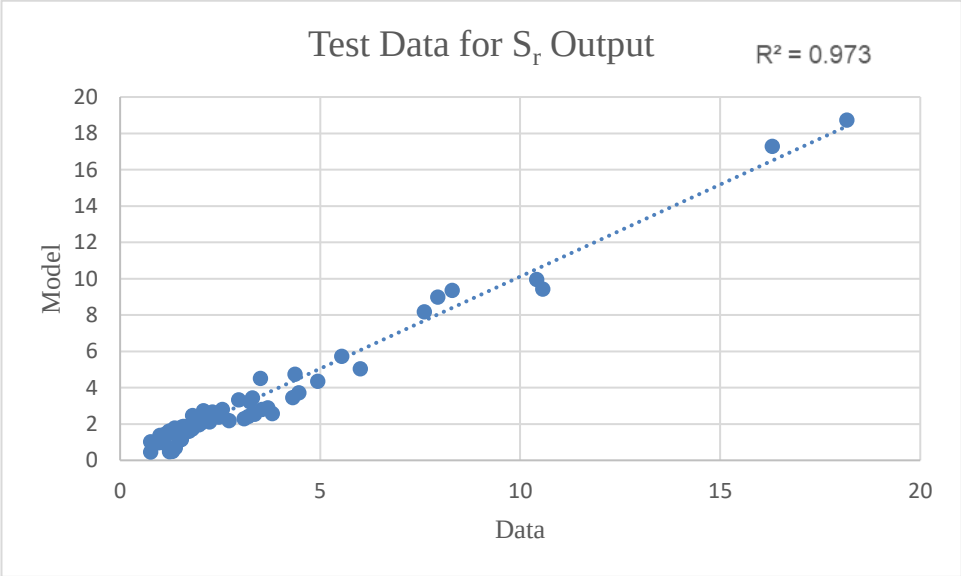
Test Data for S_r Output
R^2 = 0.973
Model
Data
0
2
4
6
8
10
12
14
16
18
20
0
5
10
15
20

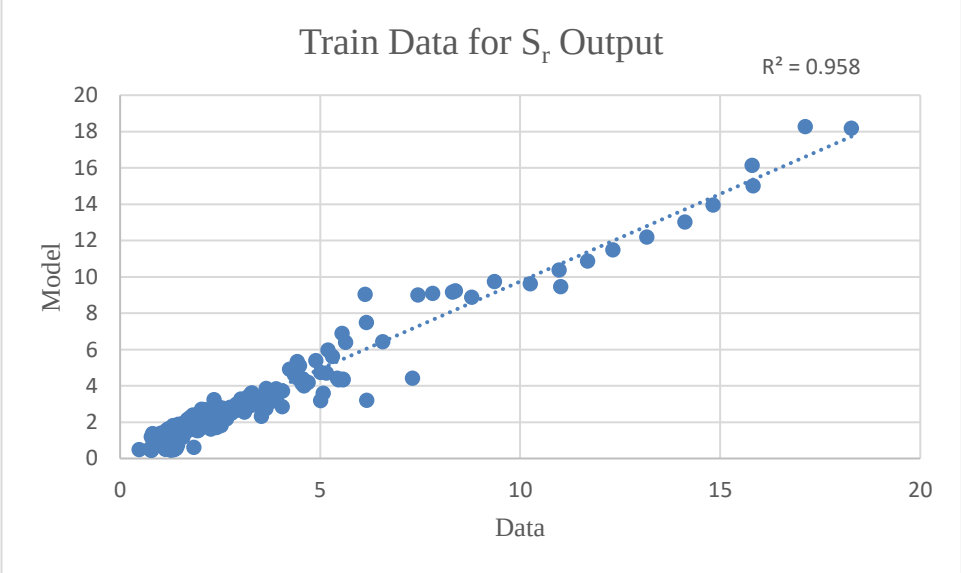
Train Data for S_r Output
R^2 = 0.958
Model
Data
0
2
4
6
8
10
12
14
16
18
20
0
5
10
15
20

b)

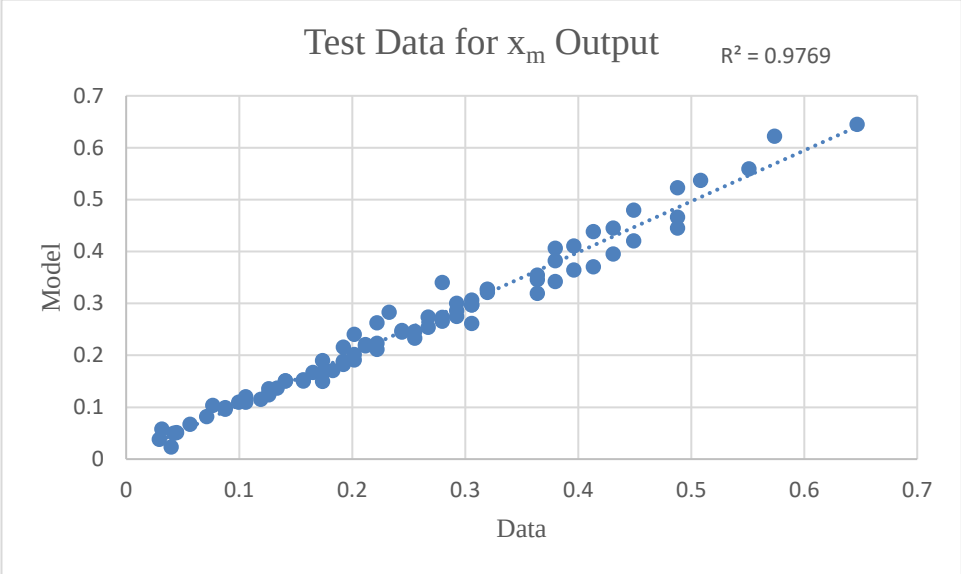
Test Data for x_m Output
R^2 = 0.9769
Model
Data
0
0.1
0.2
0.3
0.4
0.5
0.6
0.7

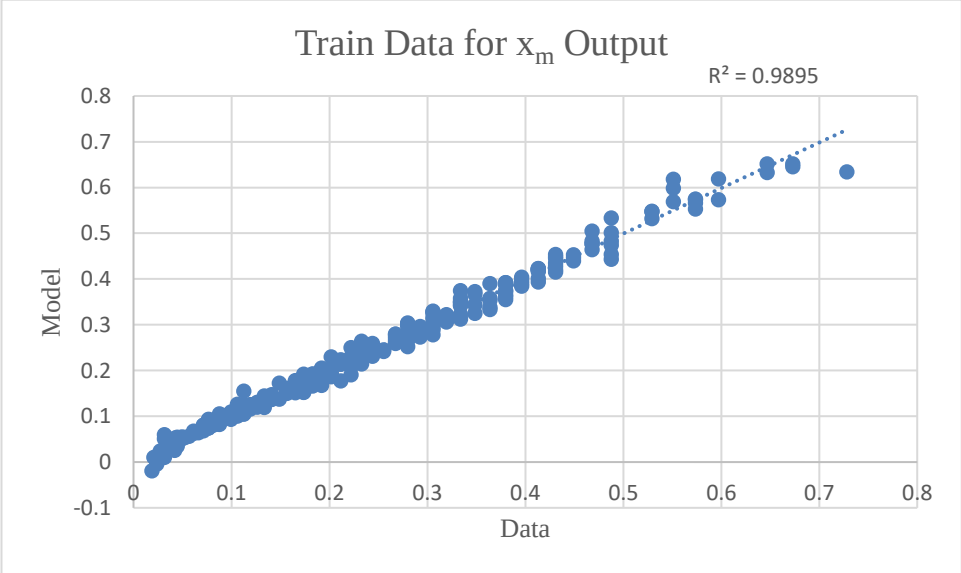
Train Data for x_m Output
R^2 = 0.9895
Model
Data
-0.1
0
0.1
0.2
0.3
0.4
0.5
0.6
0.7
0.8

c)

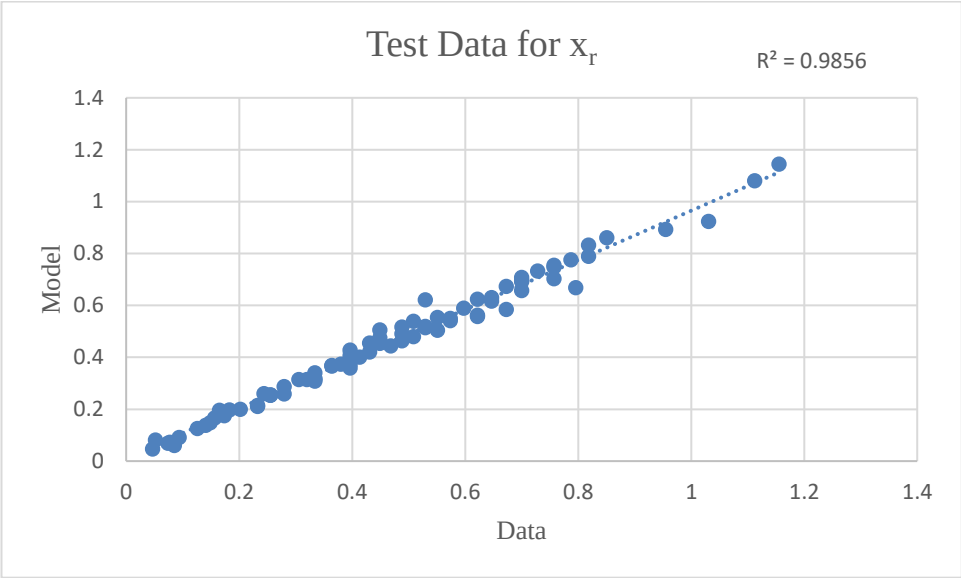
Test Data for x_r
$R^2 = 0.9856$
Model
Data
1.4
1.2
1
0.8
0.6
0.4
0.2
0
0
0.2
0.4
0.6
0.8
1
1.2
1.4

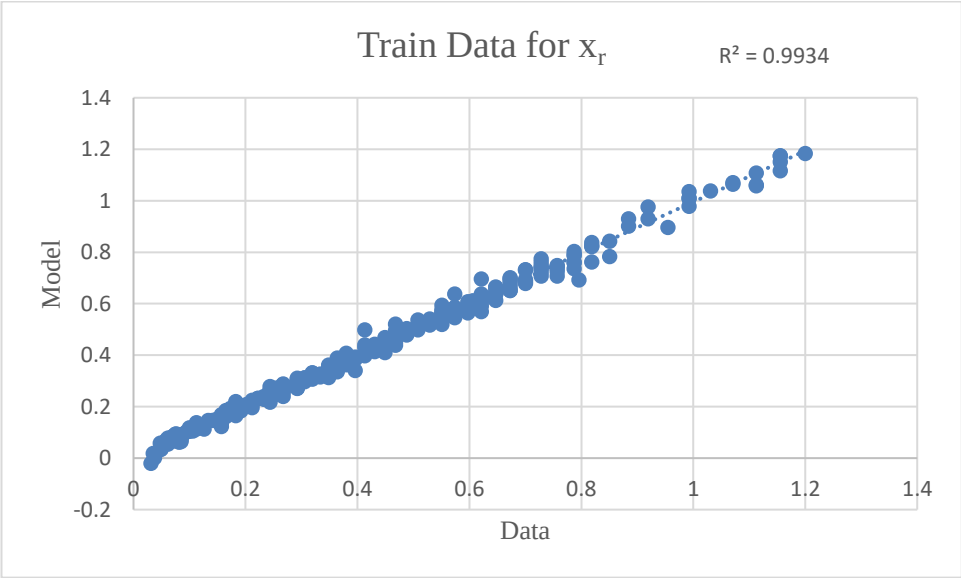
Train Data for x_r
$R^2 = 0.9934$
Model
Data
1.4
1.2
1
0.8
0.6
0.4
0.2
0
-0.2
0
0.2
0.4
0.6
0.8
1
1.2
1.4

d)

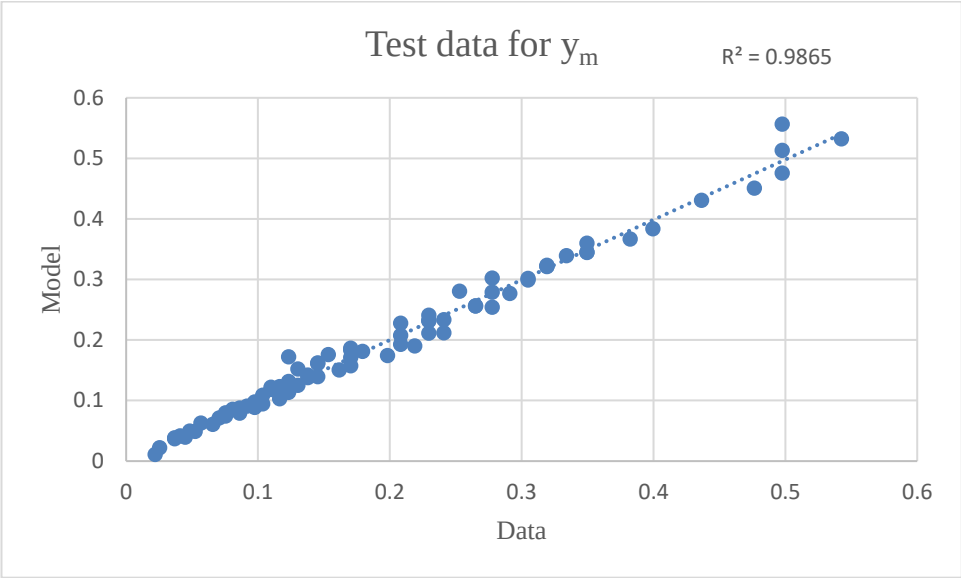
Test data for y_m
$R^2 = 0.9865$
Model
Data
0
0.1
0.2
0.3
0.4
0.5
0.6

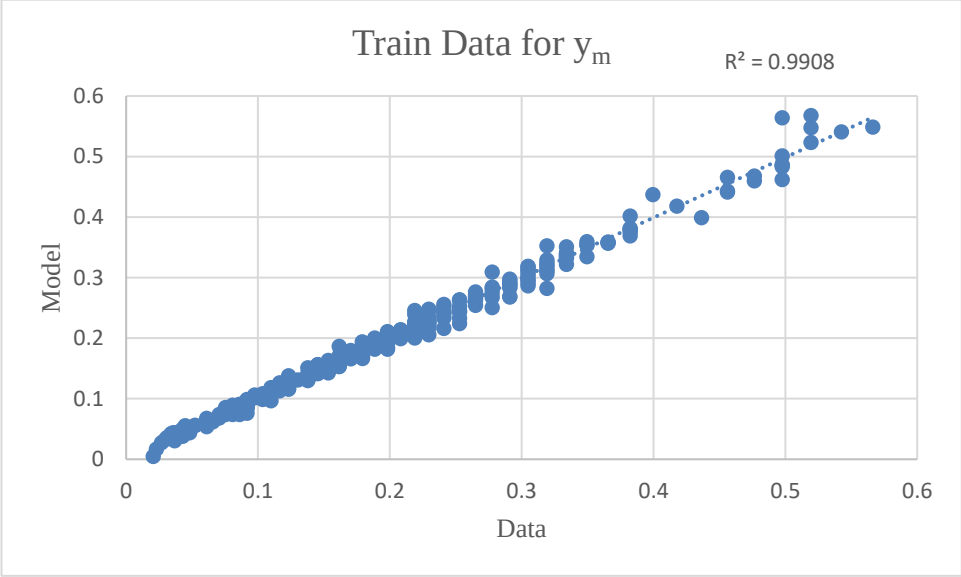
Train Data for y_m
$R^2 = 0.9908$
Model
Data
0
0.1
0.2
0.3
0.4
0.5
0.6

e)

Figure A4: Coefficient of Determination (R^2) Graphs for the Outputs of ANFIS-FFA Model a)S_m b)S_r c)x_m d)x_r e)y_m

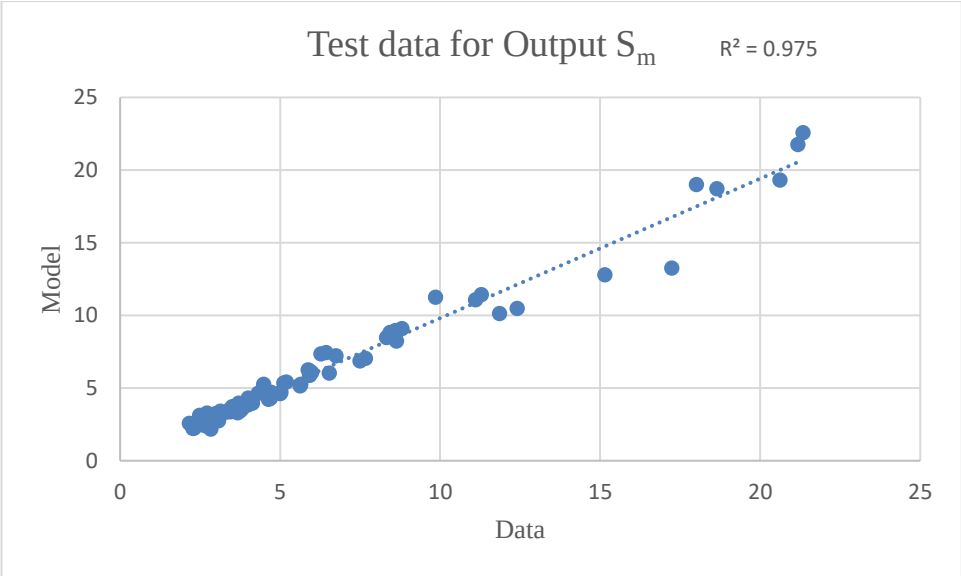

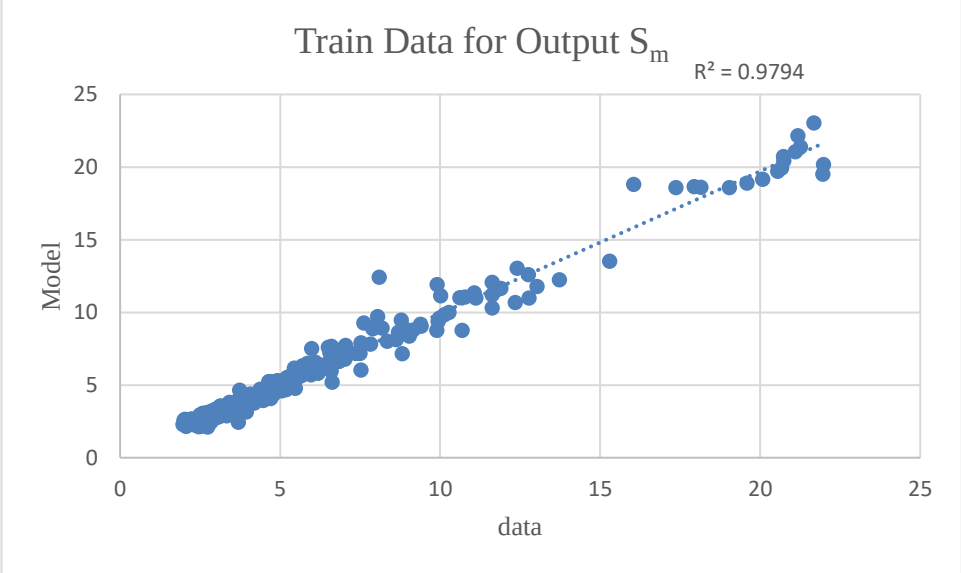

a)

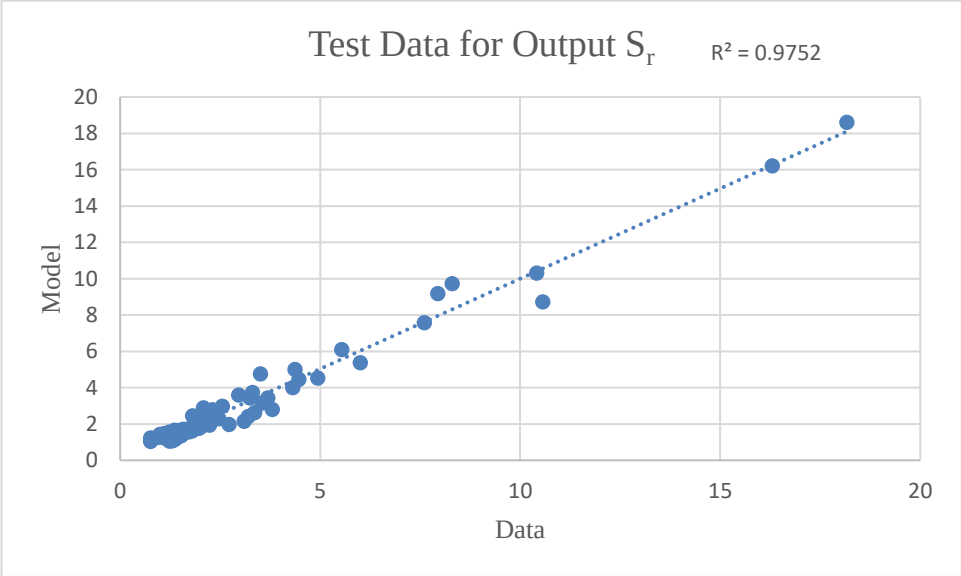
Test Data for Output S_r
$R^2 = 0.9752$
Model
Data
0
2
4
6
8
10
12
14
16
18
20
0
5
10
15
20

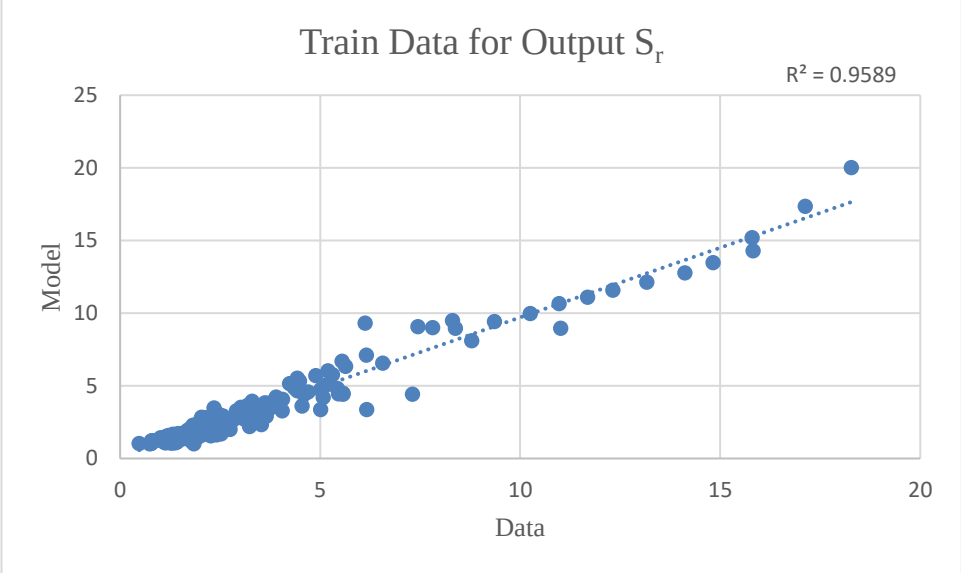
Train Data for Output S_r
$R^2 = 0.9589$
Model
Data
0
5
10
15
20
25
0
5
10
15
20

b)

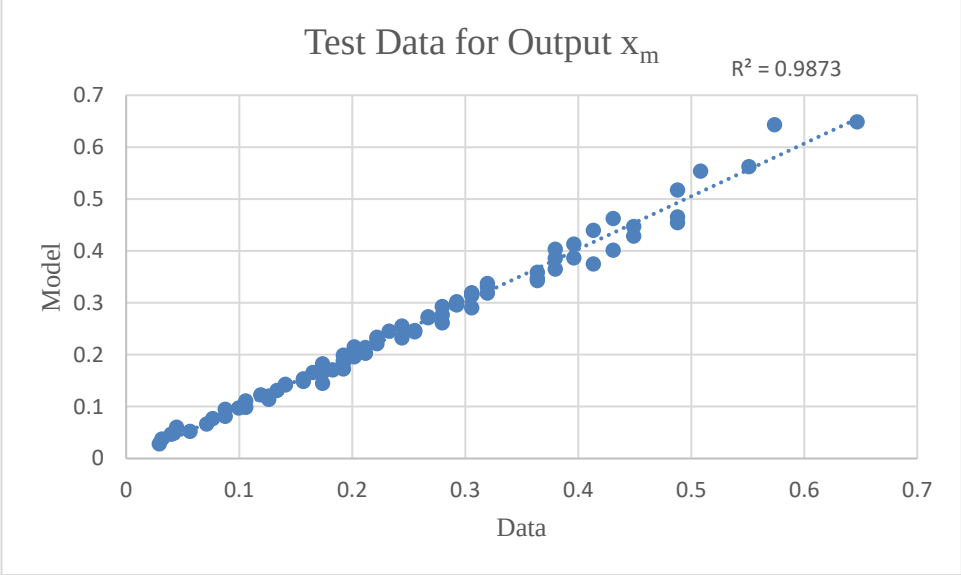
Test Data for Output x_m
R^2 = 0.9873
Model
Data
0
0.1
0.2
0.3
0.4
0.5
0.6
0.7

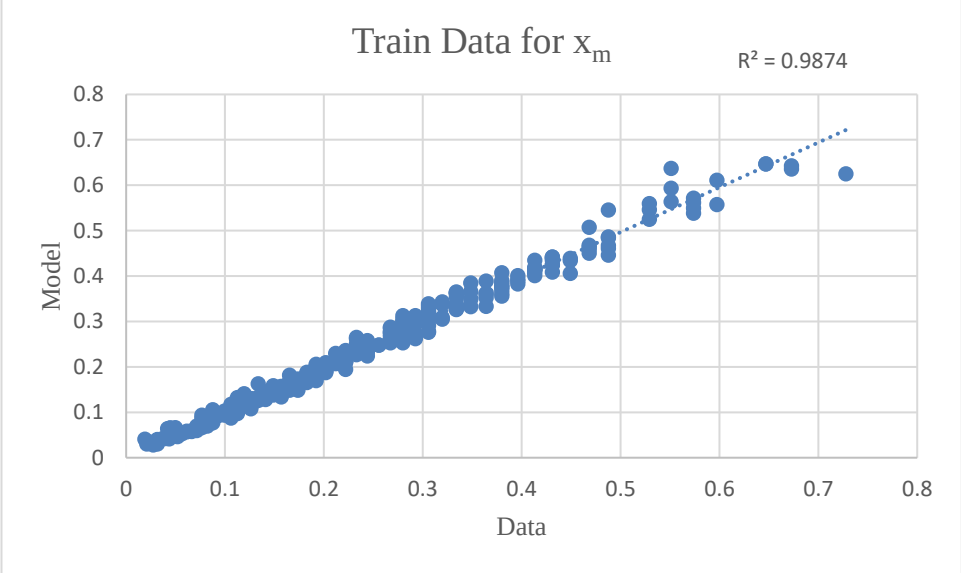
Train Data for x_m
R^2 = 0.9874
Model
Data
0
0.1
0.2
0.3
0.4
0.5
0.6
0.7
0.8

c)

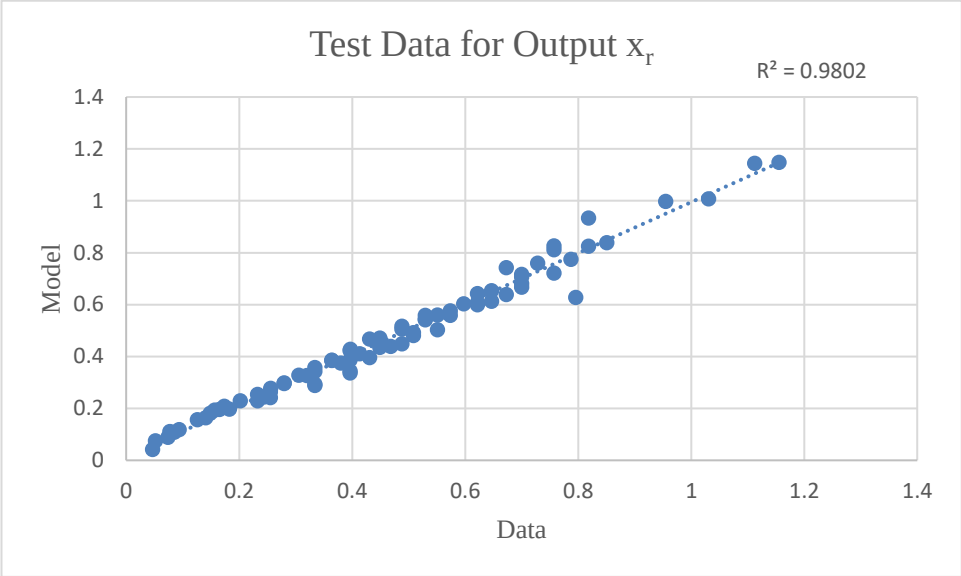
Test Data for Output x_r
R^2 = 0.9802
Model
Data
0
0.2
0.4
0.6
0.8
1
1.2
1.4

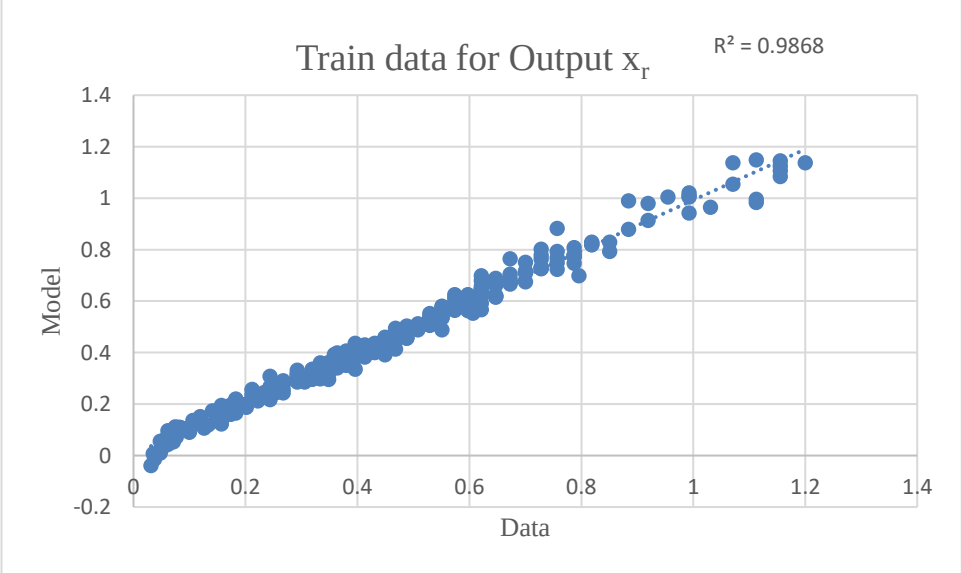
Train data for Output x_r
R^2 = 0.9868
Model
Data
-0.2
0
0.2
0.4
0.6
0.8
1
1.2
1.4

d)

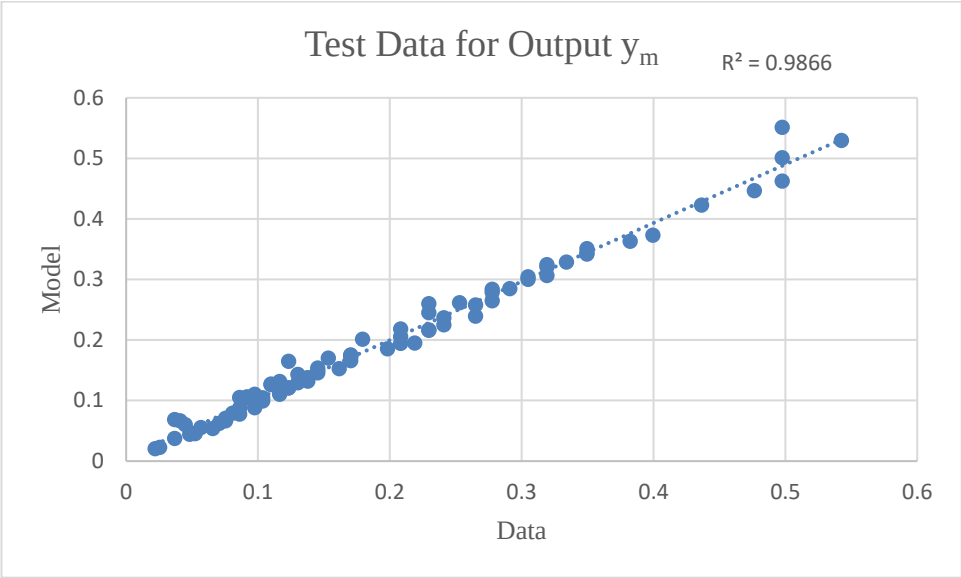
Test Data for Output y_m
R^2 = 0.9866
Model
Data
0
0.1
0.2
0.3
0.4
0.5
0.6

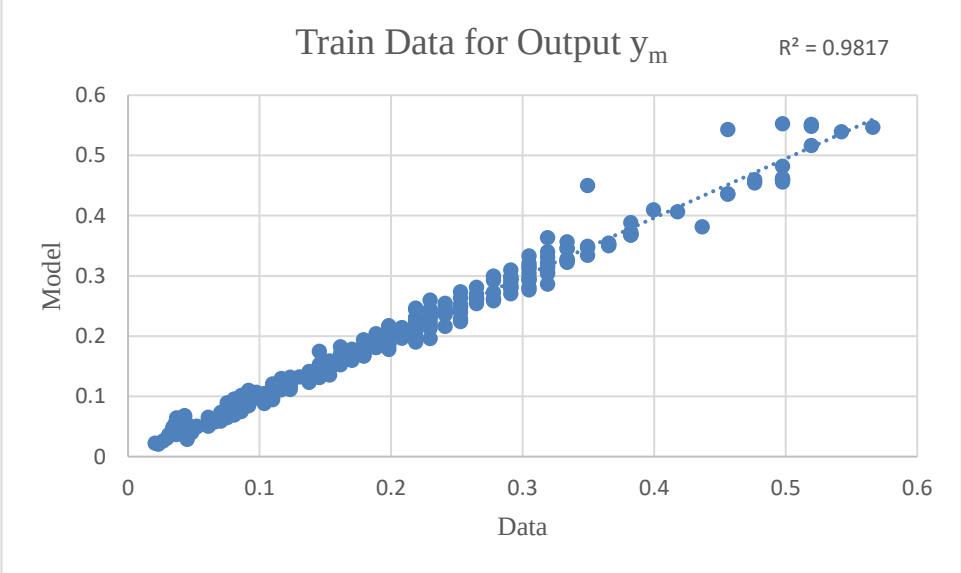
Train Data for Output y_m
R^2 = 0.9817
Model
Data
0
0.1
0.2
0.3
0.4
0.5
0.6

e)

Figure A5: Coefficient of Determination (R^2) Graphs for the Outputs of Multivariate Regression Model a)S_m b)S_r c)x_m d)x_r e)y_m

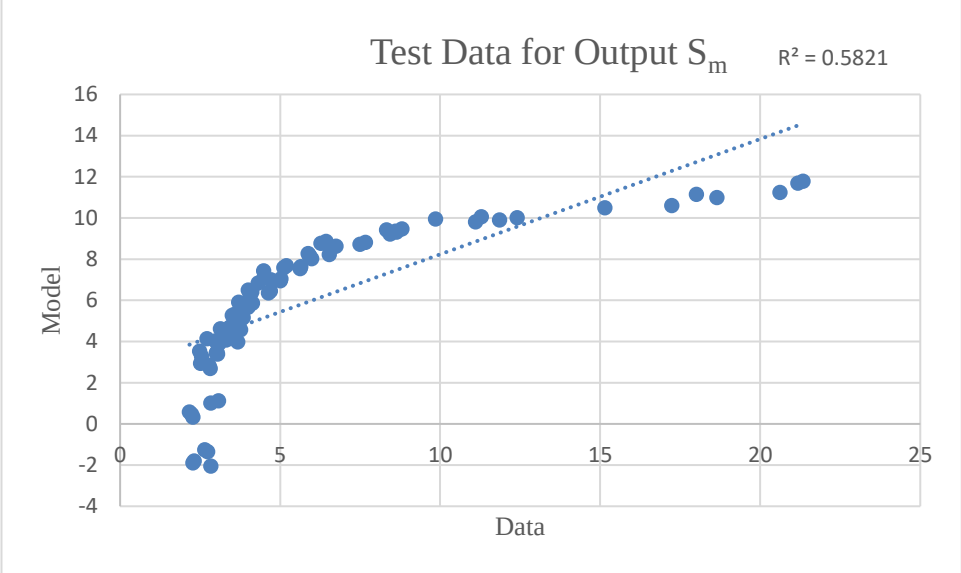

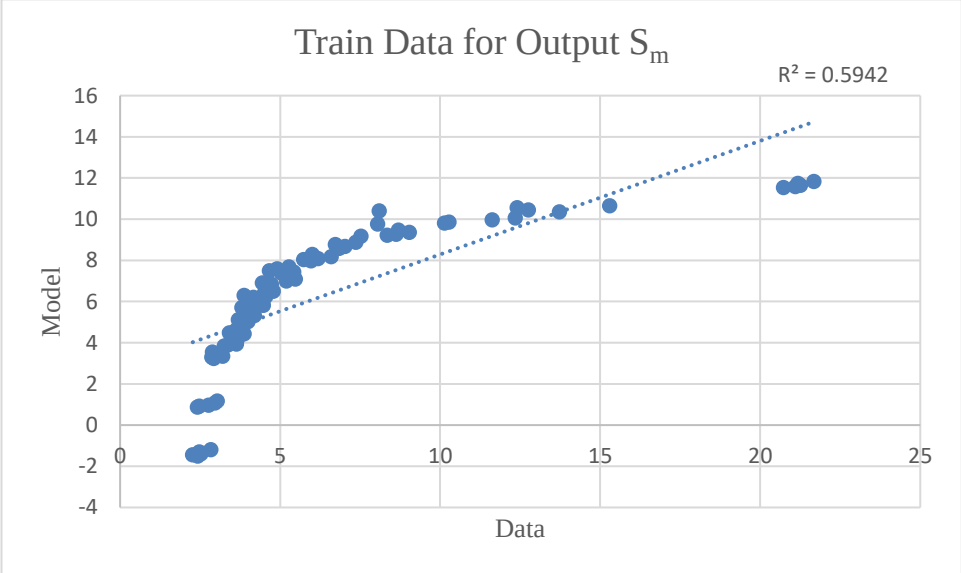

a)

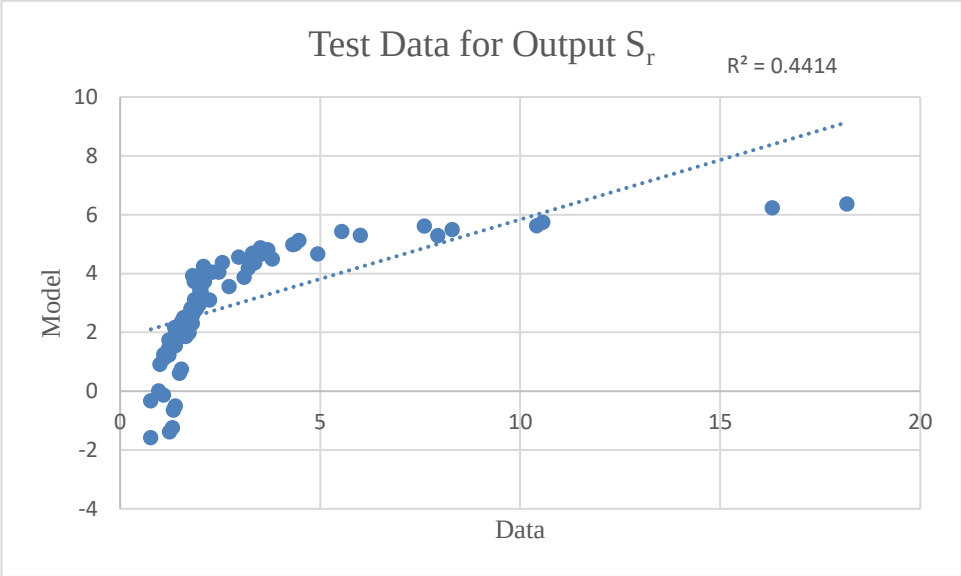
Test Data for Output S_r
R^2 = 0.4414
Model
Data
10
8
6
4
2
0
-2
-4
0
5
10
15
20

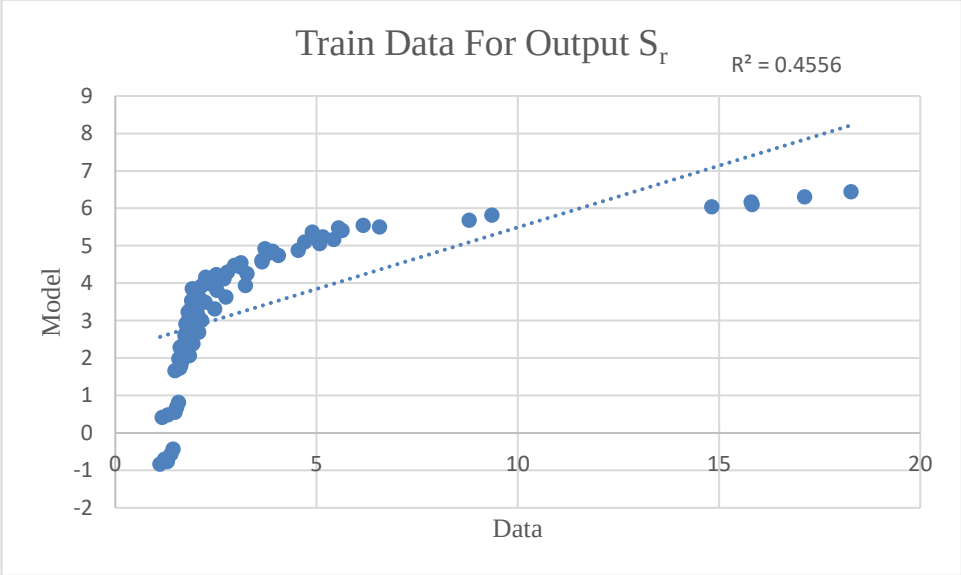
Train Data For Output S_r
R^2 = 0.4556
Model
Data
9
8
7
6
5
4
3
2
1
0
-1
-2
0
5
10
15
20

b)

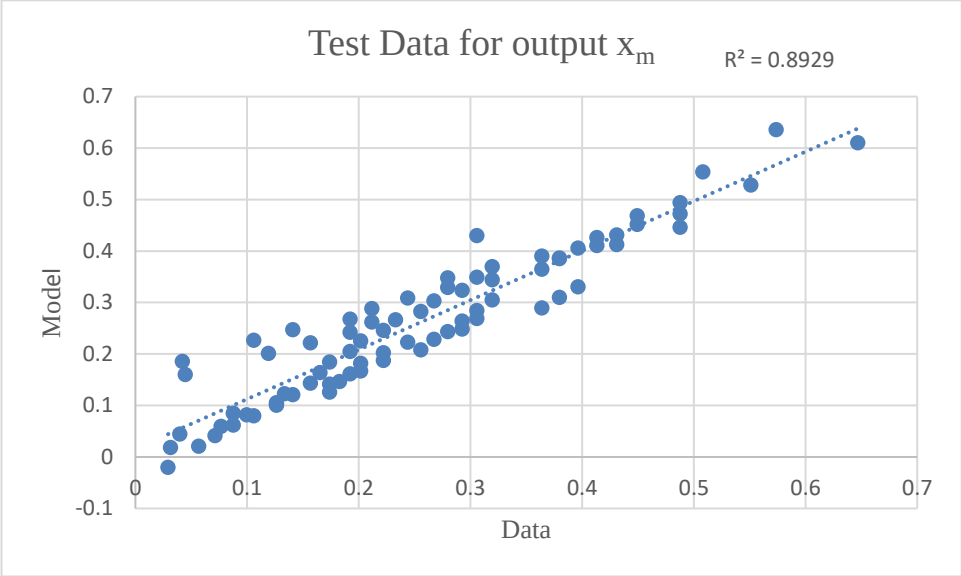
Test Data for output x_m
R^2 = 0.8929
Model
Data
0.7
0.6
0.5
0.4
0.3
0.2
0.1
0
-0.1
0
0.1
0.2
0.3
0.4
0.5
0.6
0.7

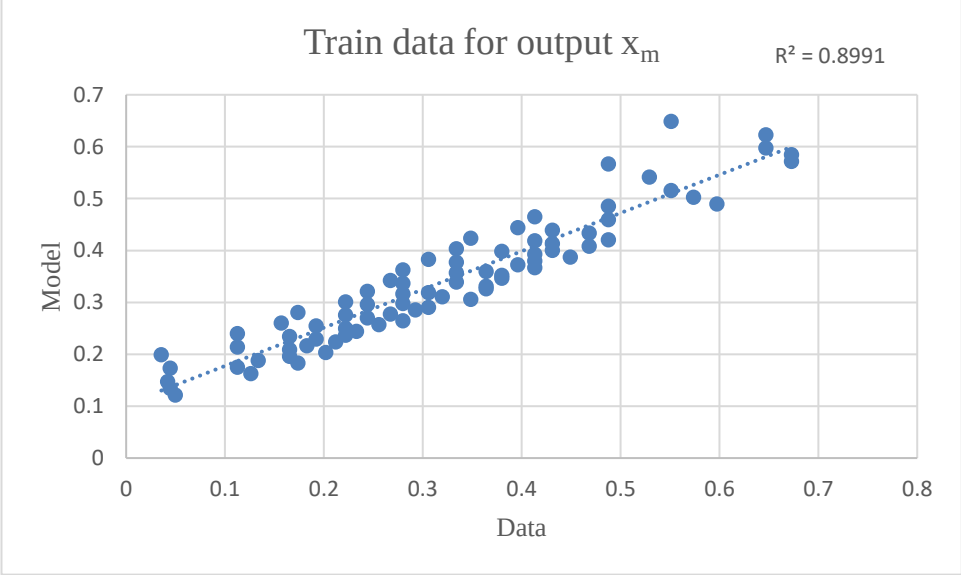
Train data for output x_m
R^2 = 0.8991
Model
Data
0.7
0.6
0.5
0.4
0.3
0.2
0.1
0
0
0.1
0.2
0.3
0.4
0.5
0.6
0.7
0.8

c)

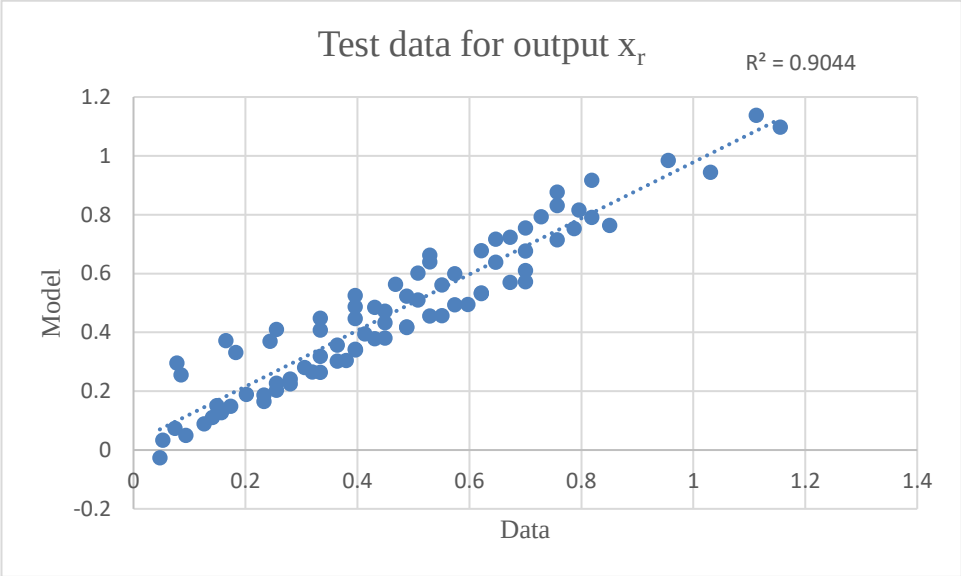
Test data for output x_r
$R^2 = 0.9044$
Model
Data
1.2
1
0.8
0.6
0.4
0.2
0
-0.2
0
0.2
0.4
0.6
0.8
1
1.2
1.4

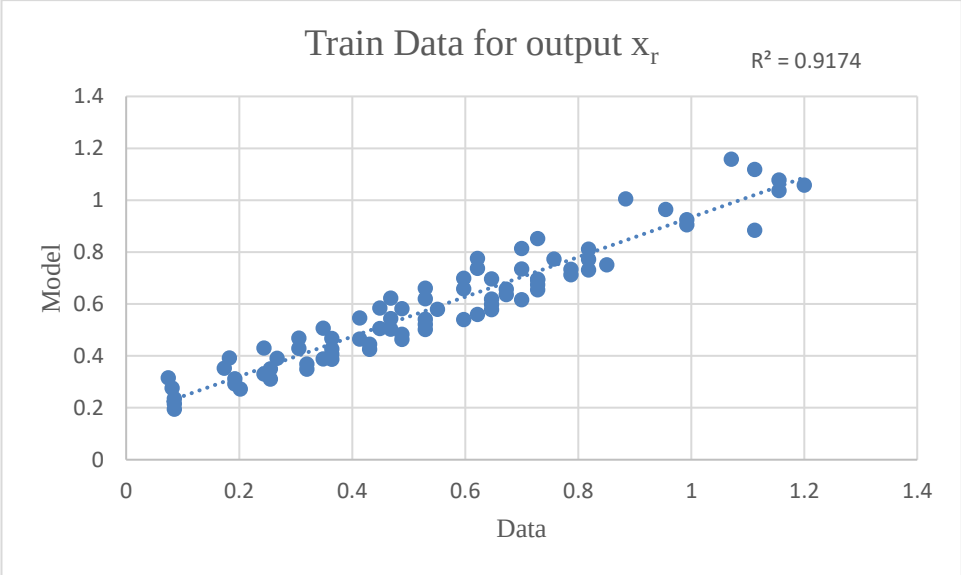
Train Data for output x_r
$R^2 = 0.9174$
Model
Data
1.4
1.2
1
0.8
0.6
0.4
0.2
0
0
0.2
0.4
0.6
0.8
1
1.2
1.4

d)

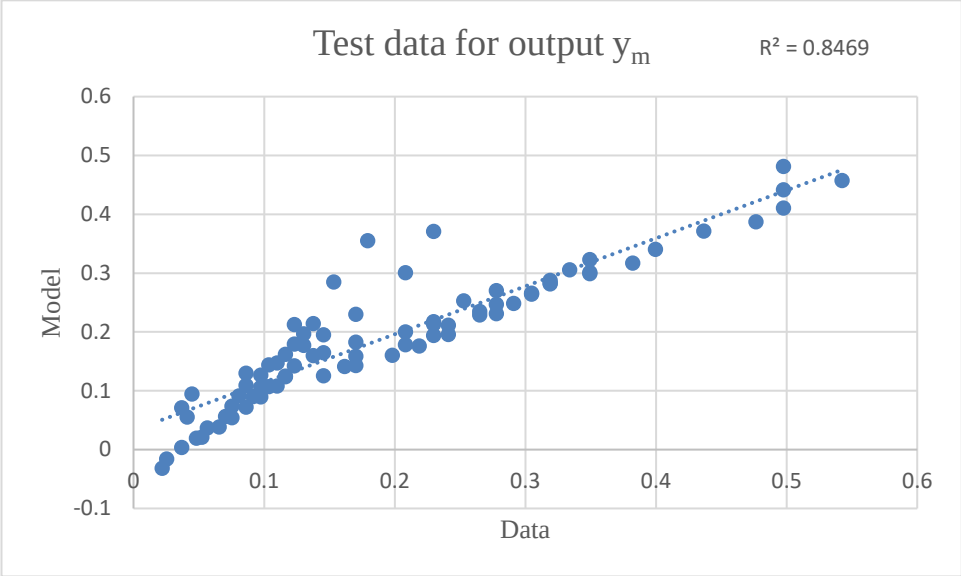
Test data for output y_m
R² = 0.8469
Model
Data
0.6
0.5
0.4
0.3
0.2
0.1
0
-0.1
0
0.1
0.2
0.3
0.4
0.5
0.6

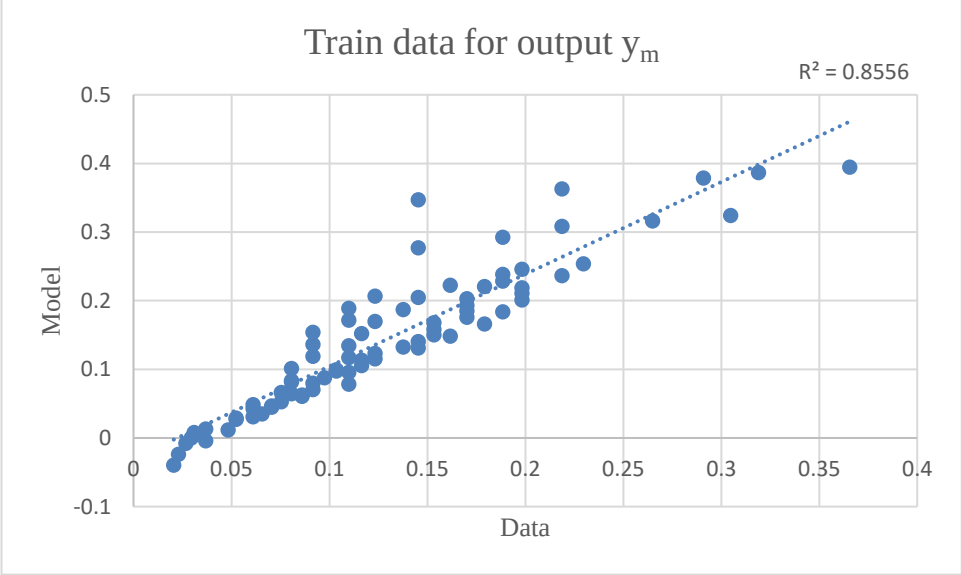
Train data for output y_m
R² = 0.8556
Model
Data
0.5
0.4
0.3
0.2
0.1
0
-0.1
0
0.05
0.1
0.15
0.2
0.25
0.3
0.35
0.4

e)

Appendix B: Training and Test Data

Table B1: Data set for S_m

Training Data			Test Data		
Fr	Angle	S_m	Fr	Angle	S_m
5	20	21.6767	5	22.5	21.3327
10	20	15.2973	10	22.5	17.2343
12.5	20	12.3489	12.5	22.5	12.408
15	20	8.69758	15	22.5	8.32761
17.5	20	7.36975	17.5	22.5	7.66958
20	20	6.00785	20	22.5	6.53465
22.5	20	5.27429	22.5	22.5	5.64901
25	20	5.47852	25	22.5	5.02429
27.5	20	4.78465	27.5	22.5	4.69427
30	20	4.45181	30	22.5	4.13045
32.5	20	4.19321	32.5	22.5	3.50586
35	20	3.70299	35	22.5	3.41944
37.5	20	3.65246	37.5	22.5	3.30972
40	20	2.88617	40	22.5	3.02299
50	20	3.03419	50	22.5	3.07581
60	20	2.83349	60	22.5	2.64123
5	25	21.1789	5	27.5	21.1808
10	25	12.4026	10	27.5	15.1466
12.5	25	11.6272	12.5	27.5	11.8553
15	25	9.03146	15	27.5	8.63699
17.5	25	6.72452	17.5	27.5	7.49809
20	25	6.59984	20	27.5	5.92225
22.5	25	4.90239	22.5	27.5	5.62618
25	25	5.19672	25	27.5	5.0024
27.5	25	4.5014	27.5	27.5	4.63904
30	25	4.47533	30	27.5	4.03468
32.5	25	3.85823	32.5	27.5	3.84142
35	25	3.62263	35	27.5	3.76815
37.5	25	3.48271	37.5	27.5	3.67828
40	25	2.94443	40	27.5	3.04872
50	25	2.96098	50	27.5	2.83779
60	25	2.476	60	27.5	2.73315
5	30	21.2605	5	50	20.6141
10	30	12.7552	10	50	11.2868
12.5	30	10.2708	12.5	50	8.80485
15	30	8.62574	15	50	6.43841
17.5	30	7.02903	17.5	50	5.87571

20	30	6.18645	20	50	5.19557
22.5	30	4.66224	22.5	50	4.49793
25	30	4.44173	25	50	4.00934
27.5	30	3.87404	27.5	50	3.70314
30	30	3.80708	30	50	3.57705
32.5	30	3.69214	32.5	50	3.46293
35	30	3.64459	35	50	2.71083
37.5	30	3.63818	37.5	50	2.48018
40	30	3.20746	40	50	2.51047
50	30	2.7671	50	50	2.16615
60	30	2.52105	60	50	2.31606
5	32.5	21.0964	5	55	18.0102
10	32.5	8.09551	10	55	9.85718
12.5	32.5	10.1305	12.5	55	8.60063
15	32.5	8.34668	15	55	6.27639
17.5	32.5	6.8494	17.5	55	5.91154
20	32.5	5.73876	20	55	5.11137
22.5	32.5	5.42903	22.5	55	4.71894
25	32.5	4.72009	25	55	4.11194
27.5	32.5	4.55025	27.5	55	3.91125
30	32.5	4.09667	30	55	3.68715
32.5	32.5	3.97496	32.5	55	3.13578
35	32.5	3.41668	35	55	2.97891
37.5	32.5	3.36279	37.5	55	3.003
40	32.5	2.86455	40	55	2.77655
50	32.5	2.47057	50	55	2.23108
60	32.5	2.26868	60	55	2.27915
5	35	20.7274	5	62.5	18.6411
10	35	13.7269	10	62.5	11.1013
12.5	35	8.04453	12.5	62.5	8.43135
15	35	7.52809	15	62.5	6.74413
17.5	35	6.84909	17.5	62.5	5.98733
20	35	5.9619	20	62.5	4.48745
22.5	35	5.03038	22.5	62.5	4.30992
25	35	4.60952	25	62.5	4.06689
27.5	35	4.16077	27.5	62.5	3.99892
30	35	4.19066	30	62.5	3.77065
32.5	35	3.99202	32.5	62.5	3.43544
35	35	3.87491	35	62.5	3.08577
37.5	35	3.25335	37.5	62.5	2.54855
40	35	2.92723	40	62.5	2.80965
50	35	2.41089	50	62.5	2.27297
60	35	2.42604	60	62.5	2.83862
5	37.5	20.7361			
10	37.5	11.623			

12.5	37.5	9.97087			
15	37.5	7.82385			
17.5	37.5	6.10001			
20	37.5	5.65584			
22.5	37.5	4.92668			
25	37.5	4.72663			
27.5	37.5	4.26575			
30	37.5	3.41674			
32.5	37.5	3.78316			
35	37.5	3.04815			
37.5	37.5	3.30678			
40	37.5	2.69586			
50	37.5	2.22139			
60	37.5	2.03441			
5	40	21.9741			
10	40	9.90228			
12.5	40	8.78431			
15	40	7.04653			
17.5	40	5.85671			
20	40	5.29356			
22.5	40	5.24598			
25	40	4.77765			
27.5	40	4.69982			
30	40	4.11327			
32.5	40	3.76206			
35	40	3.67457			
37.5	40	3.22047			
40	40	2.66196			
50	40	2.23347			
60	40	2.45425			
5	42.5	20.6695			
10	42.5	13.0238			
12.5	42.5	9.93948			
15	42.5	6.60833			
17.5	42.5	6.43253			
20	42.5	5.55445			
22.5	42.5	4.99085			
25	42.5	4.6196			
27.5	42.5	4.3619			
30	42.5	4.02395			
32.5	42.5	3.49568			
35	42.5	3.19583			
37.5	42.5	3.09191			
40	42.5	2.7744			
50	42.5	2.02564			

60	42.5	2.35383			
5	45	20.5419			
10	45	11.8967			
12.5	45	7.61941			
15	45	6.50535			
17.5	45	6.2254			
20	45	5.20751			
22.5	45	4.62463			
25	45	4.06758			
27.5	45	3.70774			
30	45	3.46223			
32.5	45	3.11816			
35	45	2.98103			
37.5	45	2.81318			
40	45	2.76119			
50	45	2.13204			
60	45	1.96151			
5	47.5	21.9528			
10	47.5	11.7586			
12.5	47.5	9.38413			
15	47.5	5.98555			
17.5	47.5	5.69962			
20	47.5	5.40914			
22.5	47.5	4.93457			
25	47.5	4.69017			
27.5	47.5	4.12578			
30	47.5	3.80147			
32.5	47.5	3.4228			
35	47.5	3.337			
37.5	47.5	3.16833			
40	47.5	2.89261			
50	47.5	2.07487			
60	47.5	2.09288			
5	52.5	20.0747			
10	52.5	11.0628			
12.5	52.5	9.40994			
15	52.5	6.8706			
17.5	52.5	6.08934			
20	52.5	5.39981			
22.5	52.5	4.69074			
25	52.5	4.29413			
27.5	52.5	3.84962			
30	52.5	3.56979			
32.5	52.5	3.48985			
35	52.5	3.27787			

37.5	52.5	2.76461			
40	52.5	2.57193			
50	52.5	1.99918			
60	52.5	2.34448			
5	57.5	19.5854			
10	57.5	11.6258			
12.5	57.5	8.1891			
15	57.5	6.84003			
17.5	57.5	5.44166			
20	57.5	5.39241			
22.5	57.5	4.3733			
25	57.5	4.26277			
27.5	57.5	3.96129			
30	57.5	3.65809			
32.5	57.5	3.20369			
35	57.5	3.14102			
37.5	57.5	3.04166			
40	57.5	2.50782			
50	57.5	2.20786			
60	57.5	2.41524			
5	60	16.0464			
10	60	10.0156			
12.5	60	7.89491			
15	60	6.82637			
17.5	60	5.8755			
20	60	4.91298			
22.5	60	4.53551			
25	60	4.23995			
27.5	60	3.76009			
30	60	3.64481			
32.5	60	3.27165			
35	60	2.90818			
37.5	60	2.58704			
40	60	2.49571			
50	60	2.21553			
60	60	2.59222			
5	65	17.9389			
10	65	10.7735			
12.5	65	8.94707			
15	65	6.55529			
17.5	65	5.67792			
20	65	4.70901			
22.5	65	3.72986			
25	65	4.10615			
27.5	65	3.82027			

30	65	3.68629			
32.5	65	3.13137			
35	65	3.212			
37.5	65	2.62716			
40	65	2.49167			
50	65	2.38482			
60	65	2.5047			
5	67.5	18.1451			
10	67.5	10.6112			
12.5	67.5	9.15341			
15	67.5	7.16637			
17.5	67.5	6.14822			
20	67.5	4.64046			
22.5	67.5	4.55502			
25	67.5	4.1519			
27.5	67.5	4.08132			
30	67.5	3.13387			
32.5	67.5	2.9897			
35	67.5	2.98434			
37.5	67.5	2.80565			
40	67.5	2.74919			
50	67.5	2.20136			
60	67.5	2.065			
5	70	17.3671			
10	70	12.779			
12.5	70	9.89316			
15	70	7.49287			
17.5	70	5.92867			
20	70	5.00393			
22.5	70	4.39882			
25	70	4.0409			
27.5	70	3.59378			
30	70	3.57219			
32.5	70	3.46984			
35	70	3.08135			
37.5	70	3.16878			
40	70	3.33163			
50	70	2.42428			
60	70	2.45079			
5	72.5	19.0327			
10	72.5	11.11178			
12.5	72.5	10.6853			
15	72.5	8.81518			
17.5	72.5	7.52977			
20	72.5	6.62171			

22.5	72.5	5.05557			
25	72.5	3.98799			
27.5	72.5	3.94526			
30	72.5	3.96534			
32.5	72.5	3.93059			
35	72.5	3.94509			
37.5	72.5	3.56575			
40	72.5	3.13281			
50	72.5	3.69913			
60	72.5	2.73213			

Table B2: Data set for S_r:

Training Data			Test Data		
Fr	Angle	Sr	Fr	Angle	Sr
5	20	18.2784	5	22.5	18.1614
10	20	9.3602	10	22.5	10.5622
12.5	20	6.56561	12.5	22.5	5.54285
15	20	5.01164	15	22.5	4.46697
17.5	20	4.54524	17.5	22.5	3.6911
20	20	3.64993	20	22.5	3.8076
22.5	20	3.27296	22.5	22.5	3.20545
25	20	3.23482	25	22.5	3.10308
27.5	20	2.74503	27.5	22.5	2.72534
30	20	2.46964	30	22.5	2.02574
32.5	20	2.13928	32.5	22.5	1.96818
35	20	2.0704	35	22.5	1.82301
37.5	20	1.93142	37.5	22.5	1.80331
40	20	1.83777	40	22.5	1.72584
50	20	1.57242	50	22.5	1.53535
60	20	1.43361	60	22.5	1.37595
5	25	17.125	5	27.5	16.2983
10	25	8.78887	10	27.5	7.60747
12.5	25	4.89228	12.5	27.5	6.00515

15	25	5.07452	15	27.5	4.3152
17.5	25	4.04824	17.5	27.5	3.54712
20	25	3.11069	20	27.5	3.3606
22.5	25	2.70052	22.5	27.5	2.46529
25	25	2.52758	25	27.5	2.10897
27.5	25	2.22807	27.5	27.5	1.99196
30	25	2.03775	30	27.5	1.85919
32.5	25	1.9087	32.5	27.5	1.82303
35	25	1.79514	35	27.5	1.75264
37.5	25	1.70692	37.5	27.5	1.69545
40	25	1.65955	40	27.5	1.64257
50	25	1.52474	50	27.5	1.48532
60	25	1.38214	60	27.5	1.33417
5	30	15.7956	5	50	10.4144
10	30	6.15602	10	50	4.37113
12.5	30	5.15949	12.5	50	3.30525
15	30	3.718	15	50	2.55455
17.5	30	3.64656	17.5	50	2.16345
20	30	2.7856	20	50	2.00091
22.5	30	2.33873	22.5	50	2.00091
25	30	2.05832	25	50	1.90476
27.5	30	1.97923	27.5	50	1.7699
30	30	1.83791	30	50	1.59017
32.5	30	1.79632	32.5	50	1.43934
35	30	1.7883	35	50	1.4027
37.5	30	1.65878	37.5	50	1.29076
40	30	1.62525	40	50	1.0896
50	30	1.47982	50	50	0.96654
60	30	1.22409	60	50	1.30494
5	32.5	15.8241	5	55	8.29772
10	32.5	5.54642	10	55	3.5048
12.5	32.5	5.43127	12.5	55	2.96689
15	32.5	3.9067	15	55	2.08454

17.5	32.5	3.12011	17.5	55	1.81155
20	32.5	2.50622	20	55	2.04096
22.5	32.5	2.13547	22.5	55	2.02738
25	32.5	1.98005	25	55	1.93684
27.5	32.5	1.86435	27.5	55	1.75396
30	32.5	1.80337	30	55	1.53789
32.5	32.5	1.75295	32.5	55	1.38603
35	32.5	1.6918	35	55	1.21921
37.5	32.5	1.62978	37.5	55	1.20274
40	32.5	1.6047	40	55	1.1007
50	32.5	1.30789	50	55	1.08004
60	32.5	1.29079	60	55	1.23216
5	35	14.823	5	62.5	7.9407
10	35	5.63618	10	62.5	4.93606
12.5	35	4.70002	12.5	62.5	3.24558
15	35	3.77262	15	62.5	2.30825
17.5	35	2.96479	17.5	62.5	1.84824
20	35	2.24768	20	62.5	2.01984
22.5	35	1.91489	22.5	62.5	2.23456
25	35	1.89718	25	62.5	1.90797
27.5	35	1.80518	27.5	62.5	1.78907
30	35	1.75201	30	62.5	1.35968
32.5	35	1.73345	32.5	62.5	1.54373
35	35	1.61406	35	62.5	1.38256
37.5	35	1.58155	37.5	62.5	1.21808
40	35	1.48545	40	62.5	0.99885
50	35	1.16865	50	62.5	0.76644
60	35	1.1112	60	62.5	0.76612
5	37.5	14.1187			
10	37.5	5.19975			
12.5	37.5	4.5968			
15	37.5	3.51518			
17.5	37.5	2.38789			

20	37.5	2.00025			
22.5	37.5	1.8875			
25	37.5	1.86218			
27.5	37.5	1.67968			
30	37.5	1.72491			
32.5	37.5	1.65706			
35	37.5	1.5948			
37.5	37.5	1.5004			
40	37.5	1.39886			
50	37.5	1.31166			
60	37.5	1.3			
5	40	13.1668			
10	40	5.30718			
12.5	40	3.90002			
15	40	2.90506			
17.5	40	2.50845			
20	40	1.92517			
22.5	40	1.80395			
25	40	1.76204			
27.5	40	1.70639			
30	40	1.65583			
32.5	40	1.57882			
35	40	1.49344			
37.5	40	1.52226			
40	40	1.32977			
50	40	1.29002			
60	40	1.40591			
5	42.5	12.3198			
10	42.5	4.4315			
12.5	42.5	4.05953			
15	42.5	2.95852			
17.5	42.5	2.2503			
20	42.5	1.81986			

22.5	42.5	1.85762			
25	42.5	1.68141			
27.5	42.5	1.8735			
30	42.5	1.59436			
32.5	42.5	1.50577			
35	42.5	1.43995			
37.5	42.5	1.44689			
40	42.5	1.49029			
50	42.5	1.18176			
60	42.5	1.33319			
5	45	11.6825			
10	45	4.48536			
12.5	45	3.30108			
15	45	3.23573			
17.5	45	2.23714			
20	45	1.98085			
22.5	45	1.74757			
25	45	1.88768			
27.5	45	1.67698			
30	45	1.54289			
32.5	45	1.4262			
35	45	1.42513			
37.5	45	1.39951			
40	45	1.34562			
50	45	1.15231			
60	45	1.12061			
5	47.5	10.9714			
10	47.5	4.23583			
12.5	47.5	3.62364			
15	47.5	2.46802			
17.5	47.5	2.17357			
20	47.5	1.97713			
22.5	47.5	1.75261			

25	47.5	1.73763			
27.5	47.5	1.73128			
30	47.5	1.45482			
32.5	47.5	1.37101			
35	47.5	1.3571			
37.5	47.5	1.33622			
40	47.5	1.31497			
50	47.5	1.04864			
60	47.5	1.13869			
5	52.5	10.2538			
10	52.5	4.35394			
12.5	52.5	3.18632			
15	52.5	2.56814			
17.5	52.5	2.00454			
20	52.5	2.04445			
22.5	52.5	2.04193			
25	52.5	1.84603			
27.5	52.5	1.80906			
30	52.5	1.5424			
32.5	52.5	1.49904			
35	52.5	1.33858			
37.5	52.5	1.20355			
40	52.5	1.1533			
50	52.5	1.08108			
60	52.5	1.35545			
5	57.5	8.31077			
10	57.5	4.42671			
12.5	57.5	3.01851			
15	57.5	2.03363			
17.5	57.5	1.94686			
20	57.5	1.91117			
22.5	57.5	1.99708			
25	57.5	1.67202			

27.5	57.5	1.57387			
30	57.5	1.3268			
32.5	57.5	1.4645			
35	57.5	1.26074			
37.5	57.5	1.15933			
40	57.5	1.10861			
50	57.5	1.0903			
60	57.5	1.27187			
5	60	6.12462			
10	60	4.56116			
12.5	60	2.34841			
15	60	2.11261			
17.5	60	2.08663			
20	60	1.98506			
22.5	60	1.82989			
25	60	1.96444			
27.5	60	1.80263			
30	60	1.50624			
32.5	60	1.3299			
35	60	1.25052			
37.5	60	1.15124			
40	60	1.07537			
50	60	1.01558			
60	60	0.79114			
5	65	7.4472			
10	65	5.57373			
12.5	65	3.16985			
15	65	2.13994			
17.5	65	1.94859			
20	65	2.16787			
22.5	65	2.16516			
25	65	2.16423			
27.5	65	1.97448			

30	65	1.73703			
32.5	65	1.5902			
35	65	1.33456			
37.5	65	1.13672			
40	65	1.008			
50	65	0.81443			
60	65	0.76854			
5	67.5	7.80999			
10	67.5	5.45657			
12.5	67.5	3.55444			
15	67.5	2.87543			
17.5	67.5	2.24137			
20	67.5	2.39576			
22.5	67.5	2.05322			
25	67.5	1.86706			
27.5	67.5	1.65359			
30	67.5	1.50533			
32.5	67.5	1.20587			
35	67.5	1.1574			
37.5	67.5	1.21729			
40	67.5	1.09577			
50	67.5	0.78088			
60	67.5	0.47814			
5	70	8.38046			
10	70	5.57373			
12.5	70	5.00874			
15	70	2.03672			
17.5	70	2.08176			
20	70	2.65811			
22.5	70	2.22555			
25	70	2.47097			
27.5	70	2.2577			
30	70	2.05832			

32.5	70	1.89097			
35	70	1.70954			
37.5	70	1.43699			
40	70	1.41585			
50	70	0.81002			
60	70	0.73773			
5	72.5	11.0094			
10	72.5	7.30844			
12.5	72.5	6.1651			
15	72.5	3.54383			
17.5	72.5	3.52969			
20	72.5	2.47385			
22.5	72.5	2.31646			
25	72.5	1.72809			
27.5	72.5	2.52182			
30	72.5	2.41281			
32.5	72.5	2.2644			
35	72.5	1.95893			
37.5	72.5	1.92965			
40	72.5	1.6461			
50	72.5	1.77155			
60	72.5	1.84395			

Table B3: Data Set for x_m

Training Data			Test Data		
Fr	Angle	x	Fr	Angle	x
5	20	0.0356	5	22.5	0.042061
10	20	0.112437	10	22.5	0.105923
12.5	20	0.156792	12.5	22.5	0.140942
15	20	0.173811	15	22.5	0.192087
17.5	20	0.22206	17.5	22.5	0.211711

20	20	0.243897	20	22.5	0.243897
22.5	20	0.267346	22.5	22.5	0.279712
25	20	0.279712	25	22.5	0.305804
27.5	20	0.305804	27.5	22.5	0.319564
30	20	0.333822	30	22.5	0.363909
32.5	20	0.348598	32.5	22.5	0.413253
35	20	0.396216	35	22.5	0.430908
37.5	20	0.413253	37.5	22.5	0.449202
40	20	0.487805	40	22.5	0.487805
50	20	0.4878	50	22.5	0.508162
60	20	0.551117	60	22.5	0.573769
5	25	0.044477	5	27.5	0.044477
10	25	0.112437	10	27.5	0.119187
12.5	25	0.16515	12.5	27.5	0.156792
15	25	0.192087	15	27.5	0.192087
17.5	25	0.22206	17.5	27.5	0.211711
20	25	0.243897	20	27.5	0.255413
22.5	25	0.279712	22.5	27.5	0.267346
25	25	0.279712	25	27.5	0.292526
27.5	25	0.333822	27.5	27.5	0.319564
30	25	0.333822	30	27.5	0.363909
32.5	25	0.379775	32.5	27.5	0.379775
35	25	0.413253	35	27.5	0.396216
37.5	25	0.430908	37.5	27.5	0.413253
40	25	0.487805	40	27.5	0.487805
50	25	0.529257	50	27.5	0.551117
60	25	0.646773	60	27.5	0.646773
5	30	0.042061	5	50	0.039729
10	30	0.133431	10	50	0.087716
12.5	30	0.16515	12.5	50	0.126182
15	30	0.192087	15	50	0.173811
17.5	30	0.22206	17.5	50	0.182786
20	30	0.243897	20	50	0.201724

22.5	30	0.305804	22.5	50	0.22206
25	30	0.319564	25	50	0.255413
27.5	30	0.363909	27.5	50	0.267346
30	30	0.379775	30	50	0.292526
32.5	30	0.396216	32.5	50	0.305804
35	30	0.413253	35	50	0.363909
37.5	30	0.430908	37.5	50	0.379775
40	30	0.46816	40	50	0.396216
50	30	0.551117	50	50	0.430908
60	30	0.646773	60	50	0.487805
5	32.5	0.044477	5	55	0.031558
10	32.5	0.112437	10	55	0.076615
12.5	32.5	0.16515	12.5	55	0.105923
15	32.5	0.182786	15	55	0.126182
17.5	32.5	0.22206	17.5	55	0.140942
20	32.5	0.255413	20	55	0.173811
22.5	32.5	0.267346	22.5	55	0.192087
25	32.5	0.279712	25	55	0.201724
27.5	32.5	0.305804	27.5	55	0.22206
30	32.5	0.333822	30	55	0.243897
32.5	32.5	0.363909	32.5	55	0.279712
35	32.5	0.413253	35	55	0.292526
37.5	32.5	0.430908	37.5	55	0.305804
40	32.5	0.487805	40	55	0.319564
50	32.5	0.573769	50	55	0.379775
60	32.5	0.672892	60	55	0.449202
5	35	0.049575	5	62.5	0.029239
10	35	0.126182	10	62.5	0.056649
12.5	35	0.173811	12.5	62.5	0.071354
15	35	0.201724	15	62.5	0.087716
17.5	35	0.211711	17.5	62.5	0.099637
20	35	0.232784	20	62.5	0.126182
22.5	35	0.279712	22.5	62.5	0.133431

25	35	0.292526	25	62.5	0.156792
27.5	35	0.348598	27.5	62.5	0.16515
30	35	0.363909	30	62.5	0.173811
32.5	35	0.379775	32.5	62.5	0.192087
35	35	0.413253	35	62.5	0.201724
37.5	35	0.449202	37.5	62.5	0.22206
40	35	0.46816	40	62.5	0.232784
50	35	0.597243	50	62.5	0.279712
60	35	0.672892	60	62.5	0.305804
5	37.5	0.044477			
10	37.5	0.119187			
12.5	37.5	0.156792			
15	37.5	0.182786			
17.5	37.5	0.211711			
20	37.5	0.232784			
22.5	37.5	0.267346			
25	37.5	0.279712			
27.5	37.5	0.305804			
30	37.5	0.379775			
32.5	37.5	0.396216			
35	37.5	0.430908			
37.5	37.5	0.449202			
40	37.5	0.46816			
50	37.5	0.573769			
60	37.5	0.728006			
5	40	0.046981			
10	40	0.126182			
12.5	40	0.16515			
15	40	0.182786			
17.5	40	0.211711			
20	40	0.243897			
22.5	40	0.267346			
25	40	0.292526			

27.5	40	0.305804			
30	40	0.348598			
32.5	40	0.379775			
35	40	0.396216			
37.5	40	0.430908			
40	40	0.46816			
50	40	0.573769			
60	40	0.597243			
5	42.5	0.044477			
10	42.5	0.112437			
12.5	42.5	0.140942			
15	42.5	0.173811			
17.5	42.5	0.192087			
20	42.5	0.22206			
22.5	42.5	0.243897			
25	42.5	0.267346			
27.5	42.5	0.279712			
30	42.5	0.305804			
32.5	42.5	0.333822			
35	42.5	0.379775			
37.5	42.5	0.413253			
40	42.5	0.430908			
50	42.5	0.529257			
60	42.5	0.551117			
5	45	0.044477			
10	45	0.112437			
12.5	45	0.148726			
15	45	0.182786			
17.5	45	0.201724			
20	45	0.22206			
22.5	45	0.255413			
25	45	0.279712			
27.5	45	0.305804			

30	45	0.333822			
32.5	45	0.363909			
35	45	0.379775			
37.5	45	0.413253			
40	45	0.430908			
50	45	0.46816			
60	45	0.573769			
5	47.5	0.042061			
10	47.5	0.099637			
12.5	47.5	0.126182			
15	47.5	0.156792			
17.5	47.5	0.182786			
20	47.5	0.201724			
22.5	47.5	0.22206			
25	47.5	0.232784			
27.5	47.5	0.267346			
30	47.5	0.292526			
32.5	47.5	0.319564			
35	47.5	0.333822			
37.5	47.5	0.348598			
40	47.5	0.379775			
50	47.5	0.487805			
60	47.5	0.529257			
5	52.5	0.039729			
10	52.5	0.087716			
12.5	52.5	0.105923			
15	52.5	0.133431			
17.5	52.5	0.156792			
20	52.5	0.16515			
22.5	52.5	0.192087			
25	52.5	0.211711			
27.5	52.5	0.243897			
30	52.5	0.267346			

32.5	52.5	0.292526			
35	52.5	0.305804			
37.5	52.5	0.319564			
40	52.5	0.333822			
50	52.5	0.413253			
60	52.5	0.487805			
5	57.5	0.031558			
10	57.5	0.076615			
12.5	57.5	0.105923			
15	57.5	0.126182			
17.5	57.5	0.140942			
20	57.5	0.173811			
22.5	57.5	0.192087			
25	57.5	0.201724			
27.5	57.5	0.22206			
30	57.5	0.243897			
32.5	57.5	0.279712			
35	57.5	0.292526			
37.5	57.5	0.305804			
40	57.5	0.319564			
50	57.5	0.379775			
60	57.5	0.449202			
5	60	0.031558			
10	60	0.071354			
12.5	60	0.087716			
15	60	0.099637			
17.5	60	0.112437			
20	60	0.133431			
22.5	60	0.156792			
25	60	0.16515			
27.5	60	0.201724			
30	60	0.211711			
32.5	60	0.232784			

35	60	0.243897			
37.5	60	0.292526			
40	60	0.305804			
50	60	0.333822			
60	60	0.363909			
5	65	0.027356			
10	65	0.052063			
12.5	65	0.061377			
15	65	0.082067			
17.5	65	0.087716			
20	65	0.112437			
22.5	65	0.126182			
25	65	0.126182			
27.5	65	0.140942			
30	65	0.156792			
32.5	65	0.173811			
35	65	0.192087			
37.5	65	0.201724			
40	65	0.22206			
50	65	0.232784			
60	65	0.232784			
5	67.5	0.020886			
10	67.5	0.043434			
12.5	67.5	0.052086			
15	67.5	0.066277			
17.5	67.5	0.071354			
20	67.5	0.087716			
22.5	67.5	0.09357			
25	67.5	0.105923			
27.5	67.5	0.119187			
30	67.5	0.126182			
32.5	67.5	0.140942			
35	67.5	0.173811			

37.5	67.5	0.173811			
40	67.5	0.192087			
50	67.5	0.211711			
60	67.5	0.22206			
5	70	0.023785			
10	70	0.031558			
12.5	70	0.039334			
15	70	0.047683			
17.5	70	0.066277			
20	70	0.076615			
22.5	70	0.082067			
25	70	0.087716			
27.5	70	0.099637			
30	70	0.105923			
32.5	70	0.112437			
35	70	0.112437			
37.5	70	0.112437			
40	70	0.119187			
50	70	0.133431			
60	70	0.148726			
5	72.5	0.018883			
10	72.5	0.031558			
12.5	72.5	0.031558			
15	72.5	0.039334			
17.5	72.5	0.047683			
20	72.5	0.056649			
22.5	72.5	0.061377			
25	72.5	0.071354			
27.5	72.5	0.076615			
30	72.5	0.076615			
32.5	72.5	0.076615			
35	72.5	0.076615			
37.5	72.5	0.087716			

40	72.5	0.087716			
50	72.5	0.105923			
60	72.5	0.112437			

Table B4: Data set for x_r

Training Set			Test Set		
Fr	Angle	xr	Fr	Angle	xr
5	20	0.07436	5	22.5	0.07759
10	20	0.18279	10	22.5	0.16515
12.5	20	0.2439	12.5	22.5	0.25541
15	20	0.3058	15	22.5	0.33382
17.5	20	0.3486	17.5	22.5	0.39622
20	20	0.41325	20	22.5	0.39622
22.5	20	0.4492	22.5	22.5	0.46816
25	20	0.46816	25	22.5	0.50816
27.5	20	0.52926	27.5	22.5	0.52926
30	20	0.59724	30	22.5	0.62157
32.5	20	0.62157	32.5	22.5	0.64677
35	20	0.62157	35	22.5	0.7
37.5	20	0.69996	37.5	22.5	0.72801
40	20	0.72801	40	22.5	0.75707
50	20	0.88425	50	22.5	0.95497
60	20	1.07095	60	22.5	1.11244
5	25	0.0813	5	27.5	0.08514
10	25	0.17381	10	27.5	0.18279
12.5	25	0.26735	12.5	27.5	0.2439
15	25	0.3058	15	27.5	0.33382
17.5	25	0.36391	17.5	27.5	0.39622
20	25	0.4492	20	27.5	0.43091
22.5	25	0.46816	22.5	27.5	0.48781
25	25	0.48781	25	27.5	0.55112

27.5	25	0.52926	27.5	27.5	0.57377
30	25	0.59724	30	27.5	0.64677
32.5	25	0.64677	32.5	27.5	0.69996
35	25	0.69996	35	27.5	0.75707
37.5	25	0.75707	37.5	27.5	0.78719
40	25	0.8184	40	27.5	0.8184
50	25	0.95457	50	27.5	1.0309
60	25	1.11244	60	27.5	1.15544
5	30	0.08514	5	50	0.07402
10	30	0.19209	10	50	0.14873
12.5	30	0.25541	12.5	50	0.20172
15	30	0.3486	15	50	0.25554
17.5	30	0.36391	17.5	50	0.31956
20	30	0.41325	20	50	0.37978
22.5	30	0.46816	22.5	50	0.39622
25	30	0.52926	25	50	0.4492
27.5	30	0.55112	27.5	50	0.48781
30	30	0.64677	30	50	0.55112
32.5	30	0.67289	32.5	50	0.59724
35	30	0.72801	35	50	0.62157
37.5	30	0.78719	37.5	50	0.69996
40	30	0.8184	40	50	0.69996
50	30	0.99226	50	50	0.85074
60	30	1.15544	60	50	0.8184
5	32.5	0.08514	5	55	0.05209
10	32.5	0.19209	10	55	0.14094
12.5	32.5	0.2439	12.5	55	0.17381
15	32.5	0.31956	15	55	0.23278
17.5	32.5	0.36391	17.5	55	0.27971
20	32.5	0.43091	20	55	0.33382
22.5	32.5	0.48781	22.5	55	0.36391
25	32.5	0.52926	25	55	0.39662
27.5	32.5	0.62157	27.5	55	0.43091

30	32.5	0.64677	30	55	0.48781
32.5	32.5	0.67289	32.5	55	0.52926
35	32.5	0.72801	35	55	0.57377
37.5	32.5	0.78719	37.5	55	0.62157
40	32.5	0.85074	40	55	0.67289
50	32.5	0.99226	50	55	0.67289
60	32.5	1.2	60	55	0.75707
5	35	0.08514	5	62.5	0.04698
10	35	0.20172	10	62.5	0.09357
12.5	35	0.25541	12.5	62.5	0.12618
15	35	0.31956	15	62.5	0.15679
17.5	35	0.36391	17.5	62.5	0.23278
20	35	0.43091	20	62.5	0.25541
22.5	35	0.48781	22.5	62.5	0.27971
25	35	0.52925	25	62.5	0.3058
27.5	35	0.59724	27.5	62.5	0.33382
30	35	0.64677	30	62.5	0.36391
32.5	35	0.7	32.5	62.5	0.41325
35	35	0.72801	35	62.5	0.4492
37.5	35	0.72801	37.5	62.5	0.44921
40	35	0.8184	40	62.5	0.50816
50	35	1.11244	50	62.5	0.52926
60	35	1.15544	60	62.5	0.79581
5	37.5	0.08514			
10	37.5	0.19209			
12.5	37.5	0.2439			
15	37.5	0.33382			
17.5	37.5	0.37978			
20	37.5	0.4492			
22.5	37.5	0.48781			
25	37.5	0.50816			
27.5	37.5	0.57377			
30	37.5	0.62157			

32.5	37.5	0.67289			
35	37.5	0.75707			
37.5	37.5	0.78719			
40	37.5	0.8184			
50	37.5	1.11244			
60	37.5	1.15544			
5	40	0.08514			
10	40	0.18279			
12.5	40	0.25541			
15	40	0.31956			
17.5	40	0.36391			
20	40	0.4492			
22.5	40	0.48781			
25	40	0.52926			
27.5	40	0.59724			
30	40	0.64677			
32.5	40	0.67289			
35	40	0.69996			
37.5	40	0.72801			
40	40	0.78719			
50	40	1.0309			
60	40	1.15544			
5	42.5	0.08514			
10	42.5	0.19209			
12.5	42.5	0.23278			
15	42.5	0.3058			
17.5	42.5	0.36391			
20	42.5	0.43091			
22.5	42.5	0.4492			
25	42.5	0.52926			
27.5	42.5	0.55112			
30	42.5	0.59724			
32.5	42.5	0.62157			

35	42.5	0.67289			
37.5	42.5	0.75707			
40	42.5	0.85074			
50	42.5	0.99226			
60	42.5	1.07095			
5	45	0.0813			
10	45	0.17381			
12.5	45	0.23278			
15	45	0.26735			
17.5	45	0.36391			
20	45	0.41325			
22.5	45	0.4492			
25	45	0.48781			
27.5	45	0.55112			
30	45	0.57377			
32.5	45	0.62157			
35	45	0.64677			
37.5	45	0.72801			
40	45	0.78719			
50	45	0.91898			
60	45	0.99226			
5	47.5	0.07759			
10	47.5	0.16515			
12.5	47.5	0.21171			
15	47.5	0.29253			
17.5	47.5	0.31965			
20	47.5	0.39622			
22.5	47.5	0.43091			
25	47.5	0.48781			
27.5	47.5	0.55112			
30	47.5	0.55112			
32.5	47.5	0.59724			
35	47.5	0.64677			

37.5	47.5	0.69996			
40	47.5	0.78719			
50	47.5	0.88425			
60	47.5	0.91898			
5	52.5	0.06724			
10	52.5	0.14094			
12.5	52.5	0.18279			
15	52.5	0.2439			
17.5	52.5	0.29253			
20	52.5	0.3486			
22.5	52.5	0.37978			
25	52.5	0.4492			
27.5	52.5	0.46816			
30	52.5	0.52926			
32.5	52.5	0.55112			
35	52.5	0.57377			
37.5	52.5	0.62157			
40	52.5	0.62157			
50	52.5	0.75707			
60	52.5	0.75707			
5	57.5	0.05794			
10	57.5	0.11919			
12.5	57.5	0.15679			
15	57.5	0.21171			
17.5	57.5	0.26735			
20	57.5	0.29253			
22.5	57.5	0.33382			
25	57.5	0.36391			
27.5	57.5	0.39622			
30	57.5	0.46816			
32.5	57.5	0.48781			
35	57.5	0.55112			
37.5	57.5	0.57377			

40	57.5	0.62157			
50	57.5	0.67289			
60	57.5	0.67279			
5	60	0.04768			
10	60	0.10592			
12.5	60	0.15679			
15	60	0.18279			
17.5	60	0.21171			
20	60	0.29253			
22.5	60	0.29253			
25	60	0.36391			
27.5	60	0.37978			
30	60	0.41325			
32.5	60	0.4492			
35	60	0.50816			
37.5	60	0.52926			
40	60	0.55112			
50	60	0.57377			
60	60	0.79581			
5	65	0.04958			
10	65	0.06138			
12.5	65	0.11244			
15	65	0.14873			
17.5	65	0.18279			
20	65	0.22206			
22.5	65	0.26735			
25	65	0.26735			
27.5	65	0.29253			
30	65	0.31956			
32.5	65	0.36391			
35	65	0.39622			
37.5	65	0.41325			
40	65	0.41325			

50	65	0.55112			
60	65	0.60667			
5	67.5	0.03538			
10	67.5	0.07135			
12.5	67.5	0.09357			
15	67.5	0.11244			
17.5	67.5	0.17381			
20	67.5	0.20172			
22.5	67.5	0.22206			
25	67.5	0.2439			
27.5	67.5	0.25541			
30	67.5	0.26735			
32.5	67.5	0.29253			
35	67.5	0.3486			
37.5	67.5	0.34598			
40	67.5	0.36391			
50	67.5	0.46816			
60	67.5	0.47814			
5	70	0.03748			
10	70	0.06138			
12.5	70	0.07135			
15	70	0.09964			
17.5	70	0.13343			
20	70	0.15679			
22.5	70	0.16515			
25	70	0.18279			
27.5	70	0.20172			
30	70	0.2439			
32.5	70	0.2439			
35	70	0.2439			
37.5	70	0.2439			
40	70	0.25541			
50	70	0.39622			

60	70	0.35909			
5	72.5	0.03119			
10	72.5	0.04768			
12.5	72.5	0.05209			
15	72.5	0.07135			
17.5	72.5	0.07661			
20	72.5	0.09964			
22.5	72.5	0.12618			
25	72.5	0.15679			
27.5	72.5	0.15679			
30	72.5	0.15679			
32.5	72.5	0.18279			
35	72.5	0.18279			
37.5	72.5	0.18279			
40	72.5	0.18279			
50	72.5	0.21171			
60	72.5	0.24377			

Table B5: Data Set for y_m

Training Set			Test Set		
Fr	Angle	y	Fr	Angle	y
5	20	0.0205	5	22.5	0.02186
10	20	0.03684	10	22.5	0.03684
12.5	20	0.03684	12.5	22.5	0.05234
15	20	0.06105	15	22.5	0.06567
17.5	20	0.06105	17.5	22.5	0.07047
20	20	0.07546	20	22.5	0.07546
22.5	20	0.08064	22.5	22.5	0.08064
25	20	0.08064	25	22.5	0.08604
27.5	20	0.09165	27.5	22.5	0.09748
30	20	0.09165	30	22.5	0.10355

32.5	20	0.09165	32.5	22.5	0.11641
35	20	0.1099	35	22.5	0.12323
37.5	20	0.10985	37.5	22.5	0.13032
40	20	0.12323	40	22.5	0.13769
50	20	0.14536	50	22.5	0.15333
60	20	0.14536	60	22.5	0.1792
5	25	0.02301	5	27.5	0.02545
10	25	0.04824	10	27.5	0.04824
12.5	25	0.05234	12.5	27.5	0.05661
15	25	0.07047	15	27.5	0.07546
17.5	25	0.08064	17.5	27.5	0.08604
20	25	0.08064	20	27.5	0.09748
22.5	25	0.10355	22.5	27.5	0.10355
25	25	0.10985	25	27.5	0.11641
27.5	25	0.10985	27.5	27.5	0.12323
30	25	0.11641	30	27.5	0.13769
32.5	25	0.12323	32.5	27.5	0.13032
35	25	0.13769	35	27.5	0.14536
37.5	25	0.14536	37.5	27.5	0.12323
40	25	0.16162	40	27.5	0.17024
50	25	0.18851	50	27.5	0.20827
60	25	0.21875	60	27.5	0.22964
5	30	0.02674	5	50	0.04096
10	30	0.05234	10	50	0.09165
12.5	30	0.07047	12.5	50	0.10985
15	30	0.08604	15	50	0.14536
17.5	30	0.09165	17.5	50	0.17024
20	30	0.10355	20	50	0.1982
22.5	30	0.12323	22.5	50	0.20827
25	30	0.13769	25	50	0.24097
27.5	30	0.15333	27.5	50	0.22964
30	30	0.15333	30	50	0.27772
32.5	30	0.17024	32.5	50	0.29096

35	30	0.17024	35	50	0.30472
37.5	30	0.1792	37.5	50	0.31903
40	30	0.18851	40	50	0.34939
50	30	0.21875	50	50	0.43651
60	30	0.29096	60	50	0.49755
5	32.5	0.02949	5	55	0.03684
10	32.5	0.06567	10	55	0.09748
12.5	32.5	0.07546	12.5	55	0.11641
15	32.5	0.09165	15	55	0.16162
17.5	32.5	0.09748	17.5	55	0.17024
20	32.5	0.11641	20	55	0.21875
22.5	32.5	0.12323	22.5	55	0.22964
25	32.5	0.14536	25	55	0.24097
27.5	32.5	0.15333	27.5	55	0.26499
30	32.5	0.17024	30	55	0.27772
32.5	32.5	0.17024	32.5	55	0.30472
35	32.5	0.1982	35	55	0.31903
37.5	32.5	0.18851	37.5	55	0.34939
40	32.5	0.1982	40	55	0.38221
50	32.5	0.26499	50	55	0.4764
60	32.5	0.31903	60	55	0.5424
5	35	0.03094	5	62.5	0.04485
10	35	0.06105	10	62.5	0.08604
12.5	35	0.08604	12.5	62.5	0.10985
15	35	0.10985	15	62.5	0.14536
17.5	35	0.10985	17.5	62.5	0.17024
20	35	0.11641	20	62.5	0.20827
22.5	35	0.14536	22.5	62.5	0.22964
25	35	0.16162	25	62.5	0.26499
27.5	35	0.1792	27.5	62.5	0.25274
30	35	0.18851	30	62.5	0.27772
32.5	35	0.1982	32.5	62.5	0.31903
35	35	0.1982	35	62.5	0.33392

37.5	35	0.21875	37.5	62.5	0.34939
40	35	0.22964	40	62.5	0.39961
50	35	0.30472	50	62.5	0.49755
60	35	0.36548	60	62.5	0.49755
5	37.5	0.03402			
10	37.5	0.07047			
12.5	37.5	0.08604			
15	37.5	0.10355			
17.5	37.5	0.12323			
20	37.5	0.13769			
22.5	37.5	0.15333			
25	37.5	0.16162			
27.5	37.5	0.16162			
30	37.5	0.21875			
32.5	37.5	0.20827			
35	37.5	0.25274			
37.5	37.5	0.22964			
40	37.5	0.22964			
50	37.5	0.30472			
60	37.5	0.43651			
5	40	0.03402			
10	40	0.07546			
12.5	40	0.09165			
15	40	0.12323			
17.5	40	0.13769			
20	40	0.14536			
22.5	40	0.17024			
25	40	0.18851			
27.5	40	0.1982			
30	40	0.20827			
32.5	40	0.21875			
35	40	0.24097			
37.5	40	0.25274			

40	40	0.29096			
50	40	0.33392			
60	40	0.39961			
5	42.5	0.03566			
10	42.5	0.07546			
12.5	42.5	0.09748			
15	42.5	0.12323			
17.5	42.5	0.13769			
20	42.5	0.15333			
22.5	42.5	0.17024			
25	42.5	0.1791			
27.5	42.5	0.1982			
30	42.5	0.21875			
32.5	42.5	0.21875			
35	42.5	0.26499			
37.5	42.5	0.26499			
40	42.5	0.29096			
50	42.5	0.38221			
60	42.5	0.45607			
5	45	0.03735			
10	45	0.08064			
12.5	45	0.10985			
15	45	0.13032			
17.5	45	0.15333			
20	45	0.1792			
22.5	45	0.1982			
25	45	0.20827			
27.5	45	0.22964			
30	45	0.24097			
32.5	45	0.27772			
35	45	0.29096			
37.5	45	0.29096			
40	45	0.30472			

50	45	0.38221			
60	45	0.49755			
5	47.5	0.03735			
10	47.5	0.08604			
12.5	47.5	0.10985			
15	47.5	0.13769			
17.5	47.5	0.16162			
20	47.5	0.17024			
22.5	47.5	0.18851			
25	47.5	0.1982			
27.5	47.5	0.22964			
30	47.5	0.24097			
32.5	47.5	0.25274			
35	47.5	0.27772			
37.5	47.5	0.30472			
40	47.5	0.31903			
50	47.5	0.4177			
60	47.5	0.49755			
5	52.5	0.04287			
10	52.5	0.09165			
12.5	52.5	0.11641			
15	52.5	0.14536			
17.5	52.5	0.16162			
20	52.5	0.18851			
22.5	52.5	0.20827			
25	52.5	0.22964			
27.5	52.5	0.25274			
30	52.5	0.27772			
32.5	52.5	0.30472			
35	52.5	0.31903			
37.5	52.5	0.34939			
40	52.5	0.36548			
50	52.5	0.45607			

60	52.5	0.51954			
5	57.5	0.04287			
10	57.5	0.09165			
12.5	57.5	0.12323			
15	57.5	0.14536			
17.5	57.5	0.1792			
20	57.5	0.20827			
22.5	57.5	0.21875			
25	57.5	0.25274			
27.5	57.5	0.26499			
30	57.5	0.29096			
32.5	57.5	0.31903			
35	57.5	0.33392			
37.5	57.5	0.34939			
40	57.5	0.38221			
50	57.5	0.4764			
60	57.5	0.5424			
5	60	0.03684			
10	60	0.09165			
12.5	60	0.12323			
15	60	0.15333			
17.5	60	0.1792			
20	60	0.22964			
22.5	60	0.22964			
25	60	0.24097			
27.5	60	0.27772			
30	60	0.29096			
32.5	60	0.31903			
35	60	0.33392			
37.5	60	0.36548			
40	60	0.38221			
50	60	0.4764			
60	60	0.56617			

5	65	0.04485			
10	65	0.09165			
12.5	65	0.11641			
15	65	0.15333			
17.5	65	0.1792			
20	65	0.21875			
22.5	65	0.22964			
25	65	0.24097			
27.5	65	0.27772			
30	65	0.30472			
32.5	65	0.30472			
35	65	0.33392			
37.5	65	0.34939			
40	65	0.38221			
50	65	0.49755			
60	65	0.49755			
5	67.5	0.04049			
10	67.5	0.08064			
12.5	67.5	0.11641			
15	67.5	0.13769			
17.5	67.5	0.17024			
20	67.5	0.1982			
22.5	67.5	0.21875			
25	67.5	0.22964			
27.5	67.5	0.26499			
30	67.5	0.30472			
32.5	67.5	0.27772			
35	67.5	0.33392			
37.5	67.5	0.33392			
40	67.5	0.38221			
50	67.5	0.49755			
60	67.5	0.51954			
5	70	0.04287			

10	70	0.08604			
12.5	70	0.10985			
15	70	0.14536			
17.5	70	0.15333			
20	70	0.1982			
22.5	70	0.20827			
25	70	0.25274			
27.5	70	0.25274			
30	70	0.29096			
32.5	70	0.30472			
35	70	0.31903			
37.5	70	0.31903			
40	70	0.31903			
50	70	0.49755			
60	70	0.51954			
5	72.5	0.04485			
10	72.5	0.07546			
12.5	72.5	0.10355			
15	72.5	0.12323			
17.5	72.5	0.14536			
20	72.5	0.17024			
22.5	72.5	0.18851			
25	72.5	0.24097			
27.5	72.5	0.24097			
30	72.5	0.26499			
32.5	72.5	0.31903			
35	72.5	0.29096			
37.5	72.5	0.30472			
40	72.5	0.33392			
50	72.5	0.34939			
60	72.5	0.45607			